CHALMERS
UNIVERSITY OF TECHNOLOGY

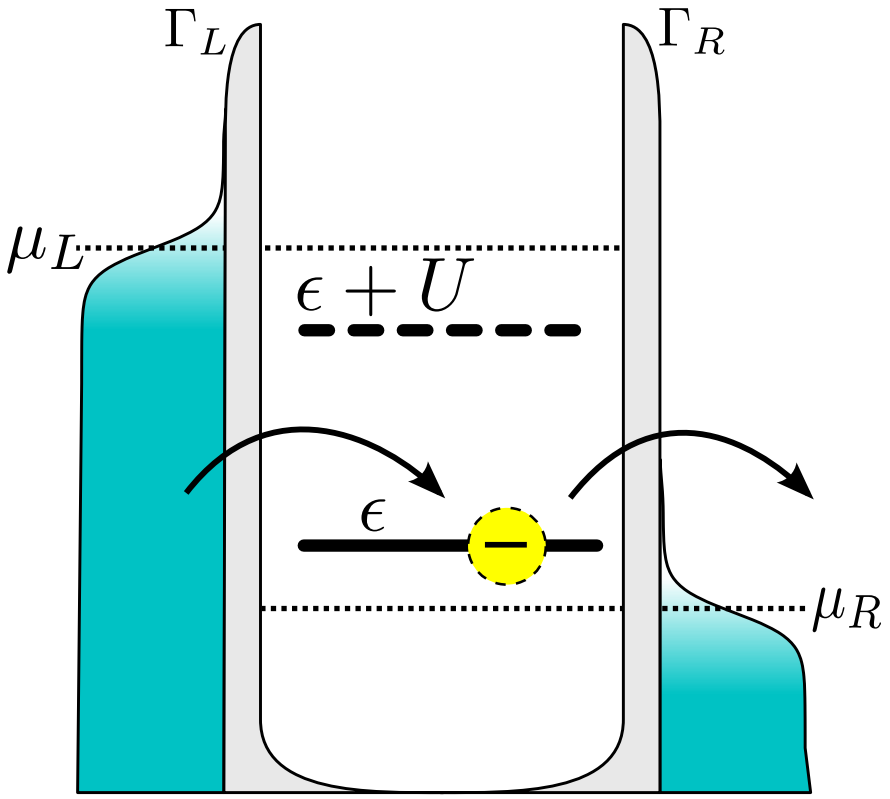

Time-dependent particle and energy currents through interacting quantum dots

Thesis for the degree of Erasmus Mundus Master of Science in Nanoscience and Nanotechnology

JOREN VANHERCK

Promoter: Prof. Janine Splettstößer
Co-promoter: Prof. Michel Houssa

KU LEUVEN

Department of Microtechnology and Nanoscience (MC2)
Applied Quantum Physics Laboratory
CHALMERS UNIVERSITY OF TECHNOLOGY
Göteborg, Sweden 2016

Erasmus Mundus

THESIS FOR THE DEGREE OF ERASMUS MUNDUS MASTER OF SCIENCE IN NANOSCIENCE AND NANOTECHNOLOGY
Specialisation Nanophysics

Time-dependent particle and energy currents through interacting quantum dots

JOREN VANHERCK

Department of Microtechnology and Nanoscience (MC2)

Applied Quantum Physics Laboratory

CHALMERS UNIVERSITY OF TECHNOLOGY

Göteborg, Sweden 2016

Time-dependent particle and energy currents through interacting quantum dots
JOREN VANHERCK

Thesis for the degree of Erasmus Mundus Master of Science in Nanoscience and Nanotechnology

This thesis was conducted in the framework of the Erasmus Mundus Master programme in Nanoscience and Nanotechnology.

Promoter: Prof. Janine Splettstößer
Co-promoter: Prof. Michel Houssa
Daily supervisor: Jens Schulenborg
External referee: Prof. Ermin Malic

Applied Quantum Physics Laboratory
Department of Microtechnology and Nanoscience (MC2)
Chalmers University of Technology
SE-412 96 Göteborg
Sweden

Faculties of Engineering Science and Science
KU Leuven
3000 Leuven
Belgium

Cover
A sketch of a typical quantum dot, tunnel-coupled to two leads, as studied in this thesis.

Printed by Chalmers Reproservice
Göteborg, Sweden 2016

Time-dependent particle and energy currents through interacting quantum dots
Thesis for the degree of Erasmus Mundus Master of Science in Nanoscience and Nanotechnology

JOREN VANHERCK

Department of Microtechnology and Nanoscience (MC2)
Applied Quantum Physics Laboratory
Chalmers University of Technology

Abstract

Recently, there has been a lot of interest in particle and energy currents through nanoscale devices. Most of these studies focus on the stationary behaviour of these devices, which can for example describe autonomous heat engines. However, for the dynamical operation of such nanosystems, e.g. for cyclic gate driving or irradiation of frequency-dependent electromagnetic fields, it is indispensable to be able to reliably model the time-dependent currents during and after executing operations.

Here, we study the time-dependence of a single level quantum dot with a strong on-site Coulomb interaction that is weakly tunnel-coupled to multiple non-interacting electronic leads and subject to non-linear driving. The leads are characterised by different electrochemical potentials and temperatures. We analyse this system up to first order in the tunnel-coupling strength, expressed in a Liouville superoperator formalism, yielding a convenient formulation of the Born-Markov master equation. Both the density operators of the open quantum dot system as well as the particle, energy and heat currents through it are evaluated within this formalism and expressed in terms of decay modes in response to the driving. We consider two important non-stationary regimes in which any of the system's parameters (dot energy level, on-site interaction, tunnel-coupling strength and electrochemical potential of the leads) can be changed time-dependently: On the one hand the currents are calculated after a sudden, instantaneous switch. On the other hand they are found for moderately fast, but otherwise arbitrary driving schemes. For both cases, fully analytical and physically insightful expressions for the time-dependent particle, energy and heat currents are derived and discussed. This is done both in the absence and presence of an externally applied magnetic field, leading to spin-dependent energy levels and tunnelling. Finally, the broadly applicable, analytic results that we obtained are employed in the study of two concrete cases. First their use is demonstrated in the study of thermoelectric efficiencies when time-dependent driving signals are applied. Secondly, we investigate the fundamental nature and the practical experimental consequences of a recently highlighted fermion-parity decay mode in the moderately fast driving regime.

Keywords: quantum dot, Coulomb charging energy, particle current, energy current, time-dependent, switch, arbitrary driving, master equation, tunnel-coupled, thermoelectric, fermion-parity

Acknowledgements

First of all, I would like to thank my promoter Janine Splettstößer for giving me the chance to work on this interesting and novel project. She was always prepared to give advice and support, in every sense possible. Her continuous motivations have really lifted this work to a higher level. Especially, I want to thank her for giving me the opportunity to attend, and present a poster with this work at the Fourth Quantum Thermodynamics Conference in Erice. This really helped to get a better view on the field, and especially related research.

Secondly, but with equal importance, I wish to thank my daily supervisor Jens Schulenborg. His knowledge and experience on the topic of this thesis are enormous and he was always happy to share this with me. Next to this topical assistance, he also provided valuable practical and technological counselling in the form of templates, figures, email management ... Apart from all of this, Jens has helped extensively on the improvement of this final thesis text.

I also want to express my gratitude for prof. Michel Houssa for his consent in being my co-promoter. I want to thank Angelo di Marco (as well as Jens and Janine) for the collaboration on thermoelectric efficiencies and the detailed explanations regarding this topic. Furthermore I would like to thank Michele Governale for the insightful discussions on the signatures of the fermion-parity rate. Of course, I also want to thank everyone whom I had the pleasure of working and meeting with, especially everyone from the applied quantum physics laboratory at MC2.

Last, but certainly not least, I want to thank everyone in my (distant) environment supporting me during the last year(s). With this, I mainly want to address my girlfriend Eline, my parents and grandparents[1], the rest of my family and of course my friends.

[1] Bedankt oma en opa!

Contents

1 Introduction

1.1 General context

The finest feature size of transistors on a computer chip steadily decreases. This reduction by fifty percent about every eighteen months was already predicted by Moore in 1965 [1]. Up to now, the downscaling was anticipated to reach its limits already many times. It however still continues today[1], and is most probably not going to stop because of technological reasons, but rather due to economical limitations. The required technological progress and continuous downscaling has some important consequences.

First of all, critical dimensions have decreased below 100 nm and will soon be reaching the 10 nm threshold. This means that we are not just entering the realm of quantum mechanics, we are already in it! Instead of fighting these quantum effects, such as tunnelling, we should try to exploit them for new applications. This asks of course for a lot of research. On the one hand, the advanced fabrication techniques open up an enormous playground for experimental physicists. On the other hand, it also requires a large effort theory-wise to be able to describe and understand the exact system's behaviour. In this thesis, an effort is done for a contribution on this theory side.

Another key consequence of the continuous downscaling is that one needs to adopt new computational paradigms (e.g. spintronics, wave-logic ...) and new device architectures. This is the contrast between two large movements in the field of nanoelectronics. "More than Moore" is the branch that goes beyond charge based devices, while "More Moore" tries to keep using charge-based technologies, but not just the classical planar transistors [3]. Examples of the latter are gate-all-around field effect transistor architectures and new device concepts such as single electron transistors. In this thesis, we study the time-dependent dynamics of a quantum dot, which is coupled to multiple leads. This is in essence a simple model of a single electron transistor.

Finally, miniaturisation goes hand in hand with increasing device speeds and heating problems. The former implies that behaviour of nanostructures during switching operations grows in importance relative to its stationary state behaviour. The latter means that keeping track of heat generation, transport and dissipations is unavoidable if we want devices to perform as expected. In this thesis, we focus on both the particle and heat currents through a quantum dot system in which all parameters - such as gate voltages and magnetic fields - can have a general time-dependence.

To summarise, this thesis is focussed on the study of a specific, single level quantum dot model with a local repulsive interaction with coupling to multiple leads. A more exact definition is provided in Chapter 2. The quantum state of this dot, as well as the (time-resolved) particle and heat current through it, are studied while any of its defining

[1] Although one of the largest chip manufacturers very recently announced a slowdown [2].

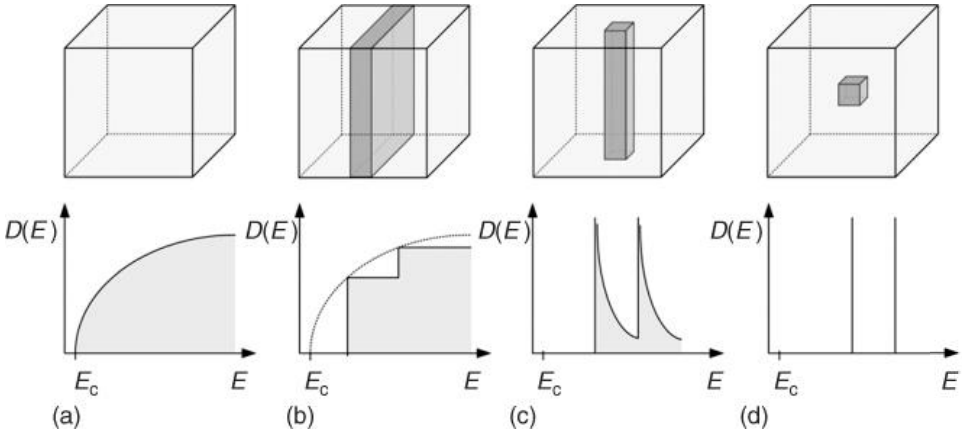

Figure 1.1: *Typical density of states as a function of energy for particles confined to* ***(a)*** *three (bulk),* ***(b)*** *two (quantum well),* ***(c)*** *one (quantum wire) or* ***(d)*** *zero (quantum dot) dimensions.* ***Source****: [8]*

parameters can be varied in time. In this introductory chapter, we will first elaborate on quantum dots and how they can be realised. In Sec. 1.3, we describe how single electrons can be manipulated using quantum dots and possible motivations for doing this. Although this thesis is self-contained, Sec. 1.4 provides a short overview of the recent advances in the theory concerning the dynamics of interacting quantum dots, of which this thesis is a continuation. Finally we outline the structure of the results part of this thesis in Sec. 1.5.

1.2 Quantum dot

This section is meant to give a brief introduction on what quantum dots are, and how they can be achieved practically. This is not a complete overview of the field, but rather intended to give an essential background. More background information can be found in the introductory solid state physics book by C. Kittel [4]. For a much more detailed treatment, I refer to the book [5] by T. Ihn and to reviews by S.M. Reimann [6] and L.P. Kouwenhoven [7]. Most information in this section is based on these sources.

Since quantum dots can in general appear in many forms, there is no clear-cut definition. They have however a characteristic that always stays the same: they are nanoscale systems in which particles are confined in all spatial dimensions. To illustrate the consequences of this confinement, we can consider the density of states $\mathcal{D}(E)$ of free electrons in a Fermi gas for different dimensions, as shown in Fig. 1.1. The density of states (DOS) is a measure for the number of states an electron can occupy in an infinitesimal energy range centered on a specific energy E. For a bulk piece of material, Fig. 1.1(a), the electrons are free to move in all three directions. No quantisation effects take place and the DOS has the energy dependence $\mathcal{D}(E) \propto \sqrt{E}$. Fig. 1.1(b) shows the situation for a system where the electrons are confined (to nanometer scale) in one direction, while free in the two other directions. This leads to a continuous two-dimensional density of states $\mathcal{D}(E) \propto$ const., with several subbands due to the quantisation of energy in the third direction [9]. This subband quantisation is visible as steps in the DOS. An electronic

system that is only free in two dimensions is often called a 2DEG (two-dimensional electron gas), but sometimes also referred to as a quantum well. Confining the system in one more dimension, Fig. 1.1(c), leads to quantisation in two dimensions, while the DOS in the third direction is still continuous and behaves as $\mathcal{D}(E) \propto E^{-\frac{1}{2}}$. Such a one-dimensional system is called a quantum wire. Typical examples are carbon nanotubes, conducting polymers or semiconducting nanowires. This brings us finally to the system of interest: the quantum dot, Fig. 1.1(d). This system is confined to nanometer scale in all three dimensions, such that the density of states is not continuous any more in any directions. This means that the system is fully quantised, it has discrete energy levels E_i. The density of states therefore consists of separated Dirac delta functions: $\mathcal{D}(E) \propto \sum_i \delta(E - E_i)$. The exact quantisation (i.e. at which energy levels there are states available) is strongly dependent on the confinement geometry. This means that the energy spectrum can be tuned by changing the confining potential. A quantum dot is sometimes also called an *artificial* atom since the discrete energy spectrum, resembling that of an atom or molecule, can be realised with highly tunable electromagnetic fields. The important difference between an atom and a quantum dot is the fact that certain quantum dots (e.g. constructed in semiconducting material with electrostatic confinement) can be contacted and that their energy level structure is highly tunable. At the end of this section, we give a brief overview of different types of quantum dots that are of interest for this thesis.

For the practical use of semiconductor based quantum dots, they are most often connected to a source and drain electrode by a tunnelling contact. This allows for the existence of a current from source to drain when a voltage is applied between them. An additional condition for this to happen is that there has to be a dot energy level within the bias window[1]. This requirement is illustrated in Fig. 1.2(a). In the upper part of the figure, the energy level E_i is situated within the bias window (indicated in orange). This means that there are electrons with sufficient energy available from the left electronic lead (source) to transfer into the dot when the level E_i is empty. Similarly, when this level is occupied, the occupying electron will have enough energy to transfer to one of the empty states in the right lead. Electrons can thus flow from the left lead, through the dot, into the right lead when there is a quantum dot level within the bias window. The lower part of the figure shows how any current is inhibited when none of the levels satisfies this requirement. The electron already occupying the dot at energy E_{i-1}, can not go into any of the lead, since there are no empty states available at this low energy. The level E_i can on its turn not get filled, since none of the lead's electrons have sufficient energy. This blockade regime is often referred to as a Coulomb blockade[2] and is most prominently present at low temperatures (since this reduces thermal broadening). The Coulomb blockade was suggested by C.J. Gorter in 1951 [10] as a solution to some anomalous conductance observations for metallic thin films (a decrease of conductance is detected in this regime). Later experiments by T.A. Fulton and J.G. Dolan [11] showed this exact effect in small-area tunnel junctions.

[1] At least in the sequential tunnelling regime and at sufficiently low temperature. We will elaborate further on this condition in Sec. 2.1.

[2] Since the energy level separation in the dot is often due to the electrostatic charging energy of the system. This will also be the case in the quantum dot that we study in this work.

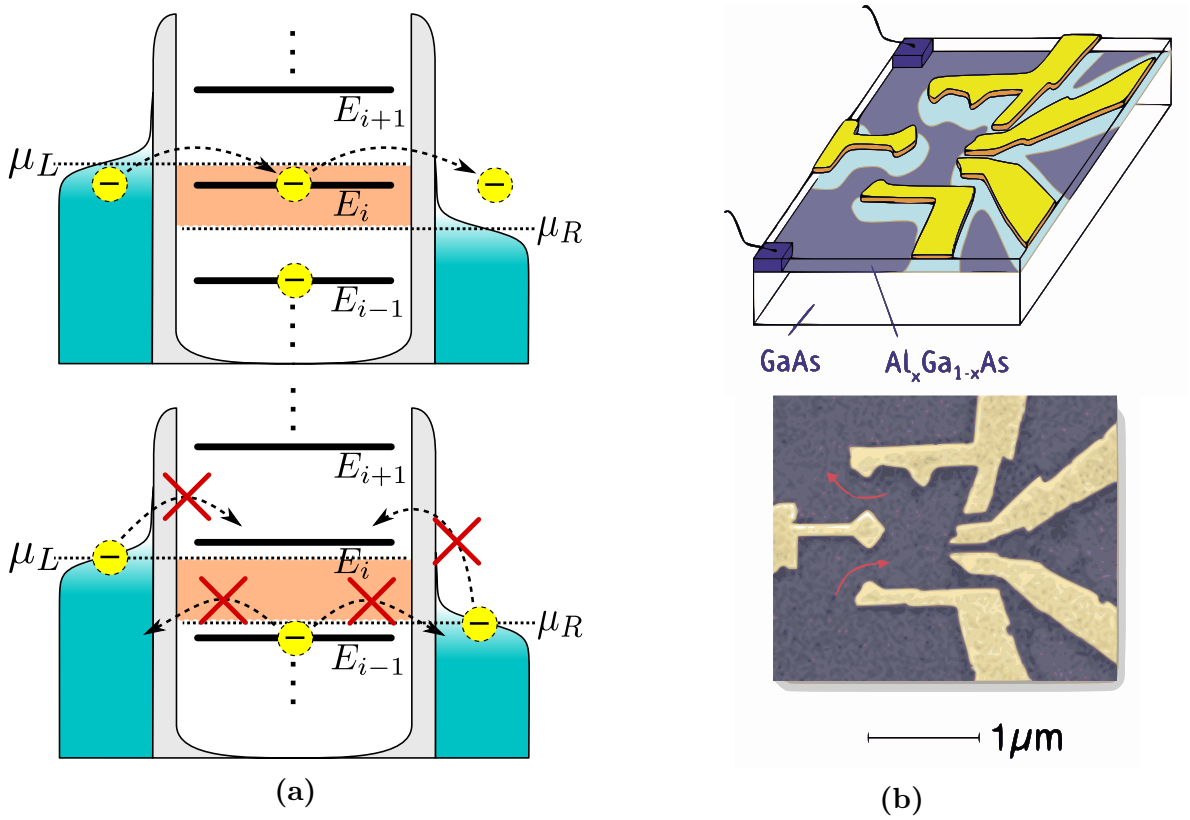

Figure 1.2: **(a)** *Illustration explaining the Coulomb blockade regime. In both figures, the quantum dot and its energy levels are shown in the centre. The turquoise regions on the left and right represent the electronic occupation (Fermi-distributions) of the leads. Electrons can tunnel from the leads into the dot and vice versa when states are available, i.e. when there is a dot energy level within the bias window (shaded in orange).* **(b)** *A typical solid state quantum dot. The upper figure is a schematic drawing, while the lower one is an actual electron micrograph. Purple regions represent the 2DEG formed at the GaAs/AlGaAs interface. The yellow structures are the confining gate electrodes that deplete the underlying 2DEG in the blue regions. Source and drain voltages can be tuned by the contacts shown in dark purple at the left-hand side of the drawing.* ***Source****: [13]*

Next to the source and drain, one often adds a third contact to the quantum dot, a capacitively coupled gate electrode which allows to shift the energy spectrum as we did in Fig. 1.2(a). This allows us to switch between the states in which a current can or can not flow, which is basically what a transistor does. Indeed: this is the device concept for a single electron transistor (SET) [11]! Already in 2001, controllable room-temperature single electron transistors made from metallic single-wall carbon nanotubes were demonstrated by a group lead by H. W. Ch. Postma at Delft University of Technology [12].

To conclude this section, it is instructive to briefly consider the practical realisation of quantum dots. Typically, we can distinguish two large classes of quantum dots. The first category are the solid state quantum dots [14]. In general, these artificial atoms are a combination of semiconductors in different forms: in bulk, as thin layers or as small gate electrodes. An example of such a system is shown in Fig. 1.2(b) [13]. First a two-dimensional electron gas is formed from a GaAs/AlGaAs heterostructure.

Next, electrodes are fabricated on top of this to further confine the electrons in the two remaining dimensions. By tuning the voltages and shapes of these electrodes, the confining potential can be altered. These devices are typically fabricated top-down. This means that one starts with a macroscopic material and uses lithography to define for example the gate electrodes. The top-down fabrication is typically very successful down to about 50 nm, although advanced lithography techniques allow to go far beyond this. The second category are the nanoclusters and molecules [15]. This class spans a very wide range. There are metallic or semiconducting nanoclusters that are highly tunable by changing their size and adding different functional groups. But there are also highly ordered structures such as nanotubes made from carbon or semiconducting materials. The fabrication techniques for these kind of assemblies are typically bottom-up. This means that larger structures are formed from smaller ones, by e.g. self-assembly. The bottom-up approach has most advantages below about 50 nm. The study of the synthesis and characterisation of these materials is a whole field of chemistry on its own, namely nanochemistry. We refer the interested reader to the excellent books [16] and [17] on the chemical synthesis of these types of nanostructures. The distinction between the two classes of quantum dots and their fabrication techniques is often not as clear-cut as it seems to be from the above explanation. The two strategies are often combined, for example to fabricate nanotubes bottom-up, while the connecting electrodes are made top-down.

1.3 Single electron dynamics

Understanding the dynamics of nanoscale systems at the single electron level is crucial for many, very different applications. Here, we highlight two of them. A first example is quantum information processing. The most advanced technologies in this field at the moment, are based on controlling single photons, i.e. quantum optics [18]. However, there is in theory nothing that inhibits the use of single electrons instead of photons. Quantum electron optics would allow for on-chip or table-top experiments instead of rather large photonic experiments. Using electrons could moreover offer additional opportunities over the use of photons, since it is easier to let electrons interact with each other and they obey Fermi-Dirac instead of Bose-Einstein statistics. This is thus an active field of research, and most of the papers cited in this section are related to this research. A second application is the completion of the quantum metrology triangle [19]. This triangle directly relates three of the most important metrological quantities in electricity and magnetism (the electrical current, voltage and frequency) using only fundamental constants of nature. The relations between frequency and voltage respectively voltage and current are well established due to the Josephson effect and the quantum Hall effect. Indirectly, the frequency and current are thus related as well. However, to check for consistency of the three quantum electrical effects, a direct relation has to be made using single-electron currents. By investigating new single electron sources and detectors, one tries to reduce the uncertainty on these single-electron current measurements. In a new revision of the International System of Units (SI), that is scheduled for 2018, the Ampère will already be linked directly to the exact numerical values of the charge of an electron.

The three key elements that are necessary for doing quantum information processing using electrons (i.e. quantum electron optics) are a single-electron source, a means of propagation and a detector. The source can be made from a quantum dot, using many different methodologies. Since this source is most closely related to the contents of this thesis, we will focus more on a specific example later in this section. The propagation of a single electron has to take place in a shielded environment from the other electrons in order not to disturb the electron's quantum state. One possibility to do this is to use a combination of a 2DEG and surface acoustic waves [20–22]. The electrons are then "surfing" on the moving potential that in turn is excited by the surface acoustic wave. With this technique, single electrons can be transferred between two quantum dots (a source and a detector) with a quantum efficiency above 90 %. To obtain such high efficiencies, a good knowledge of the exact time-dependence of the emission and propagation of electrons is absolutely necessary. The detector is typically based on the charge measurement of a quantum dot.

The electron source has to reliably emit single electrons, and this preferably at a high frequency[1] if one wants to measure and effectively use them. Fève et al. [23] showed experimentally that these requirements could be met in a system similar to the one in Fig. 1.2(a), but with only one connected electrode. The device was fabricated in a 2DEG and tunnel-coupled to a lead with a quantum point contact. By changing the height of the gate switch, the electronic energy could be tuned. Frequencies in the gigahertz regime were shown to be possible. The main restriction to the frequency was the finite tunnel rate. When the tunnel rate gets too high, the electronic levels in the quantum dot become effectively broadened due to virtual processes[2], which in turn leads to dot charge fluctuations. This is not desirable for a single electron source. The tunnelling time is thus basically the limiting factor in this experimental setup.

Another approach that solves this problem was proposed and realised by Blumenthal et al. [24], and is schematically shown in Fig. 1.3. In this experiment, the electrons "surf" on the potential instead of tunnelling through barriers. Next to changing the quantum dot energy level itself (here: M), also the two tunnel barriers (L and R) can be tuned. This setup was realised in a 2DEG, with three surface finger gates to modify the different parts of the potential surface. The voltage at the left electrode is changed time-dependently in order to control the barrier height. However, this also has an effect on the potential at M, and to lesser extend on R. The tunnel barriers can be lowered such that there is no effective quantum dot any more. But they can also be raised up to a point where no tunnelling through them is possible at all. Since there is always one barrier at a very high point (barrier R), the current will always be independent of the source-drain voltage. Moreover, the quantisation of this current can be precisely controlled by the exact time-dependent tuning of the left barrier height. The elimination of the limiting tunnelling time with respect to the experiment by Fève et al., was the enabling factor to reach slightly higher frequencies.

[1] More single electrons emitted in a short time, leads to a higher accuracy.

[2] Remember Heisenberg's uncertainty principle that relates the lifetime of an energy level to its uncertainty in energy.

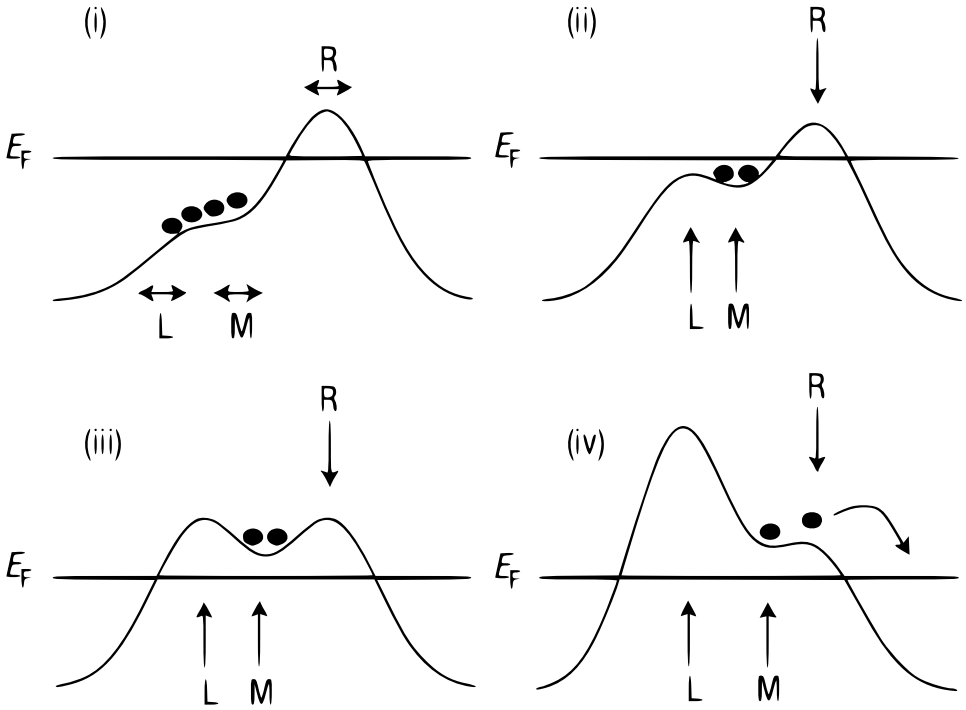

Figure 1.3: *Pictures showing changes in the potential surface that allow for quantised charge pumping. The changes can be achieved by tuning the surface finger electrode at position L, M and R. L and R tune the barriers of the quantum dot, while M tunes the energy levels of the quantum dot itself. E_F is the Fermi-level of the 2DEG in which the quantum dot is embedded. By tuning the exact time-dependence of the electrode voltages (specifically by driving L, which in turn also influences the voltage at M and to lesser extend the barrier R), the number of electrons transferred during each pumping cycle can be adjusted.* ***Source****: [24]*

More recent experiments on gigahertz quantised charge pumping comprise pumping through a graphene-based double quantum dot [25] and through a quantum dot made from a semiconducting nanowire [26]. Note that especially the experiments by Blumenthal et al. [24] and d'Hollosy et al. [26] crucially depend on the exact time-dependent control of the different system parameters. The transfer of single electrons using surface acoustic waves on the other hand relied strongly on the exact emission times from the quantum dot.

However, quantum transport has preliminarily only been studied using stationary, non-equilibrium electron distributions. A good theoretical description and understanding of the time-dependent currents of a dynamically driven quantum dot will thus certainly be valuable in the design of new experiments in this field. It is crucial to understand the currents flowing in and out of a quantum dot before quantum information processing using electrons can catch up with the more advanced quantum optics.

1.4 Relaxation rates of an interacting open system

This thesis work is inserted into an ongoing research effort in the domain of interacting open quantum systems. It is therefore instructive to give a brief overview of the line of research that will be continued in this thesis. Most of the concepts that are stated here are also explained in more detail in the remainder of this thesis. For a more exhaustive overview, both in depth and width, we refer to the papers cited in this section and the references therein.

All these papers study the same basic system: a single level quantum dot with strong Coulomb interaction in the Anderson model. This is also the system under investigation in this thesis and it will be carefully explained in Sec. 2.1. In general this quantum dot is (weakly) tunnel-coupled to a single electronic lead. It can be considered as the most basic setup to study time-dependence in interacting open quantum systems.

First, Splettstoesser et al. [27] were interested in the response of this system to a fast switch of the gate potential, or to the slow harmonic variation of this gate potential. They used an expansion in the tunnel-coupling strength up to fourth order in the tunnelling matrix elements. This allows not only to describe sequential tunnelling events, but also cotunnelling effects and virtual tunnelling processes. For the harmonic variation of the gate potential, they limit their approach however to first order in the driving frequency, which means that the driving has to be very slow. They find that the Coulomb interaction leads to two different time scales in the system, that both depend on the dot's energy level. These time scales can be related to charge and spin relaxation processes respectively. On the contrary, without the Coulomb interaction, both spin and charge relax by the same rate, which is independent of the energy level of the dot.

Contreras-Pulido et al. [28] identified a third time scale necessary to fully describe this system. This additional time scale is independent of the level position and the strength of the Coulomb interaction. Moreover, it only appears for the evolution of physical quantities related to two-particle processes. There was however not yet a good interpretation for this additional rate.

Finally, Schulenborg et al. [29] found very peculiar features in the heat current after a gate voltage switch: there are signatures of electron-electron attraction, while the system has a repulsive Coulomb interaction. These features, as well as the third rate that was found earlier, turned out to be related to a very general duality relation. This duality relation holds for a large class of open fermionic quantum systems, and can be derived from the fermion parity superselection postulate[1]. Next to explaining the peculiar features, it also helps to express the used equations in quantities with a physical meaning (instead of complex combinations of Fermi function, which are often difficult to interpret). To demonstrate the duality, the example of a simple gate switch in a quantum dot connected to one electronic lead is worked out in detail.

In this thesis, we will now use the newly found duality relation under more general conditions. We will exploit the duality to extend the example of a simple gate switch in three major directions. At first, we extend the model to allow for fast switches in any of the system parameters (e.g. dot energy level, on-site interaction, coupling

[1] This postulate basically tells that quantum states with even and odd fermion number cannot be superposed.

strength to the leads ...), while the dot is connected to an arbitrary number of leads. Secondly, we investigate the usefulness of the duality for the calculation of currents through the quantum dot when there is an arbitrary (but rather slow) driving in any of the parameters. In a third phase, we repeat the previous two points, but now when an external magnetic field is applied, such that the spin-degeneracy is lifted.

1.5 Organisation of this thesis

We now have a basic understanding of quantum dots and the relevance of single-electron dynamics in nanosystems. The remainder of this thesis will focus on a continuation of the research that we outlined in the last section. The structure of this work can be seen as consisting of two parts: the first three chapters extend these works in the three major directions just mentioned, while the two chapters thereafter present the first results of ongoing research that makes use of the general formalism presented in the first three chapters.

First, in chapter 2, we introduce the single level quantum dot with strong on-site interaction weakly coupled to multiple electronic leads, which is the main system studied in this thesis. We explain the Born-Markov master equation that is used to describe this system and calculate its relevant eigenmodes. The general employed strategy is the same as used by Schulenborg et al. [29, 30]. However, the quantum dot is now coupled to multiple leads (instead of one). The chapter ends with the dynamics after a sudden switch in any of the system parameters. This is a limiting case scenario of the full description of the system dynamics for arbitrary (slow) driving in any parameter, which is presented in chapter 3. This chapter comprises the *main results* of this thesis: *practical analytic* equations that allow for a dynamical system description in terms of the *density operator* and the different *currents* through the quantum dot. Chapter 4 then lifts the spin-degeneracy of the system by introducing a magnetic field. We investigate to which extend the results of chapters 2 and 3 translate to this more complicated system. Interesting similarities and new phenomena are carefully analysed.

In chapter 5, we see how the expression for the currents through the quantum dot system can be used in the description of thermoelectric devices. They can be used to calculate Onsager coefficients and as such the thermoelectric efficiency when time-dependent driving is present. Possibly they can help to better understand the presumed increased efficiency under certain driving schemes [31]. Finally, in chapter 6 we initiate further research concerning a time-averaged detection of, and a better understanding of, the fermion-parity mode and the related inverted dot model, in continuation of [29, 32].

2 Strongly interacting quantum dot

Before any time-dependent currents can be calculated, we should get acquainted with the precise system model that we are studying, some notation and the equations describing the dynamics of the system. In Sec. 2.1 we explain the quantum dot model and some of the assumptions that we make with respect to its parameters. Next, in Sec. 2.2, we introduce the notation that will be used throughout this thesis. Also the Born-Markov master equation, which fully describes the dynamics of the system, is introduced. Section 2.3 starts by stating the duality relation [29] that allows for physical interpretations of many of the results in this thesis. It also paves the way to calculate the different eigenmodes of the kernel of the Born-Markov master equation. The chapter is concluded in Sec. 2.4 by calculating a first time-dependent result: the decay dynamics of the quantum dot after a sudden switch in any of the system's parameters. This is also the appropriate place to extend on the different decay rates of the system.

Please note that the general strategy of this chapter is similar to calculations by Schulenborg et al. [29, 30]. There are however two main differences. Firstly, the dot is now connected to multiple leads instead of only one. Secondly, the switch at the end of the chapter is generalised to incorporate changes in any of the system's parameters, instead of only the gate voltage.

2.1 Anderson quantum dot model

The system under consideration consists of a single level quantum dot which is weakly tunnel-coupled to multiple non-interacting leads (see Fig. 2.1). The Anderson Hamiltonian [33]

$$H_{\mathrm{And}} = H + H_{\mathrm{Leads}} + H_{\mathrm{Tun}} \tag{2.1}$$

is used to describe the system. H, H_{Leads} and H_{Tun} are the Hamiltonians of the dot, the leads and the tunnel-coupling respectively.

The Hamiltonian of the quantum dot itself is given by

$$H = \sum_{\sigma=\uparrow,\downarrow} \epsilon n_\sigma + U n_\uparrow n_\downarrow, \tag{2.2}$$

where the number operator is written as $n_\sigma = d_\sigma^\dagger d_\sigma$. The operators $d_\sigma^\dagger$ and d_σ are respectively the creation and annihilation operators for an electron with spin $\sigma = \uparrow, \downarrow$ in the dot. The quantum dot has one discrete energy level ϵ and can accommodate two fermions with opposite spin. There is only one energy level ϵ because we consider the dot without an external magnetic field, such that the level is spin degenerate. The single dot level results in four possible physical states of the isolated dot system: unoccupied ($|0\rangle$), singly occupied with a spin-up fermion ($d_\uparrow^\dagger|0\rangle = |\uparrow\rangle$), singly occupied with a spin-down

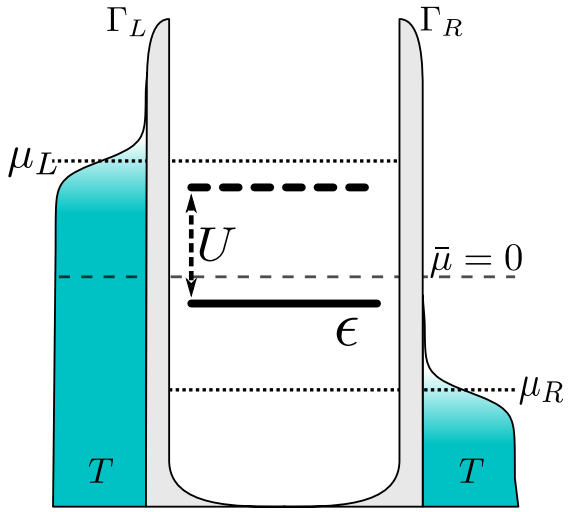

Figure 2.1: *Model of the strongly interacting quantum dot, tunnel-coupled to two leads. There is one energy level ϵ in the dot. If the dot is doubly occupied, there is an additional charging energy U. For simplicity, the dot is only coupled to two leads: left ($\alpha = \mathrm{L}$) and right ($\alpha = \mathrm{R}$). The tunnel-coupling strengths are Γ_L and Γ_R. The leads are in the Grand-Canonical ensemble with electrochemical potentials μ_L and μ_R and at temperature T. All energies are measured with respect to the average chemical potential $\bar{\mu} = 0$.*

fermion ($d_\downarrow^\dagger|0\rangle = |\downarrow\rangle$) or doubly occupied ($d_\uparrow^\dagger d_\downarrow^\dagger|0\rangle = |2\rangle$). These physical occupation states span the four-dimensional Hilbert space of the dot. When two particles occupy the dot, there is an on-site Coulomb repulsion, which increases the energy of the dot system by U. The total energy of the dot occupied by two particles is thus $2\epsilon + U$.

The Hamiltonian describing the non-interacting electrons in the leads is

$$H_\mathrm{Leads} = \sum_\alpha H_\alpha = \sum_{\alpha,k} \sum_{\sigma=\uparrow,\downarrow} \epsilon_{\alpha k\sigma} c_{\alpha k\sigma}^\dagger c_{\alpha k\sigma}. \tag{2.3}$$

The leads connected to the dot are labeled with an index α. Most often we will consider the quantum dot coupled to two leads, in which case the leads are labeled by left (L) and right (R). The creation (annihilation) operator for electrons with spin σ and momentum k in lead α is $c_{\alpha k\sigma}^\dagger$ ($c_{\alpha k\sigma}$). The leads are assumed to be in equilibrium and can be described by the Grand-Canonical ensemble. They are furthermore seen as infinite reservoirs of both spin-up and spin-down particles following a Fermi distribution function. These Fermi-Dirac distributions are characterised by different electrochemical potentials μ_α and a temperature[1] T. All energies in the system are measured with respect to the average electrochemical potential of the leads: $\bar{\mu} = \sum_\alpha \frac{\mu_\alpha}{Z} = 0$, where Z is the total number of leads. It is also useful to introduce $\mathrm{e}V = \mu_\mathrm{L} - \mu_\mathrm{R}$ in the case of two leads, or more general $\mathrm{e}V_{\alpha\alpha'} = \mu_\alpha - \mu_{\alpha'}$, where e is the absolute value of the unit electronic charge and V is the potential difference between leads $\alpha = \mathrm{L}$ and $\alpha' = \mathrm{R}$. From now on, we will also use the convention $k_\mathrm{B} = \hbar = \mathrm{e} = 1$ for notational simplicity (occasionally we still use these symbols for clarity).

[1] Most often we assume all leads to have the same temperature, but in general this can also be a different temperature T_α for every lead α.

The Hamiltonian

$$H_{\text{Tun}} = \sum_{\alpha,k} \sum_{\sigma=\uparrow,\downarrow} \left(V_\alpha c_{\alpha k\sigma} d_\sigma^\dagger + \text{H.c.} \right), \tag{2.4}$$

where H.c. denotes the Hermitian conjugate, describes the tunnel-coupling between the leads α and the dot. V_α is the spin- and momentum-independent tunnelling matrix element which couples lead α to the dot. The tunnel-coupling strength can be characterised by $\Gamma_\alpha = 2\pi\rho_\alpha |V_\alpha|^2$, which is spin-independent since no magnetic field is assumed to be present. ρ_α is the density of states of the lead. Both V_α and ρ_α are assumed to be energy-independent. This important assumption guarantees that the tunnel-coupling strengths Γ_α are also energy-independent. This is called the wide band limit. The total coupling strength of the dot is defined as $\Gamma = \sum_\alpha \Gamma_\alpha$.

In describing the quantum dot model, we should also clearly define some of the assumptions that we make. For now, these assumptions are related to two important parts of the system: the energy structure of the dot and the tunnel-coupling strength to the electronic leads.

As explained in Sec. 1.2, the energy structure of a quantum dot consists in general of many discrete energy levels E_i. In this specific model, we assume that the energy spacing $\Delta E = E_{i+1} - E_i$ is very large compared to the thermal energy of the system $k_\text{B}T$ as well as in comparison with the on-site interaction U and the applied potential difference between the different leads. This allows to consider only the energy level $E_i = \epsilon$ that is closest to $\bar{\mu} = 0$. Indeed, all the lower energy levels will always be occupied, while the higher energy levels will continue to be empty. Next, we also assume the Coulomb interaction energy U, often called the charging energy, to be larger (but still of the same magnitude) than the thermal energy: $k_\text{B}T \lesssim U$. This charging energy is due to the close confinement of multiple electrons and is inversely proportional to the total electrostatic capacitance of the quantum dot. The exact magnitude of U depends on both the geometry (size, shape ...) and the environment (e.g. metals or dielectrics in close proximity reduce U due to screening effects) of the dot. We will treat U in this thesis as being one of the parameters that has a time-dependence. This dependence can for example be introduced when varying the energy level ϵ of the dot by changing the gate voltage (which indeed typically changes the environment and geometry of the potential by which the dot is formed). Notice that if we combine the two previous assumptions, we get the inequalities $\Delta E \gg U \gtrsim k_\text{B}T$. Since both the energy spacing and interaction energy increase with decreasing dot size, it is not a priori clear that this condition can be met. It turns out however that there is typically a cross-over point where the relative importance of ΔE and U changes. Energy spacing is found to be dominant for the smaller dot sizes in semiconductor quantum dots (typically $\approx 10\,\text{nm}$ for a GaAs/AlGaAs quantum dot) [5, 34, 35]. In metallic systems on the other hand are the scales typically inverted, i.e. the level spacing ΔE stays much smaller (no quantum confinement effects, except when dealing with few-atom systems) than the charging energy U [36, 37].

The tunnel-coupling strength with the electronic leads is assumed to be weak: $\Gamma_\alpha \ll k_\text{B}T$ for all leads α. Moreover, we assume in general that the tunnel-coupling is the smallest energy scale present in the system. This has some important consequences. First of all, it allows to assume that the electronic leads will be in equilibrium for all events that happen. This is true because after each tunnelling event (in which the equilibrium

Fermi distribution is shortly distorted) there is enough time to equilibrate before a new event happens[1]. Another consequence is that we can assume that no two events will ever happen at the same time (e.g. two electrons can not tunnel simultaneously into the dot). In other words, we assume to be in the sequential tunnelling regime and we will only take the lowest order in the tunnel-coupling Γ into account. Hereby, we neglect effects such as cotunnelling and the Kondo effect [5]. The weak coupling assumption allows to use the Born-Markov master equation for the description of the system and has a large experimental relevance [38, 39].

2.2 Notation and Born-Markov master equation

Before introducing and discussing the Born-Markov master equation, it is useful to define some notation that recurs regularly in this thesis. This notation concerns either the description of the quantum dot itself (1.) or the electronic reservoirs (2.).

1. In general, the state of the quantum dot can be described by a density operator $\rho(t)$. The exact form of this density operator, depends on the basis of the Hilbert space in which the quantum dot is described. Here, a representation in the orthonormal basis of physical states $i = \{0, \uparrow, \downarrow, 2\}$ is chosen. These states are all pure states. Since we are studying an open quantum system (i.e. the quantum dot is coupled to an environment represented by the leads), we will be using a description in Liouville space [40]. From now on, an operator x will be denoted as $|x) := |x\rangle\langle x|$. The covector of the operator x acting on the argument $\bullet$ will be written as $(x|\bullet = (|x))^\dagger \bullet := \mathrm{Tr}\left(x^\dagger \bullet\right)$. This is the same notation as used in [29]. The completeness relation for basis states i in this notation reads $\sum_i |i)(i|/(i|i) = 1$, where the denominator can account for non-unit scalar products. For the chosen normalised basis (so with $\langle i|i\rangle = 1$) however, this is

$$(i|i) = \mathrm{Tr}\left[(|i\rangle\langle i|)^\dagger |i\rangle\langle i|\right] = \mathrm{Tr}\left[|i\rangle\langle i|i\rangle\langle i|\right] = \mathrm{Tr}\left[|i\rangle\langle i|\right] = (\langle i|i\rangle)^2 = 1.$$

For properly normalised basis states, the completeness relation hence simplifies to

$$\sum_i |i)(i| = 1. \tag{2.5}$$

Another property of the chosen basis states is that they have unit trace. For example, for the basis state operator $|\uparrow)$, one can calculate the trace as:

$$(\mathbb{1}|\uparrow) = (0|\uparrow) + (\uparrow|\uparrow) + (\downarrow|\uparrow) + (2|\uparrow) = (\uparrow|\uparrow) = 1.$$

Analogous calculations prove that this property also holds for the other basis states.

Using the completeness relation (2.5), the density operator may be written as

$$|\rho(t)) = \sum_i |i)(i|\rho(t)) = \sum_i P_i|i), \text{ with } P_i = (i|\rho(t)). \tag{2.6}$$

The factors P_i can be interpreted as the probabilities to find the dot in the physical state i. These results also hold for more general (possibly time-dependent) orthonormal basis sets i.

[1] The typical tunnelling time $\sim \frac{1}{\Gamma}$ is much larger than the memory time of the leads $\sim \frac{1}{T}$.

2. Since the environment is described by a grand-canonical ensemble, explicit results often depend on Fermi functions. Hence, these functions also deserve some dedicated, compact notation. A typical Fermi function is written as

$$f^+(E) = \frac{1}{\exp(\beta E) + 1}, \text{ where } \beta = \frac{1}{k_B T}.$$

This gives the probability of finding a particle with energy E in a reservoir of fermions at a temperature T and with chemical potential $\mu_\alpha = 0$. k_B is the Boltzmann constant. On the other hand, one can also introduce

$$f^-(E) = 1 - f^+(E) = f^+(-E) = \frac{1}{\exp(-\beta E) + 1},$$

which gives the probability of finding an empty state at the energy E. With these Fermi-functions, the following notation is established:

$$f_\epsilon^+ = \sum_\alpha \Gamma_\alpha f^+(\epsilon - \mu_\alpha) \qquad f_\epsilon^- = \sum_\alpha \Gamma_\alpha f^-(\epsilon - \mu_\alpha)$$
$$f_U^+ = \sum_\alpha \Gamma_\alpha f^+(\epsilon + U - \mu_\alpha) \qquad f_U^- = \sum_\alpha \Gamma_\alpha f^-(\epsilon + U - \mu_\alpha),$$

where the chemical potentials μ_α and tunnel-coupling strengths Γ_α can all be different for different leads α.

With these conventions and notations in place, we are now ready to describe the dynamics of the quantum dot. We make use of a master equation approach, in which the state of the quantum dot is described in terms of occupation probabilities of basis states. As explained at the end of Sec. 2.1, we describe the system for weak tunnel-coupling, i.e. in the sequential tunnelling regime. In this weak-coupling regime, the dynamics of the system can be described by the Born-Markov master equation

$$\partial_t |\rho(t)) = W |\rho(t)). \tag{2.7}$$

The resulting solution $|\rho(t))$ to this equation is exact up to first order in the tunnel-coupling Γ. For a detailed explanation on how to get to this Born-Markov master equation, we refer to [30, 41, 42]. In Eq. (2.7), W is a kernel which in general describes the transitions between all the elements of the density operator. In this work however, only transitions between the populations are considered, such that W has only $4 \times 4 = 16$ entries. This is allowed, since the dynamics of the diagonal and off-diagonal elements decouple in first order in Γ. Using the completeness relation (2.5) on both the left- and right-hand side of W, the kernel can be expressed in terms of state transition rates:

$$W = \sum_{i,j} |i)(i|W|j)(j| = \sum_{i,j} W_{ij} |i)(j|, \text{ with } W_{ij} = (i|W|j). \tag{2.8}$$

In this equation, W_{ij} is the rate at which a transition from state j to state i happens.

By substituting the relations for W, Eq. (2.8), and $|\rho(t))$, Eq. (2.6), into the Born-Markov master equation (2.7), one finds

$$\begin{aligned}\partial_t|\rho(t)) &= W|\rho(t)) \\ &= \sum_{j,k} W_{jk}|j)(k|\left(\sum_i P_i|i)\right) = \sum_{i,j,k} W_{jk}P_i|j)(k|i) = \sum_{i,j} W_{ij}P_j|i) \\ &= \partial_t\left(\sum_i P_i|i)\right) = \sum_i \partial_t P_i|i).\end{aligned} \tag{2.9}$$

In the last equality we assumed the basis states $|i)$ to be time-independent, which is true for the physical basis states. For the equality to hold, the factor in front of each $|i)$ should be the same. So the eigenvalue relation

$$\partial_t P_i = \sum_j W_{ij}P_j \tag{2.10}$$

must be fulfilled for every i. The Born-Markov master equation thus reduces to the usual Markov equation for probabilities when the chosen basis state are time-independent.

Now, let us find an explicit form for the kernel W. Because of probability conservation, we know that $\sum_j P_j = 1$ for all times t. This adds the extra condition $\sum_i W_{ij} = 0$ to the elements of the kernel. This additional condition can be combined with Fermi's golden rule to find an explicit form of the matrix W_{ij}. This explicit form also depends on the chosen basis. In the basis of physical states $i = \{0, \uparrow, \downarrow, 2\}$, W_{ij} is given by

$$W = \begin{bmatrix} -2f_\epsilon^+ & f_\epsilon^- & f_\epsilon^- & 0 \\ f_\epsilon^+ & -f_\epsilon^- - f_U^+ & 0 & f_U^- \\ f_\epsilon^+ & 0 & -f_\epsilon^- - f_U^+ & f_U^- \\ 0 & f_U^+ & f_U^+ & -2f_U^- \end{bmatrix}. \tag{2.11}$$

As an example, the rate at which transitions from state $|0)$ to state $|\uparrow)$ happen, is given by $W_{\uparrow 0} = f_\epsilon^+$. This rate is related to both the tunnel-coupling strengths Γ_α (a strong coupling to lead α allows for a higher rate) and to the number of electron states occupied in lead α at energy ϵ (the more spin-up electrons at this energy in lead α, the more likely it is that an electron can get into the dot). Notice that since we consider the spin degenerate case, we in principle do not need to make the distinction between spin-up or -down electrons. We could just introduce a state for single occupation of the dot. Indeed, this can also be seen in the symmetry of W: interchanging the indices $\uparrow$ and $\downarrow$ does not change anything. We however chose to keep the four-dimensional notation in order to have more similarity with the non-spin degenerate system that we will consider in chapter 4.

2.3 Duality and eigenmodes

Notice that the kernel W is in general not Hermitian, as it would usually be the case in quantum mechanics of isolated systems. This is a consequence of the fact that we only describe a part of the model (the quantum dot) by the *reduced* density operator $\rho(t)$ instead of the full system (quantum dot tunnel-coupled to leads). In other words: we consider the quantum dot to be an open quantum system, which is coupled to an environment (represented by electronic leads). Hermiticity is the property that allows us in quantum mechanics to relate the left and right eigenvectors of an eigenmode by a Hermitian conjugation. This in turn provides a way to interpret the time-evolution of closed quantum systems: the amplitude at which a certain energy eigenmode contributes in the time-evolution of some quantum state is given by the overlap of the energy eigenstate with that quantum state. For open quantum systems however, the left and right eigenvectors are in general very different, such that this simple interpretation is no longer possible.

This is the point at which the duality relation that we hinted at in Sec. 1.4 becomes very useful. Indeed, it was shown in [29] that for a large class of fermionic open quantum systems another duality relation holds. This duality (cross-)links different left and right eigenvectors of W. It is thus in a certain sense a superhermiticity relation. Here, we will only show and explain the explicit form of the duality that is useful for our system. We will call the right eigenvectors of the kernel W (decay) modes $|x)$, while the left eigenvectors are called amplitude covectors $(x'|$. The decay rates γ_x are the negated eigenvalues of W: $\gamma_x = -\lambda_x$. Indeed, in contrast to closed quantum systems, open systems exhibit a certain decay dynamics. This becomes apparent in the decay rates γ_x that characterise the dynamics of the system. For a mode $|x) = x$ which is known and has a decay rate γ_x, application of the duality relation shows that $(y'|\bullet$ is an amplitude covector (possibly of another eigenmode) with

$$y' = (-\mathbb{1})^N \mathcal{I} x \text{ and rate } \gamma_y = 2\Gamma - \mathcal{I}\gamma_x. \tag{2.12}$$

The parity operator $|(-\mathbb{1})^N) = \mathcal{P} = |0) - |\uparrow) - |\downarrow) + |2)$ adds a factor -1 for uneven parity (occupations of the $\uparrow$ or $\downarrow$ states). $\mathcal{I}$ denotes a parameter substitution that constructs a dual model:

$$\mu_\alpha \to -\mu_\alpha,\ \epsilon \to -\epsilon \text{ and } U \to -U.$$

So $\mathcal{I}$ has the effect of inverting all the energies of the system, including the interaction energy U within the dot. This means that the interaction within the dot becomes attractive upon applying $\mathcal{I}$. The effect of $\mathcal{I}$ is shown in figure 2.2. We will often call this the *inverted dot model* or dual dot model.

Since the kernel W is four-dimensional, it will have a four-dimensional eigenspace and the density operator $|\rho)$ can be expanded in terms of the four eigenmodes of W. This eigenbasis will often turn out to be more useful than the eigenbasis of physical states that we always used up to now. Before we can exploit the eigenmodes of W, we first need to determine them of course. We here follow [29] and employ the superhemiticity relation (2.12), which is immediately a good opportunity to show how it can be used. Importantly, this duality relation allows both for a more elegant derivation of the eigenmodes as well as a better interpretation of them.

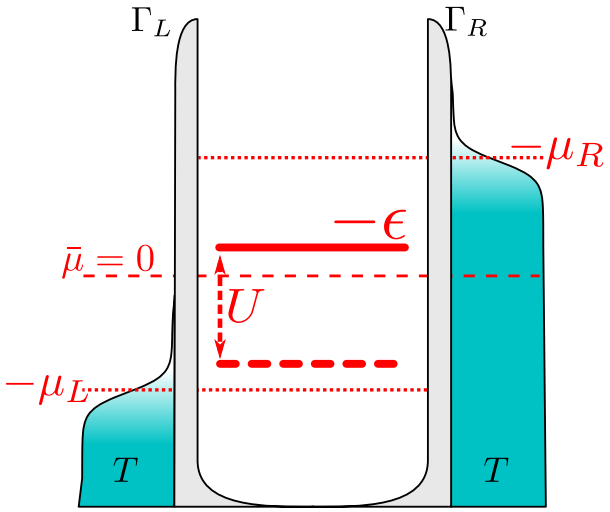

Figure 2.2: *The same system as in Fig. 2.1, but after the parameter substitution $\mathcal{I}$, which construct the dual model by inverting all the energies.*

2.3.1 Stationary state

By construction, one of the eigenvalues of W is zero, as there should be probability conservation at all times t:

$$\mathrm{Tr}\,\rho(t) = (\mathbb{1}|\rho(t)) = 1, \text{ which implies } \mathrm{Tr}\,\partial_t\rho(t) = (\mathbb{1}|W|\rho(t)) = 0,$$

and hence that the kernel is traceless: $(\mathbb{1}|W = 0$. So, the amplitude covector associated with the zero eigenvalue is $(z'| = (\mathbb{1}|$. By means of linear algebra, we can then infer that there is also a trace-normalised mode, $(\mathbb{1}|z) = 1$, with vanishing decay rate, $W|z) = 0$. It was argued, e.g., in [30] that for the system with a kernel as given in (2.11) and temperatures $T > 0$, this mode is the unique stationary state $|z) = \lim_{t\to\infty}|\rho(t))$ that is assumed by $\rho(t)$ in the long-time limit. By explicitly solving the eigenvalue equation (2.10), one can obtain an explicit form for $|z)$:

$$\begin{aligned} \gamma_z &= 0 \\ (z'| &= (\mathbb{1}| \\ |z) &= \frac{1}{\Gamma\left(f_\epsilon^+ + f_U^-\right)}\left[f_\epsilon^- f_U^-|0) + f_\epsilon^+ f_U^-\left(|\uparrow) + |\downarrow)\right) + f_\epsilon^+ f_U^+|2)\right] \end{aligned} \tag{2.13}$$

This stationary state, can also be rewritten without explicitly using Fermi functions:

$$\begin{aligned} |z) &= \left(\frac{3}{4} - \frac{1}{2}N_z + \frac{1}{4}p_z\right)|0) + \left(\frac{1}{4} - \frac{1}{4}p_z\right)[|\uparrow) + |\downarrow)] + \left(-\frac{1}{4} + \frac{1}{2}N_z + \frac{1}{4}p_z\right)|2) \\ &= \left(\frac{1}{4} - \frac{1}{2}\Delta N_z + \frac{1}{4}p_z\right)|0) + \left(\frac{1}{4} - \frac{1}{4}p_z\right)[|\uparrow) + |\downarrow)] + \left(\frac{1}{4} + \frac{1}{2}\Delta N_z + \frac{1}{4}p_z\right)|2) \end{aligned} \tag{2.14}$$

In the two last lines, some new notation was introduced. First we denote N the occupation operator, which is defined as $|N) = |\uparrow) + |\downarrow) + 2|2)$. With this occupation operator and the parity operator $\mathcal{P}$, one can write

$$N_z = (N|z) = \frac{2f_\epsilon^+}{f_\epsilon^+ + f_U^-} \quad , \quad p_z = ((-\mathbb{1})^N|z) = \frac{f_\epsilon^- f_U^- + f_\epsilon^+ f_U^+ - 2f_\epsilon^+ f_U^-}{\Gamma\left(f_\epsilon^+ + f_U^-\right)}. \tag{2.15}$$

These are respectively the stationary occupation number of the dot and the parity of the stationary state. A quantity X_z will in general denote the expectation value of the operator X for the dot in its stationary state: $X_z = (X|z)$. In this way, we also define $\Delta N_z = (N - \mathbb{1}|z) = -(0|z) + (2|z) = N_z - 1$ as the variable that represents the deviation from having a single particle on the dot.

Especially the second line of Eq. (2.14) has an interesting structure. Inherently, all states (i.e. empty, spin-up or -down and double occupation) have the same weight of one in four. The stationary parity expectation value p_z then introduces an asymmetry between even and odd parity states by adding to their weights with opposite signs. On top of this, ΔN_z changes the weight for the empty state and double occupation, depending on the charge of the dot. If the charge expectation is higher then one, the double occupation naturally gets a higher weight, in the other case this weight decreases.

The occupation number N_z is plotted as function of the dot energy level ϵ in Fig. 2.3(d). For clarity of the figure, the quantum dot that was described in Sec. 2.1 is only coupled to one lead, which then by definition has chemical potential $\mu = 0$. The top row of figures (a), (b) and (c) shows a schematic representation of the stationary state z in three typical regimes. When $\epsilon < -U$, both energy levels of the dot are lower then the Fermi level of the coupled lead (Fig. 2.3(a)). As a result, the dot is mostly doubly occupied. When ϵ approaches $-U$, more and more free electron states in the leads become accessible. The occupation number N_z thus starts to decrease. As ϵ increases above $\epsilon = -U$, the dot level at $\epsilon + U$ of the doubly occupied dot becomes higher then $\mu = 0$, such that the second electron in the dot is more likely to tunnel into the lead, whereas the probability for a second electron to tunnel from the lead into the dot decreases. The average stationary occupation thus decreases from 2 to 1 (Fig. 2.3(b)). At $\epsilon \geq 0$, also the first electron in the dot is more likely to tunnel out of the dot, such that the average stationary particle number decreases further from 1 to 0 (Fig. 2.3(c)). It is however important to emphasise that this is the *average* and *stationary* particle number. If the dot did not get enough time to relax to its stationary state, the average occupation can be entirely different. But even in its stationary state the number of electrons in the dot can be different at every instant of time. This is because we are working at a finite temperature. It is only the average over multiple measurements that will result in Fig. 2.3.

2.3.2 Fermion-parity mode

The next eigenmode of W can now be obtained without any effort by using the duality relation (2.12). Applying this relation to the stationary mode equations for γ_z, $|z)$ and $(z'|$ gives us the fermion-parity eigenmode:

$$\begin{aligned}
\gamma_p &= 2\Gamma \\
(p'| &= [\mathcal{P}\mathcal{I}|z)]^\dagger = ((-\mathbb{1})^N z_i| \\
&= \frac{1}{\Gamma\left(f_\epsilon^- + f_U^+\right)} \left[f_\epsilon^+ f_U^+ (0| - f_\epsilon^- f_U^+ \left[(\uparrow| + (\downarrow|\right] + f_\epsilon^- f_U^- (2| \right] \\
|p) &= [(z'|\mathcal{I}\mathcal{P}]^\dagger = |(-\mathbb{1})^N) \\
&= |0) - [|\uparrow) + |\downarrow)] + |2)
\end{aligned} \tag{2.16}$$

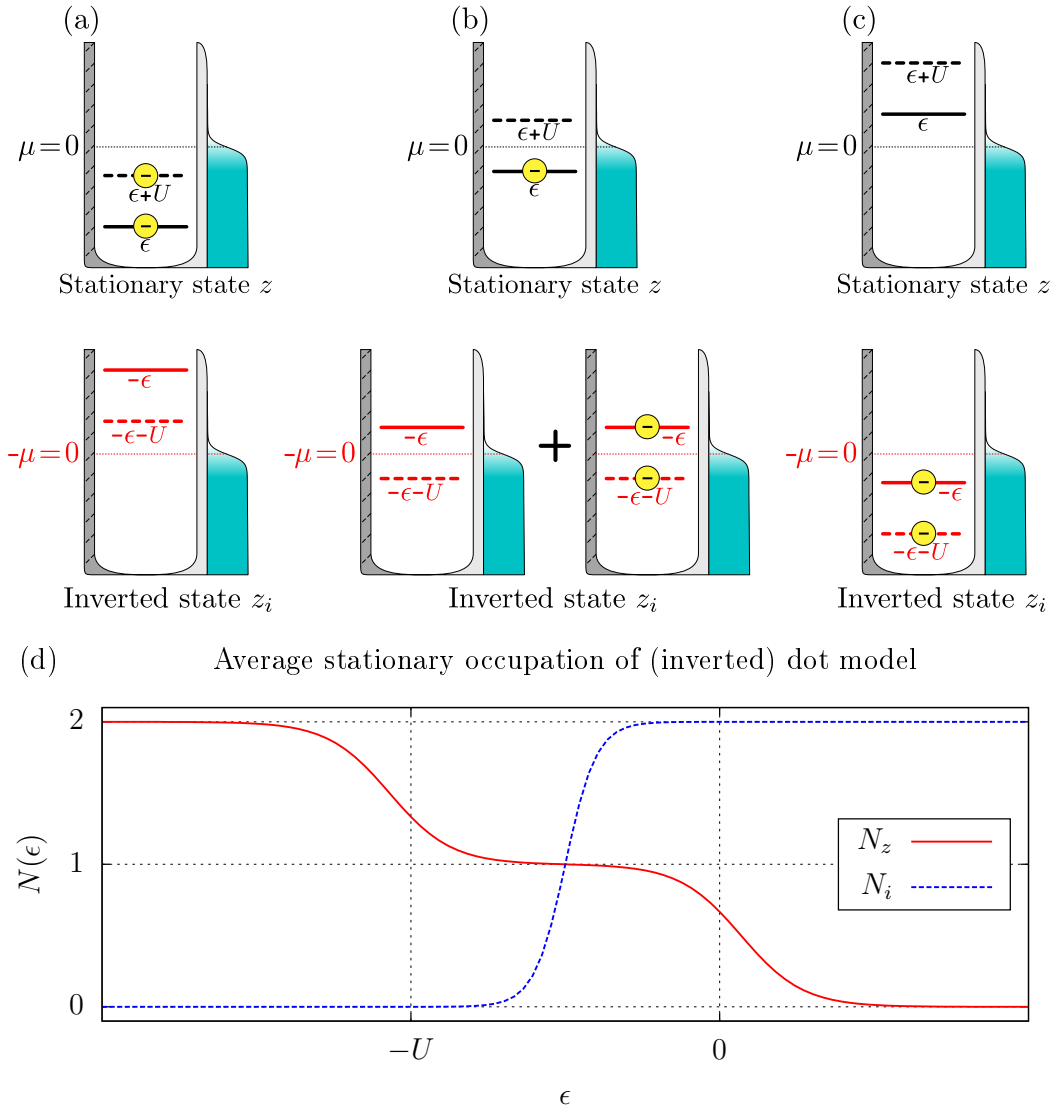

Figure 2.3: *The average stationary occupation of the dot model $N_z = (N|z)$ and of the inverted dot model $N_i = (N|z_i)$ as a function of the energy level ϵ in the case of a dot with interaction energy U connected to a single lead. Above the plot, the situations of the quantum dot corresponding to several values of ϵ are drawn schematically for both the stationary state z and the inverted state z_i. The average particle number N_z decreases from 2 to 1 at $\epsilon = -U$ and from 1 to 0 at $\epsilon = 0$. These declines correspond to the crossing of the upper, respectively the lower dot level with the chemical potential μ of the lead. The average particle number of the inverted dot model N_i shows a steep increase for 0 to 2 at $\epsilon = -\frac{U}{2}$. From the moment the dot is occupied by one particle, it immediately gets occupied by a second electron due to the attractive interaction. In the plot the internal interaction is strong, $U = 10T$. For an even stronger U or a smaller T, the slopes would become steeper.*

This fermion-parity mode is the third mode that we discussed in Sec. 1.4. These equations contain $z_i = \mathcal{I}z = z\,(-\epsilon,\, -U,\, -\mu)$, the stationary state of the dual quantum dot model with attractive interaction, obtained by the parameter substitution $\mathcal{I}$, i.e. by inverting all the energies. Therefore, $|z_i)$ is called the inverted stationary state. In the notation with Fermi functions, the energy inversion is done by swapping $f^+ \leftrightarrow f^-$ in the stationary state $|z)$:

$$|z_i) = \mathcal{I}|z) = \frac{1}{\Gamma\left(f_\epsilon^- + f_U^+\right)}\left[f_\epsilon^+ f_U^+|0) + f_\epsilon^- f_U^+\left[|\uparrow) + |\downarrow)\right] + f_\epsilon^- f_U^-|2)\right]. \tag{2.17}$$

From this, one can see that $|z_i)$ is a physical state with non-negative occupation probabilities. The inverted stationary state can, just as was done with $|z)$, also be written without Fermi-functions:

$$\begin{aligned} |z_i) &= \left(\frac{3}{4} - \frac{1}{2}N_i + \frac{1}{4}p_i\right)|0) + \left(\frac{1}{4} - \frac{1}{4}p_i\right)\left[|\uparrow) + |\downarrow)\right] + \left(-\frac{1}{4} + \frac{1}{2}N_i + \frac{1}{4}p_i\right)|2) \\ &= \left(\frac{1}{4} - \frac{1}{2}\Delta N_i + \frac{1}{4}p_i\right)|0) + \left(\frac{1}{4} - \frac{1}{4}p_i\right)\left[|\uparrow) + |\downarrow)\right] + \left(\frac{1}{4} + \frac{1}{2}\Delta N_i + \frac{1}{4}p_i\right)|2). \end{aligned} \tag{2.18}$$

In these equations, $N_i = (N|z_i)$ and $p_i = \mathcal{P}|z_i)$ were used. These are the occupation number and parity of the inverted stationary state. A quantity X_i will again also in general denote the expectation value of the operator X for the dot in its inverted stationary state: $X_i = (X|z_i)$. We also define again $\Delta N_i = (N - \mathbb{1}|z_i) = -(0|z_i) + (2|z_i)$ as the deviation between the inverted stationary state and having a single particle on the dot.

Just as in Eq. (2.14), all physical states have an equal weight in the inverted stationary state Eq. (2.18) when both $\Delta N_i = p_i = 0$. When these two expectation values are non-zero, the symmetry is broken in a similar way as was the case for the normal stationary state. The variables $\Delta N_i = N_i - 1$ and p_i have however a completely different dependence on the dot parameters (such as ϵ or U).

N_i as a function of ϵ is shown in Fig. 2.3(d) for the same system as N_z in the previous section. For $\epsilon < -\frac{U}{2}$, the occupation of the inverted state z_i is 0 (Fig. 2.3(a)). Notice that nothing special happens when $\epsilon = -U$. Indeed, the lowest dot level (with energy $\epsilon - U$) shown in Fig. 2.3(a) can only be occupied after the highest dot level (with energy ϵ) is occupied, since its energy is lowered due to an attractive interaction within the dot. The average inverted stationary particle number has a steep incline from 0 to 2 when ϵ passes $-\frac{U}{2}$ (Fig. 2.3(b)). This is the particle-hole symmetric point. When at this point one particle occupies the dot with attractive interactions, it either immediately attracts a second electron into the dot, or it leaves the dot again since its energy is larger than $\mu = 0$. The fact that $N_i(-\frac{U}{2}) = 1$, is due to the fact that this is again the *average* inverted stationary particle number. At this point, the probabilities of finding the inverted dot doubly occupied or empty are equal, as depicted in Fig. 2.3(b). The dot will (almost) never be found singly occupied when in its inverted stationary state with $U \gg T$. This statement is no longer true when the dot is connected to two leads and a bias $V > U$ is applied. That situation will be discussed in Sec. 6.3. Finally, when $\epsilon > -\frac{U}{2}$, the inverted state z_i is favourably doubly occupied as shown in Fig. 2.3(c).

2.3.3 Charge decay

Next, there is the charge mode $|c)$, its covector $(c'|$ and the charge decay rate γ_c. These are given by

$$\begin{aligned}
\gamma_c &= f_\epsilon^+ + f_U^- \\
(c'| &= (N| - N_z(\mathbb{1}| \\
&= \frac{1}{f_\epsilon^+ + f_U^-}\left[-2f_\epsilon^+(0| + \left(-f_\epsilon^+ + f_U^-\right)[(\uparrow| + (\downarrow|] + 2f_U^-(2|\right] \\
|c) &= \frac{1}{2}\mathcal{P}\left[|N) - N_i|\mathbb{1})\right] = \frac{1}{2}(-\mathbb{1})^N\left[|N) - N_i|\mathbb{1})\right] \\
&= \frac{1}{f_\epsilon^- + f_U^+}\left[-f_\epsilon^-|0) + \frac{1}{2}\left(-f_\epsilon^+ + f_U^-\right)[|\uparrow) + |\downarrow)] + f_U^+|2)\right]
\end{aligned} \tag{2.19}$$

Notice that the charge-decay rate is self-dual, $\gamma_c = 2\Gamma - \mathcal{I}\gamma_c$, under the duality (2.12). This means that its amplitude and mode are also connected by the duality, up to a normalisation factor: $|c) = \frac{1}{2}[(c'|\mathcal{I}\mathcal{P}]^\dagger$. The normalisation was chosen such that the overlap of the charge amplitude covector with the density operator $(c'|\rho(t))$ gives the deviation of the instantaneous occupation of the dot $(N|\rho(t))$ from the stationary occupation of the dot N_z. The occupation of the dot is of course proportional to the charge on the dot, hence the name charge mode. In Sec. 2.4 we will see that - when the dot has been brought out of its stationary state - the overlap $(c'|\rho(t))$ determines how much the charge mode $|c)$ contributes to the decay dynamics of the system. It is thus the deviation of the actual charge on the dot from its stationary charge that determines the importance of the charge mode in the dynamics. The decay rate γ_c determines the rate at which its amplitude decreases.

2.3.4 Spin mode

Finally, there is also a spin mode $|s)$ with covector $(s'|$ and decay rate γ_s:

$$\begin{aligned}
\gamma_s &= f_\epsilon^- + f_U^+ \\
(s'| &= (\uparrow| - (\downarrow| \\
|s) &= \frac{1}{2}(|\uparrow) - |\downarrow))
\end{aligned} \tag{2.20}$$

This mode was not yet part of [29, 30]. Notice that also this spin-decay rate is self-dual $\gamma_s = 2\Gamma - \mathcal{I}\gamma_s$, under the duality (2.12). Also its amplitude and mode are then connected, namely by $|s) = -\frac{1}{2}[(s'|\mathcal{I}\mathcal{P}]^\dagger$. The normalisation was again chosen such that the amplitude covector applied to the density operator $(s'|\rho(t))$ has a physical meaning. It is the deviation of the total spin of the dot from its total spin when it is in the stationary state $\sigma_z = (s'|z)$. Since no magnetic field is applied to the dot[1], there is a symmetry between spin up and down particles. In this case, the average total spin of the stationary state is zero. This mode can however still get excited when one wants to describe the time evolution of a system that is initially prepared in a state that is not spin-symmetric. The overlap $(s'|\rho(t))$ thus gives the net spin of the dot without applied magnetic field, hence the name spin mode.

[1] We will relax this constraint in chapter 4.

2.4 Sudden switch and decay rates

We are now in a position to study the evolution of the density operator after a sudden switch at time $t = 0$. In [29], only a gate voltage switch (corresponding to an instantaneous change of the energy level in the dot from ϵ_0 to ϵ) applied to a quantum dot connected to a single lead was considered. Here, the switch can be in any (or multiple) of the system parameters (ϵ, U, μ_α or Γ_α) and the dot can be connected to multiple leads α. We will denote the set of parameters that change during the switch as G. A switch corresponds to an instantaneous change of the parameters from G_0 to G, where G_0 are the parameters just before $t = 0$ and G are the parameters after the switch. Immediately after $t = 0$, the occupation probabilities of the dot (and thus the density operator) are the same as before the switch. This initial density operator will be denoted[1] by $|\rho_0(G_0)) = |z(G_0)) = |z_0)$. Using the Born-Markov master equation (2.7), the problem can easily be solved formally for times $t > 0$. The result is

$$|\rho(t)) = e^{Wt}|\rho_0) = e^{Wt}|z_0).$$

This can be further solved by expanding $\rho(t)$ in the eigenmodes of W:

$$|\rho(t)) = |z)(z'|z_0) + e^{-\gamma_p t}|p)(p'|z_0) + e^{-\gamma_c t}|c)(c'|z_0) + e^{-\gamma_s t}|s)(s'|z_0). \tag{2.21}$$

There is no exponential decay of the first term, since $e^{-\gamma_z t} = 1$. This equation tells us that after a sudden switch, the different components of $|\rho(t))$ (which are the eigenmodes of W) decay with their corresponding decay rate γ_x. In the limit of $t \to \infty$, the density operator will have relaxed to the new stationary state $|z)$. The amplitudes of the different decay modes are given by the overlap of their corresponding amplitude covector with the initial state $(x'|z_0)$. Denoting the observables of the dot state at $t = 0$ with a subscript $z0$ and observing that $(z'|z_0) = 1$, one finally finds

$$|\rho(t)) = |z) + (z_i|\mathcal{P}|z_0)e^{-\gamma_p t}|p) + (N_{z0} - N_z)\, e^{-\gamma_c t}|c) + \sigma_{z0}e^{-\gamma_s t}|s). \tag{2.22}$$

In the case without an applied magnetic field which we are considering here, σ_{z0} is typically zero. However, in principle nothing prevents us from preparing the quantum dot in an initial state with non-vanishing spin.

It is interesting to have a look at the behaviour of the decay rates γ_p, γ_c and γ_s as a function of the dot level position ϵ and for different applied voltages V between the leads. This is shown in Fig. 2.4 for a quantum dot connected to two leads with the same tunnel-coupling strength $\Gamma_\alpha = \frac{\Gamma}{2}$. The decay rates can in general be interpreted as representing the number of possible decay channels. In this interpretation, every lead can be seen as two channels: one for spin-up, and one for spin-down electrons.

[1] This notation seems to imply that the dot is in its stationary state just before the switch. Although this is usually the case, it is not strictly necessary. The time evolution after the switch can always be calculated, as long as the initial state $|\rho_0(G_0))$ is known.

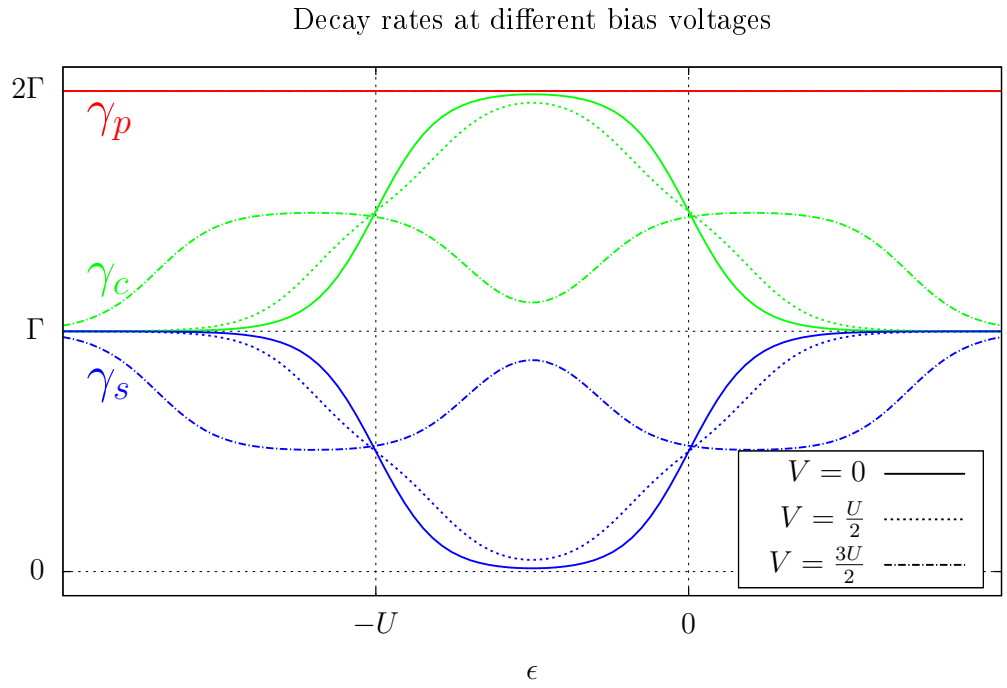

Figure 2.4: *The decay rates of the fermion-parity mode γ_p, the charge mode γ_c and the spin mode γ_s as a function of the dot energy level. The dot is connected to two leads, with an equal tunnel-coupling strength $\Gamma_\alpha = \frac{\Gamma}{2}$, where Γ is the total tunnel-coupling. The internal interaction strength is $U = 10T$. The rates are shown for the unbiased case $V = 0$ (solid line), a relatively small bias $V = \frac{U}{2}$ (dotted) and a large bias $V = \frac{3U}{2}$ (dash-dotted) between the leads.*

Let us start with the unbiased case. This is equivalent to having only one lead with double the tunnel-coupling strength, which was already discussed in [28, 29, 32]. Remarkably, the fermion-parity rate (2.16) is always the highest possible[1], and completely independent of the level position, temperature or strength of the interaction U. However, looking at Eq. (2.22), we see that the amplitude by which the parity mode is excited is $(z_i|\mathcal{P}|z_0)$. Since the inverted stationary state z_i is almost never singly occupied for $U \gg T, \Delta V$, this can be approximated by $(z_i|z_0)$. The parity mode is thus only excited when there is a large overlap between the final inverted stationary state and the initial "normal" stationary state. This typically only happens when the dot occupation has to change from two to zero or vice versa. This tells us, as we also already mentioned in Sec. 1.4, that the fermion-parity mode is related to two-particle processes. More arguments to support this claim can be found in [30]. There, it is also noted that the fermion-parity mode can be related to the first of several tunnelling processes. Since the fermion-parity rate is related to a two-particle effect, it can only show up in multi-particle observables [28, 30]. It can thus be observed for example in heat or energy currents of interacting systems, which naturally contain the $Un_\uparrow n_\downarrow$ term in their Hamiltonian, but not in particle currents.

[1] Namely 2Γ, which means that all decay channels are possible.

The relaxation rates γ_c and γ_s do have a level dependence. In the region $-U < \epsilon < 0$, the charge rate is enhanced, while the spin rate is suppressed. The transition at these boundaries is smeared out because we are working at finite temperatures. Inside this region, there are two decay channels per lead open for charge relaxation and none for spin relaxation. Indeed, the charge can decay using both spin up and down channels. However, spin-flip processes are not possible[1] in first order in Γ, such that no channels for spin relaxation are open in this region. Outside the region $-U < \epsilon < 0$, there is always one decay channel open per lead for both spin and charge. See also [27, 28] for a more detailed discussion.

Figure 2.4 also shows the results for both a relatively small ($V = \frac{U}{2}$, dotted) and large ($b = \frac{3U}{2}$, dash-dotted) applied bias. What happens can be understood using the unbiased case (full line). The dot can be seen as being coupled to each lead, with its own electrochemical potential μ_α and coupling strength $\Gamma_\alpha = \frac{\Gamma}{2}$ separately. This results for each lead in decay rates which are only half as high (reduced coupling strength) and an energy dependence shifted by their electrochemical potential. Summing these rates for the two leads gives indeed the results as presented in Fig. 2.4. This procedure immediately allows us to know what the decay rates will be for an arbitrary number of leads.

[1] Imagine the dot in a state with $\epsilon < \mu$ and $\epsilon + U > \mu$, such as in Fig. 2.3(b). If an electron occupies the level ϵ, it can not leave the dot since there are no free state in the leads. On the other hand, none of the electrons in the lead have enough energy to enter the level $\epsilon + U$. As a consequence, the spin of the dot can not change.

3 Dynamics for arbitrary driving schemes

At the end of the previous chapter, we found the evolution of the density operator after a fast switch of any of the system parameters. However, we want to be able to describe the dynamics of the quantum dot for an arbitrary driving scheme. To achieve this, we describe two different techniques in this chapter. First we show how one can efficiently obtain a numerical solution to the Born-Markov equation. This is useful for a quick analysis and validation of results. Next, an analytical solution of the density operator $\rho(t)$ is presented, which is more insightful than a numerical solution. For the achievement of this *key result*, the eigenmodes that we found in Sec. 2.3 play a crucial role.

In the second part of this chapter, we present formulas to calculate the time-resolved particle, energy and heat currents through any lead coupled to the quantum dot. These equations can directly be applied to the fast switch case, but we supplement them with the analytical solution of the density operator for arbitrary driving schemes. Examples for the instantaneous contribution and first adiabatic correction are worked out explicitly. These first corrections are of interest because they show the first "real" time-dependence and allow for adiabatic pumping [41, 42]. More specific examples for the use of these equations and further analysis of these expressions will be given in chapters 5 and 6.

3.1 Density operator

In order to find the density operator $|\rho(t))$ for an arbitrary time-dependent driving, we need to solve the Born-Markov master equation (2.7), which we repeat here for convenience:

$$\partial_t |\rho(t)) = W(t)|\rho(t)).$$

For clarity, the time-dependence is stated explicitly. Notice that the kernel $W(t)$ as well as its eigenmodes are now dependent on time. Here, we intend to treat the problem without a magnetic field, and thus we assume all variables to be spin-independent. An extension to include possible spin-dependence is given in chapter 4. Solving the Born-Markov equation exactly can be done in two ways. Either it is put in a form that allows for a rapid numerical solution, which we will briefly discuss in the first part of this section. To gain more insight in the system's dynamics however, we obtain analytical expressions for the density operator in the second part of this section. This analytical solution is based on the good knowledge of the eigenmodes of W and valid when the time-dependence is sufficiently slow (which will be quantified later). It is the main result of this thesis, and will result in applicable formulas to calculate currents through arbitrarily driven quantum dot systems.

3.1.1 Numerical solution

We start by expanding the density operator in the time-dependent eigenbasis of the kernel $W(t)$ as

$$|\rho(t)) = |z(t)) + a_p(t)|p) + a_c(t)|c(t)),$$

where $a_p(t)$ and $a_c(t)$ are the (yet unknown) expansion coefficients for the parity and charge mode that we are looking for. Because of probability conservation, the expansion coefficient of the stationary state has to be one. Moreover, because of the assumed spin-independence, the spin-mode $|s)$ is not present[1]. Substituting this expansion in the Born-Markov master equation, we find

$$\partial_t|z(t)) + \partial_t a_p(t)|p) + \partial_t a_c(t)|c(t)) + a_c(t)\partial_t|c(t)) = -\gamma_p(t)a_p(t)|p) - \gamma_c(t)a_c(t)|c(t)).$$

On the right-hand side, we used the fact that $|c(t))$ and $|p)$ are eigenvectors of the kernel W. We now use Eq. (3.5), that we will derive in the next subsection, to replace $\partial_t|z(t))$. Furthermore we can calculate $\partial_t|c(t)) = -\frac{1}{2}\mathcal{P}\partial_t N_i|\mathbb{1}) = -\frac{1}{2}\partial_t N_i|p)$. The above expression then becomes

$$\left[\frac{1}{2}\left(N_i(t)-1\right)\partial_t N_z(t) + \frac{1}{4}\partial_t p_z(t) + \partial_t a_p(t) - \frac{1}{2}a_c(t)\partial_t N_i(t) + \gamma_p(t)a_p(t)\right]|p) \\ + \left[\partial_t N_z(t) + \partial_t a_c(t) + \gamma_c(t)a_c(t)\right]|c(t)) = 0.$$

Since the basis vectors $|p)$ and $|c(t))$ are orthogonal, both expressions in the square brackets need to be zero. We thus find the set of equations (here written in matrix notation)

$$\partial_t \begin{bmatrix} a_p(t) \\ a_c(t) \end{bmatrix} = \begin{bmatrix} -\gamma_p(t) & \frac{1}{2}\partial_t N_i(t) \\ 0 & -\gamma_c(t) \end{bmatrix} \begin{bmatrix} a_p(t) \\ a_c(t) \end{bmatrix} + \begin{bmatrix} -\frac{1}{2}\left(N_i(t)-1\right)\partial_t N_z(t) - \frac{1}{4}\partial_t p_z(t) \\ -\partial_t N_z(t) \end{bmatrix}.$$

This is a set of coupled ordinary differential equations that can be solved numerically. Notice that this can even be done sequentially because the matrix that couples both equations is an upper triangular matrix. To solve the set of equations, one also needs to decide on the initial conditions. However, in systems with periodic driving, one is often interested in the solution for $t \to \infty$. In this limit, also called the periodic limit or attractor, the solution is independent on the initial conditions. Typically, one reaches this regime already after a few periods. Testing whether one has reached the periodic limit can be done by comparing the calculated values for an observable of interest in successive periods. The periodic limit is reached if the relative changes of the observable between subsequent periods are small compared to the desired numerical accuracy.

Having found this set of equations to which the solution can easily be determined numerically, we have in principle solved the problem under consideration. However, this solution does not provide much insight in the mechanisms at play. Moreover, we would like to learn more about the role of the fermion parity mode $|p)$. This exact solution

[1] As in Sec. 2.4, the system could in principle be prepared in a state with definite initial spin. This would add the relation $\partial_t a_s(t) = -\gamma_s(t)a_s(t)$ to the final matrix equation. Notice that this additional equation is decoupled from the other equations, such that it does not influence the results for $a_p(t)$ and $a_c(t)$.

is however useful for two other reasons. First of all, in the view of the remainder of this thesis, it is useful to have a reference to cross-check the results with. Secondly, by comparing this exact solution with the instantaneous solution $|z(t))$ (which is just the stationary eigenmode of the time-dependent kernel $W(t)$) we can get an idea how far the time-dependence drives the system out of its steady-state. This gives a first idea of how the rate of change of the driving compares to the typical decay rates of the system.

3.1.2 Analytical solution

In order to get more insight into the solution for the density operator and later the different currents through the quantum dot coupled to multiple leads, we will now solve the Born-Markov master equation in a systematic way. From here on, the time-dependence of the different parameters will be implicitly assumed for notational simplicity. We now expand $|\rho)$ in orders of $\frac{\Omega}{\Gamma}$, where Ω is the 'driving frequency' of the time-dependent parameter (or the parameters). This follows the approach of [41, 42]. Although we will always call Ω the driving frequency, *periodicity* is certainly *not a requirement* for the solution. One should thus rather interpret Ω as a rate of change of the time-dependent parameter. The expansion of $|\rho)$ is allowed whenever this rate of change is small compared to the characteristic decay rates of the system. As seen in chapter 2, these are proportional to the tunnel-coupling strength Γ. The contribution of order n in $\frac{\Omega}{\Gamma}$ to $|\rho)$ is written as $|\rho^{(n)})$. The kernel is always the instantaneous (time-dependent) kernel $W = W^{(0)}$ that we used before. In doing this expansion, we find a set of equations to solve:

$$\begin{cases} 0 = W|\rho^{(0)}) & \text{with solution } |\rho^{(0)}) = |z) \\ \partial_t|\rho^{(n-1)}) = W|\rho^{(n)}) & \text{for } n \geq 1 \end{cases} \tag{3.1}$$

Once all orders are found, the full density operator can be obtained as a summation over all corrections $|\rho) = \sum_{n\geq 0}|\rho^{(n)})$. For more details on this expansion, we refer to [41, 42]. This is strictly speaking only reasonable as long as $\delta_X\Omega \ll \Gamma T$, where δ_X is the amplitude of driving parameter X [43]. However, if we in any case *assume* the Born-Markov master equation (2.7) to be valid, we can always use the numerical solution discussed in Sec. 3.1.1 to check whether the expansion in orders of $\frac{\Omega}{\Gamma}$ converges to the correct solution of the Born-Markov master equation. This will typically be true whenever the time-dependence drives the system not too far out of its steady-state, as discussed at the end of that section.

The second expression in the set of equations can formally be solved as

$$|\rho^{(n)}) = \widetilde{W}^{-1}\partial_t|\rho^{(n-1)}), \tag{3.2}$$

where $\widetilde{W}^{-1}$ represents the pseudo-inverse of the kernel and can be obtained by writing $|\rho^{(n)})$ and W in terms of their eigenvectors. W has no 'true' inverse, since it has a zero eigenvalue, corresponding to the stationary state. In general, the pseudo-inverse $\widetilde{W}^{-1}$ can be written as

$$\widetilde{W}^{-1} = \sum_{j=1}^{3}\frac{1}{\lambda_j}|v_j)(v_j'|,$$

where λ_j are the *nonzero* eigenvalues of W, and $|v_j)$ and $(v_j'|$ the corresponding left and right eigenvectors. Notice that, because $\gamma_z = 0$, the stationary mode is not present in $\widetilde{W}^{-1}$. The trace of $|\rho^{(0)})$ is $(z'|\rho^{(0)}) = (\mathbb{1}|\rho^{(0)}) = 1$, so $|\rho^{(n)})$ with $n > 0$ should be traceless to guarantee probability conservation. The modes present in the expansion of $\widetilde{W}^{-1}$ are then the parity, charge and spin mode. If we assume however that the spin-degeneracy is preserved at any moment (remember that we are considering the non-magnetic system), we find $(s'|\rho(n)) = 0$ for all n. Thus, the spin mode does not need to be included in the expansion of $\widetilde{W}^{-1}$.

Using the formal expression for $|\rho^{(n)})$ (3.2) and the first expression of the set of equations (3.1), it is possible to determine $|\rho^{(n)})$ for all orders n recursively. The set of equations to be solved becomes

$$\begin{cases} |\rho^{(0)}) = |z) \\ |\rho^{(n)}) = \left(-\frac{1}{\gamma_p}|p)(p'| - \frac{1}{\gamma_c}|c)(c'|\right)\partial_t|\rho^{(n-1)}) \quad \text{for } n > 0. \end{cases}$$

Here, we want to find a formula to directly calculate all orders n. We will thus solve the recursion. Since $\partial_t|\rho^{(n-1)})$ is a linear combination of $|c)$ and $|p)$ (as can be inferred from the second line of Eq. (3.1)), we can use the identity $\partial_t|\rho^{(n-1)}) = (c'|\partial_t|\rho^{(n-1)})|c) + (p'|\partial_t|\rho^{(n-1)})|p)$ to write the second, recursive relation of this set of equations for $n > 0$ as

$$|\rho^{(n)}) = -\frac{1}{\gamma_p}(p'|\partial_t|\rho^{(n-1)})|p) - \frac{1}{\gamma_c}(c'|\partial_t|\rho^{(n-1)})|c) \tag{3.3a}$$

$$= -\frac{1}{\gamma_c}\partial_t|\rho^{(n-1)}) + \left(\frac{1}{\gamma_c} - \frac{1}{\gamma_p}\right)(p'|\partial_t|\rho^{(n-1)})|p). \tag{3.3b}$$

Especially the last of these formulations turns out to be very useful, because $\partial_t|p) = 0$. From here on, the equations in the derivation become rather long, so we choose to omit them from the main text. The remainder of the derivation can however be found in App. A.1. The final result, which expresses the nth order of $|\rho)$ in the expansion in $\frac{\Omega}{\Gamma}$ in terms of only the eigenmodes of W and their derivatives, reads (for $n \geq 1$):

$$\boxed{|\rho^{(n)}) = \left(-\frac{1}{\gamma_c}\partial_t\right)^n |z) + \left[\sum_{l=1}^{n}\left(-\frac{1}{\gamma_p}\partial_t\right)^{l-1}\left(\frac{1}{\gamma_c} - \frac{1}{\gamma_p}\right)(p'|\partial_t\left(-\frac{1}{\gamma_c}\partial_t\right)^{n-l}|z)\right]|p).} \tag{3.4}$$

This is the main result of this thesis. It gives the density operator $|\rho) = \sum_{n\geq 0}|\rho^{(n)})$ in a *generally applicable closed* form for arbitrary time-dependently driven systems. We will use this formula later in this chapter to evaluate the expressions for particle and energy currents. In chapter 5 we will then use these to study thermoelectrics in time-dependent systems and in chapter 6 we will study a specific driving in depth and use it to learn more about the fermion-parity mode. In App. A.1, we prove an expression, Eq. (A.2) that is even more general than Eq. (3.4): it relates $|\rho^{(n)})$ not specifically to $|\rho^{(0)}) = |z)$ as Eq. (3.4) does, but to $|\rho^{(n-k)})$, with $n \geq k \geq 1$.

3.1.3 Adiabatic correction

As an example of the use of Eq. (3.4), we will calculate the first adiabatic correction $|\rho^{(1)})$, which is the first order in the expansion of the density operator in $\frac{\Omega}{\Gamma}$. It thus takes into account all linear contributions in the driving rate. The zeroth order correction is the time-dependent instantaneous density operator, given by $|\rho^{(0)}) = |z)$. This is the solution that is obtained by fixing all parameters at each instant of time t, and solving this as a stationary problem. In some sense, the first adiabatic correction $|\rho^{(1)})$ is thus the first "real" time-dependent effect. This adiabatic correction already allows to describe for example situations in which adiabatic pumping takes place [41, 42].

Since we will calculate the first order ($n = 1$) correction, Eq. (3.4) is still equivalent to Eq. (3.3b), which is in turn equal to Eq. (3.3a). It is this form of the general result (3.4) that we will use here, since it immediately leads to a nice form of the final expression. Direct usage Eq. (3.4) will of course give the same result in the end.

The only unknowns in Eq. (3.3a) are $(p'|\partial_t|z)$ and $(c'|\partial_t|z)$, where we already substituted $|\rho^{(n-1)}) = |z)$. First we calculate

$$\partial_t|z) = \left(-\frac{1}{2}\partial_t N_z + \frac{1}{4}\partial_t p_z\right)|0) - \frac{1}{4}\partial_t p_z|\uparrow) - \frac{1}{4}\partial_t p_z|\downarrow) + \left(\frac{1}{2}\partial_t N_z + \frac{1}{4}\partial_t p_z\right)|2), \quad (3.5)$$

where we used the alternative formula (2.14) of the stationary state $|z)$. Combining this with the equations (2.16) and (2.19), we can directly write the two unknowns $(p'|\partial_t|z)$ and $(c'|\partial_t|z)$ in terms of physical quantities. We have then found the adiabatic correction of the density operator to be

$$|\rho^{(1)}) = -\frac{1}{2\gamma_p}\left((N_i - 1)\,\partial_t N_z + \frac{1}{2}\partial_t p_z\right)|p) - \frac{1}{\gamma_c}\partial_t N_z|c). \quad (3.6)$$

Notice that in principle nothing inhibits us from doing this calculation straight away without the duality. The expression that would then be obtained, would however contain complicated combinations of Fermi functions. These are typically very difficult to link to physical variables. This physical link is what we get for free by using the duality relation (2.12), the eigenmodes of W from Sec. 2.3 and our newly found expansion relation (3.4). The physical meaning of the terms in Eq. (3.6) will also become more clear when calculating physical observables, such as the current, which we will do in the next section.

3.2 Currents

3.2.1 Particle current

We will now find compact and insightful expressions for the time-dependent currents through the system. We start with the particle current. We define the current $I_{N\alpha}$ as the current of particles flowing *from* lead α *into* the dot. In the total system (dot and leads), there is conservation of total particle number $N^{\text{tot}} = N + \sum_\alpha N^{\text{lead}\alpha}$. The time-dependent particle current out of lead α can then be expressed in terms of the change of the expectation value of the number of particles in the dot due to lead α:

$$I_{N\alpha} = -\partial_t \left\langle N^{\text{lead}\alpha} \right\rangle = \left[\partial_t \langle N \rangle\right]_\alpha = \left[\partial_t \operatorname{Tr}(N\rho)\right]_\alpha = (N|\left[\partial_t|\rho)\right]_\alpha = (N|W_\alpha|\rho). \tag{3.7}$$

This result follows from the fact that the tunnelling Hamiltonian that couples each lead α to the dot conserves the total number of particles of each "lead α - dot subsystem" separately. The quantity $W_\alpha|\rho)$ represents the change in the density operator solely due to tunnelling to lead α.

Here, we introduced an important notation, which plays an essential role in the formulation and calculation of the currents. Whenever[1] a subscript α is added to a variable, this means that we consider the same system as in section 2.1, but now with respect to only one lead α. So one forgets for a moment all the other leads, and reintroduces for the then obtained system all the notation from section 2.1 to section 2.3. The variables which are defined in this way are denoted with a subscript α and will be called the "variables restricted to lead α", "variables with respect to lead α" or simply "lead resolved". For $W_\alpha|\rho)$, we notice that the time-dependence of $|\rho)$ is still given by the kernel W of the entire system. When we then calculate $W_\alpha|\rho)$, we consider the part of the total evolution that happens through the interaction with lead α.

Now notice that $(\mathbb{1}|W_\alpha = 0$ because $(\mathbb{1}| = (z'| = (z'_\alpha|$ is the left eigenvector of W_α corresponding to the zero eigenvalue. This can be used to write

$$(N|W_\alpha|\rho) = (N - N_{z\alpha}\mathbb{1}|W_\alpha|\rho) = -\gamma_{c\alpha}(N - N_{z\alpha}\mathbb{1}|\rho),$$

where the last equality is obtained by noticing that $(N - N_{z\alpha}\mathbb{1}| = (c'_\alpha|$ is the left charge eigenvector of W_α. The resulting particle current through lead α, for general $|\rho)$, then is

$$I_{N\alpha} = \gamma_{c\alpha}\left[N_{z\alpha} - (N|\rho)\right]. \tag{3.8}$$

This is a remarkably simple result: the particle current through lead α is proportional to the difference between the stationary occupation[2] of the dot $N_{z\alpha}$ with respect to that lead and the actual occupation of the dot within the whole system $(N|\rho)$. The proportionality constant is the charge decay rate restricted to the lead α under consideration.

Since we have analytical expressions for $|\rho^{(n)})$ for all n, we can calculate the contributions of order n in $\frac{\Omega}{\Gamma}$ to the time-resolved particle current through lead α: $I^{(n)}_{N\alpha}(t)$. Summing all these orders will then finally result again in the total particle current. The

[1] Except for the particle $I_{N\alpha}$, energy $I_{E\alpha}$ and heat $I_{Q\alpha}$ currents, for which the subscript simply means that we are looking at the current through lead α, with all leads still connected.

[2] Notice here that, with respect to a single lead α, the stationary state is also the equilibrium state.

first term of Eq. (3.8) derives from the instantaneous contribution (since this is the contribution with unit trace), so it will only appear in the current expression for $n = 0$. The instantaneous particle current can thus be found by substituting $|\rho^{(0)}) = |z)$ into Eq. (3.8):

$$I_{N\alpha}^{(0)} = \gamma_{c\alpha} \left(N_{z\alpha} - N_z \right). \tag{3.9}$$

For the higher order contributions ($n \neq 0$), we only need to consider the second term of Eq. (3.8). We write this as

$$I_{N_\alpha}^{(n)} = -\gamma_{c\alpha}(N|\rho^{(n)}) = -\gamma_{c\alpha} \left[(N| - N_z(\mathbb{1}| \right] |\rho^{(n)}) = -\gamma_{c\alpha}(c'|\rho^{(n)}),$$

where we made use of $(\mathbb{1}|\rho^{(n)}) = 0$ for $n \neq 0$. At this point, we can plug in the result for $|\rho^{(n)})$ that we found in Eq. (3.4), to express $|\rho^{(n)})$ in terms of $|\rho^{(0)}) = |z)$. We then finally find the contribution of order $\left(\frac{\Omega}{\Gamma}\right)^n$ to the particle current trough lead α:

$$\boxed{I_{N\alpha}^{(n)} \overset{n\neq 0}{=} -\gamma_{c\alpha}(c'| \left(-\frac{1}{\gamma_c}\partial_t \right)^n |z).} \tag{3.10}$$

Together with Eq. (3.9), this gives a very practical and compact way of calculating the particle current through a system with arbitrary driving schemes. The only thing one needs to do is to calculate the eigenvectors of the kernels W and W_α (for which the expressions where found already in Sec. 2.3) and take the necessary derivatives. In chapter 5, we will show how this general result for the particle current can contribute in the calculation of Onsager coefficients for the study of thermoelectrics in time-dependently driven systems. Notice that only the stationary state and charge mode play a role for the particle currents.

We will now make a specific example of how Eq. (3.10) can be used. As we did for the density operator, we calculate the adiabatic correction ($n = 1$) of the particle current. Using the result for $|\rho^{(1)})$, Eq. (3.6), we immediately find

$$I_{N\alpha}^{(1)} = -\gamma_{c\alpha}(c'|\rho^{(1)}) = \frac{\gamma_{c\alpha}}{\gamma_c}\partial_t N_z, \tag{3.11}$$

where we made crucially use of the biorthonormality of the charge and parity modes. Whereas the instantaneous contribution $I_{N\alpha}^{(0)}$ gives the particle current at every moment as if the system is in a stationary state, this first adiabatic contribution $I_{N\alpha}^{(1)}$ gives a correction for the non-instantaneous response of the system to time-dependent variations. The ratio of the charge relaxation rates $\frac{\gamma_{c\alpha}}{\gamma_c}$ determines how large the correction is for every lead. If there is no bias applied between different leads, the instantaneous current vanishes and this adiabatic correction is the largest contribution to the particle current. Introducing on top of this a time-varying asymmetry between the leads, results in the phenomenon of adiabatic pumping, which we mentioned before.

3.2.2 Energy and heat current

The energy current $I_{E\alpha}$ through lead α (from the lead into the dot) can be obtained completely similar to the particle current. The only, very important difference is that we now have to count the variation in energy instead of the change of number of particles. The tunnel-couplings between the leads and the dot do not store any energy since the tunnel-coupling is assumed to be weak (the equations that we use are correct for first order in Γ), such that the total energy in the dot and the leads is conserved [30]. The obtained expression for the energy current through lead α is then

$$I_{E\alpha} = -\partial_t \left\langle H^{\text{lead}\alpha} \right\rangle = (H|W_\alpha|\rho), \tag{3.12}$$

where the dot Hamiltonian H from Eq. (2.2) can be written as

$$(H| = \epsilon(N| + U(2|. \tag{3.13}$$

The heat current through lead α is directly related to the particle and energy currents [43] by

$$I_{Q\alpha} = I_{E\alpha} - \mu_\alpha I_{N\alpha}. \tag{3.14}$$

This heat current is positive when the heat flow is into the quantum dot. Since the heat current can here always be obtained using this expression, we will focus on the energy current in this section.

To calculate this energy current, we first use the completeness relation to expand $(2|W_\alpha$ in terms of the orthonormal eigenbasis of W_α:

$$\begin{aligned}(2|W_\alpha &= (2|z_\alpha)(z'_\alpha|W_\alpha + (2|p_\alpha)(p'_\alpha|W_\alpha + (2|c_\alpha)(c'_\alpha|W_\alpha + (2|s_\alpha)(s'_\alpha|W_\alpha \\ &= -\gamma_{p\alpha}(p'_\alpha| + (2|c_\alpha)(c'_\alpha|W_\alpha,\end{aligned}$$

where we intensively used the properties of the eigenmodes to eliminate $(z'_\alpha|W_\alpha = 0$ and $(2|s_\alpha) = 0$. We also used the identities $(2|p_\alpha) = (2|\mathcal{P}|2) = 1$ and $-\gamma_{p\alpha}(p'_\alpha|$. Now notice that $(N|W_\alpha|\rho) = (c'_\alpha|W_\alpha|\rho) = I_{N\alpha}$ (see Sec. 3.2.1). The energy current for any time-dependent ρ can thus be written as

$$I_{E\alpha} = (\epsilon + U(2|c_\alpha))\, I_{N\alpha} - \gamma_{p\alpha} U(p'_\alpha|\rho) \tag{3.15}$$

We can now continue using our analytical expressions for $|\rho^{(n)})$. The result for $n = 0$ is obtained immediately, and we state it together with the result for $n > 0$ that we calculate now. We can substitute the particle current in Eq. (3.15) to obtain

$$I^{(n)}_{E\alpha} = -\gamma_{c\alpha}\left(\epsilon + U(2|c_\alpha)\right)(c'|\rho^{(n)}) - \gamma_{p\alpha} U(p'_\alpha|\rho^{(n)})$$

for $n > 0$, $|\rho^{(n)})$ is a linear combination of $|p)$ and $|c)$. So we can expand $(p'_\alpha|\rho^{(n)}) = \underbrace{(p'_\alpha|p)}_{=1}(p'|\rho(n)) + (p'_\alpha|c)(c'|\rho(n))$ and find

$$\begin{aligned}I^{(n)}_{E\alpha} &= \left[-\gamma_{c\alpha}\left(\epsilon + U(2|c_\alpha)\right) - \gamma_{p\alpha} U(p'_\alpha|c)\right](c'|\rho^{(n)}) - \gamma_{p\alpha} U(p'|\rho^{(n)}) \\ &= \left[-\gamma_{c\alpha}\epsilon - \left(\gamma_{c\alpha}(2|c_\alpha) + \gamma_{p\alpha}(p'_\alpha|c)\right) U\right](c'|\rho^{(n)}) - \gamma_{p\alpha} U(p'|\rho^{(n)}).\end{aligned}$$

We finally arrive at an expression for the energy current through lead α of order n in $\frac{\Omega}{\Gamma}$ by using equations (3.4) and (3.10):

$$\boxed{\begin{aligned} I_{E\alpha}^{(n)} &\overset{n=0}{=} \left[\epsilon + (2|c_\alpha)U\right] I_{N\alpha}^{(0)} - \gamma_{p\alpha} U (p'_\alpha|z) \\ &\overset{n\neq 0}{=} \left[\epsilon + \left((2|c_\alpha) + \frac{\gamma_{p\alpha}}{\gamma_{c\alpha}}(p'_\alpha|c)\right) U\right] I_{N\alpha}^{(n)} - \gamma_{p\alpha} U (p'|\rho^{(n)}), \end{aligned}} \tag{3.16}$$

where

$$\begin{aligned} (p'|\rho^{(n)}) =& (p'| \left(-\frac{1}{\gamma_c}\partial_t\right)^n |z) + \sum_{l=1}^{n} \left(-\frac{1}{\gamma_p}\partial_t\right)^{l-1} \left(\frac{1}{\gamma_c} - \frac{1}{\gamma_p}\right) (p'|\partial_t \left(-\frac{1}{\gamma_c}\partial_t\right)^{n-l} |z) \\ (2|c_\alpha) =& \frac{1}{2}(2 - N_{i\alpha}) \\ (p'_\alpha|c) =& (\mathcal{P} z_{i\alpha}| \frac{1}{2}\mathcal{P}\left[|N) - N_i|\mathbb{1})\right] = \frac{1}{2}(N_{i\alpha} - N_i)\,. \end{aligned}$$

On evaluating this expression, it is often also useful to remember

$$\partial_t|z) = \left(\frac{1}{2}(N_i - 1)\,\partial_t N_z + \frac{1}{4}\partial_t p_z\right)|p) + \partial_t N_z|c),$$

which can be found from Eq. (3.6). The n^{th} order contribution in Ω to the heat current through lead α is of course immediately found as

$$I_{Q\alpha}^{(n)} = I_{E\alpha}^{(n)} - \mu_\alpha I_{N\alpha}^{(n)} \tag{3.17}$$

The expression Eq. (3.16) for the energy (and heat) current contributions of order n in Ω is another useful expression that derives from the main result Eq. (3.4). Already in its general form (without specifying a concrete time-dependence) it allows for interesting interpretations. Equation (3.16) consists of one term that is proportional to the particle current of the same order n. When the energy or heat current is simply proportional to the particle current, one often says that the currents are tightly coupled. We will thus refer to this term as the tight coupling term or contribution (TC). The proportionality constant can be perceived as a certain renormalised energy that is transported per particle. It accounts for the additional charging energy carried by electrons when a transition involving double occupation occurs. This becomes even more clear by looking at the currents when an external magnetic field is applied, as we will do in chapter 4. Since this first term is proportional to the particle current, we expect it to be transport related. The second term in Eq. (3.16) will often be referred to as the non-tight coupling contribution (NTC). This term is, except for the tunnel coupling Γ_α, independent of the lead under consideration for $n > 0$. As such, no directionality is present in the NTC term. The second term can therefore be assumed to be only related to the generated heat, and not to the transported heat. Furthermore, since it contains the fermion-parity amplitude covector $(p'|$, it might teach us something more about the fermion-parity mode and the inverted state $|z_i)$. We will come back to this later in chapter 6. Just as for the particle current, also the formula for the heat current can be used in the study of time-dependent thermoelectrics, as we will see in chapter 5.

As an example for the use of Eq. (3.16), the instantaneous ($n = 0$) energy current and the adiabatic correction ($n = 1$) are calculated in App. A.2.

4 Dynamics in the presence of a magnetic field

In this chapter, we will consider the quantum dot model discussed in the previous chapters, but in a more general case. Specifically, we now assume that the spin-degeneracy in the quantum dot is lifted, and that the tunnel-coupling to the leads is also spin-dependent. This situation can be achieved by applying a magnetic field. The spin-dependence of the model can be exploited in emerging technologies such as spintronics. Since the quantum dot is operating using individual spins, it can - together with its time-dependence - be used for controlled single-spin currents. We will repeat in this chapter several of the steps taken in chapters 2 and 3, while focussing on the changes compared to the spin-degenerate model presented there. Several expressions and derivations in this chapter are rather long and are given in App. B.

4.1 Model

The system under consideration is exactly the same as the one introduced in Sec. 2.1, except for the presence of an externally applied magnetic field on the dot. This magnetic field lifts the spin degeneracy of the energy levels (Zeeman effect) of the dot and it makes the tunnel-couplings spin-dependent. The magnetic field is furthermore assumed to be applied locally on the dot and barriers, such that the leads themselves remain spin-independent. The model is shown in Fig. 4.1. If not indicated differently here, the variables and assumptions from Sec. 2.1 are retained.

The Hamiltonian describing the system is the Anderson Hamiltonian [33], Eq. (2.1), $H_{\text{And}} = H + H_{\text{Leads}} + H_{\text{Tun}}$. The Hamiltonian of the quantum dot itself, H, becomes

$$H = \sum_{\sigma=\uparrow,\downarrow} \epsilon_\sigma n_\sigma + U n_\uparrow n_\downarrow. \tag{4.1}$$

Notice that the spin-degeneracy is lifted by making the dot energy level ϵ_σ spin-dependent. With this Hamiltonian, the total energy of the dot occupied by two fermions is $\epsilon_\uparrow + \epsilon_\downarrow + U$. We will also use $\epsilon = \frac{1}{2}(\epsilon_\uparrow + \epsilon_\downarrow)$ to denote the average of the spin-up and -down dot level energies. With this average dot level, we can write the spin-dependent dot levels as $\epsilon_\uparrow = \epsilon + \Delta\epsilon$ and $\epsilon_\downarrow = \epsilon - \Delta\epsilon$, where $2\Delta\epsilon = \epsilon_\uparrow - \epsilon_\downarrow$ is the Zeeman splitting. Since the magnetic field is applied locally on the dot, the Hamiltonian describing the leads H_{Leads} remains the same as before.

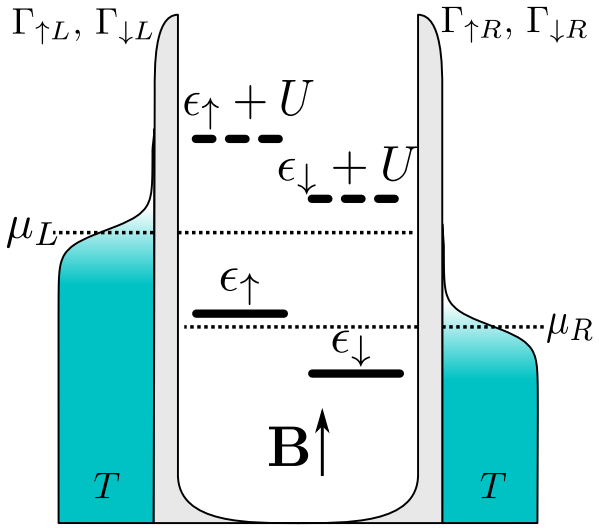

Figure 4.1: *Model of the strongly interacting quantum dot, tunnel-coupled to two leads and in a locally applied magnetic field. Compared to Fig. 2.1, the magnetic field induces a splitting of the spin-degenerate energy level ϵ into $\epsilon_\uparrow$ and $\epsilon_\downarrow$. Moreover, the tunnel-coupling strengths Γ_α become spin-dependent. Since the magnetic field is applied locally, the leads are unchanged compared to Fig. 2.1.*

Finally, the tunnel-coupling between the leads α and the dot is now described by

$$H_{\text{Tun}} = \sum_{\alpha,k} \sum_{\sigma=\uparrow,\downarrow} \left(V_{\sigma\alpha} c_{\alpha k\sigma} d_\sigma^\dagger + H.c. \right). \tag{4.2}$$

The tunnelling matrix element $V_{\sigma\alpha}$, which couples lead α to the dot, is still momentum-independent, but the magnetic field induces a spin-dependence. This spin-dependence is then also present in the tunnel-coupling strength $\Gamma_{\sigma\alpha} = 2\pi\rho_{\sigma\alpha} |V_{\sigma\alpha}|^2$. We still consider the wide band limit, in which both $\Gamma_{\sigma\alpha}$ and $\rho_{\sigma\alpha}$ are energy-independent. Here, we have $2\Gamma_\alpha = \Gamma_{\uparrow\alpha} + \Gamma_{\downarrow\alpha}$, $\Gamma_\sigma = \sum_\alpha \Gamma_{\sigma\alpha}$ and $\Gamma = \sum_\alpha \Gamma_\alpha$.

The results from Sec. 2.2 remain valid, apart from some small adaptations that we will discuss in this paragraph. The kernel W that was given in Eq. (2.11) becomes spin-dependent. Based on Fermi's Golden rule, we find the matrix elements W_{ij} in the orthonormal basis $i = \{0, \uparrow, \downarrow, 2\}$ to be

$$W = \begin{bmatrix} -f_{\epsilon\uparrow}^+ - f_{\epsilon\downarrow}^+ & f_{\epsilon\uparrow}^- & f_{\epsilon\downarrow}^- & 0 \\ f_{\epsilon\uparrow}^+ & -f_{\epsilon\uparrow}^- - f_{U\downarrow}^+ & 0 & f_{U\downarrow}^- \\ f_{\epsilon\downarrow}^+ & 0 & -f_{\epsilon\downarrow}^- - f_{U\uparrow}^+ & f_{U\uparrow}^- \\ 0 & f_{U\downarrow}^+ & f_{U\uparrow}^+ & -f_{U\uparrow}^- - f_{U\downarrow}^- \end{bmatrix}. \tag{4.3}$$

Where the notation for the Fermi-functions is similar as before:

$$f_{\epsilon\sigma}^\pm = \sum_\alpha \Gamma_{\sigma\alpha} f^\pm (\epsilon_\sigma - \mu_\alpha) = \sum_\alpha f_{\epsilon\sigma\alpha}^\pm$$
$$f_{U\sigma}^\pm = \sum_\alpha \Gamma_{\sigma\alpha} f^\pm (\epsilon_\sigma + U - \mu_\alpha) = \sum_\alpha f_{U\sigma\alpha}^\pm.$$

4.2 Eigenmodes

We will now calculate and discuss the different eigenmodes of the magnetic kernel (4.3). The first two eigenmodes (stationary and fermion-parity mode) are very similar to the ones in the non-magnetic case, Sec. 2.3. On the other hand, the charge and spin modes get mixed into new modes. Where possible, we will give compact expression for the quantities under consideration. Often however, other ways to express these quantities (e.g. in terms of Fermi-functions) and explicit derivations can be found in App. B.

4.2.1 Stationary state and fermion-parity mode

Both the mode corresponding to the zero eigenvalue and the fermion-parity mode can be obtained in exactly the same way as in section 2.3, namely by using the existence of a stationary state, probability conservation and the duality relation (2.12).

The first eigenmode, corresponding to the zero eigenvalue of the magnetic kernel W Eq. (4.3) is the stationary mode:

$$\begin{aligned} \gamma_z =& 0 \\ (z'| =& (\mathbb{1}| \\ |z) =& \left(\frac{1}{4} - \frac{1}{2}\Delta N_z + \frac{1}{4}p_z\right)|0) + \left(\frac{1}{4} + \frac{1}{2}\sigma_z - \frac{1}{4}p_z\right)|\uparrow) \\ &+ \left(\frac{1}{4} - \frac{1}{2}\sigma_z - \frac{1}{4}p_z\right)|\downarrow) + \left(\frac{1}{4} + \frac{1}{2}\Delta N_z + \frac{1}{4}p_z\right)|2). \end{aligned} \tag{4.4}$$

Although, the expressions of these quantities in terms of Fermi-functions are different now, they still simplify to the values discussed before when the external magnetic field is turned off. Next to the total stationary particle number $N_z = (N|z)$, it is now useful to also introduce spin-resolved quantities such as the average number of spin-up and spin-down electrons on the dot when in the stationary state. The spin-up and -down occupation operators can be introduced as $|N_\uparrow) = |\uparrow) + |2)$ and $|N_\downarrow) = |\downarrow) + |2)$, with $|N) = |N_\uparrow) + |N_\downarrow)$. The expectation values of these occupation operators for the dot in its stationary state are denoted by $N_{\uparrow z} = (N_\uparrow|z)$ and $N_{\downarrow z} = (N_\downarrow|z)$. In Eq. (4.4), also the new quantity σ_z was introduced. It can be calculated as $\sigma_z = (\sigma|z)$, the total spin expectation value of the dot in its stationary state. The spin operator is defined as $|\sigma) = |\uparrow) - |\downarrow) = |N_\uparrow) - |N_\downarrow)$. The other quantities in equations (4.4) and (B.1), namely p_z and ΔN_z, were introduced before in section 2.3.

The dependence of the occupations N_z, $N_{\uparrow z}$ and $N_{\downarrow z}$ on the level position ϵ can be seen in Fig. 4.2 for the cases without an applied bias $V = 0$ and with a large applied bias $V \gg U$. In both cases, the total occupation N_z increases monotonically for a decreasing energy level ϵ as expected. The exact way this happens is however rather different. When no bias is applied, Fig. 4.2(a), a spin-down electron always occupies the dot first, as soon as $\epsilon_\downarrow$ crosses the resonance of the leads. A spin-up electron can only enter once the Coulomb blockade can be overcome, i.e. when $\epsilon_\uparrow + U$ crosses the resonance of the leads. Between these two resonances, the dot occupation is completely due to spin-down electrons, which have the lower energy. This changes when a bias is applied between the leads, as shown in Fig. 4.2(b). For clarity, a very large bias $V \gg U$ was chosen, and only

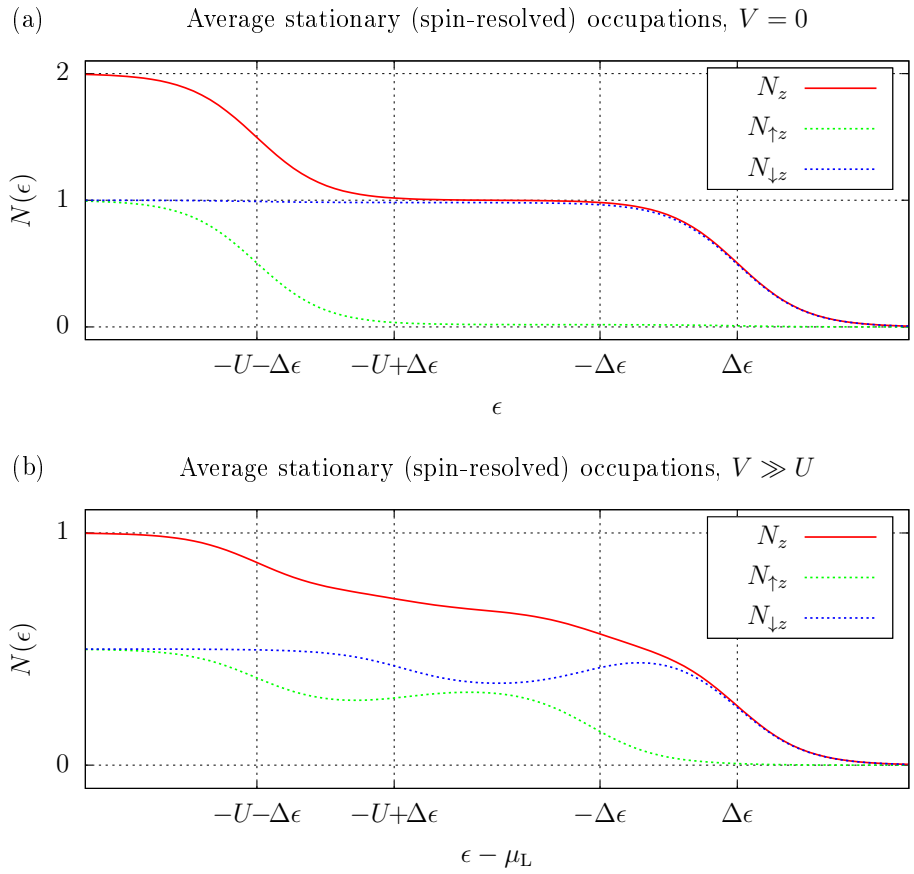

Figure 4.2: *The average full stationary occupation N_z and spin-resolved occupations $N_{\uparrow z}$ and $N_{\downarrow z}$ for the quantum dot in a magnetic field as a function of energy level position ϵ. The dot is coupled to two leads, with a spin- and lead-independent tunnel-coupling strength. The ticks on the axis with $+\Delta\epsilon$ are the resonances for spin-down electrons, while the ticks with $-\Delta\epsilon$ are the resonances for spin-up electrons. In* **(a)**, *the bias between the leads is zero, such that this is equivalent to having only one lead, as in Fig. 2.3. In* **(b)**, *a large bias $V \gg U$ is applied symmetrically over the leads. This is the model as depicted in Fig. 4.1, but with a much larger bias. Only the behaviour around $\mu_{\mathrm{L}} = \frac{V}{2}$ is shown for clarity. Around μ_{R} the behaviour is similar.*

the resonances with the left lead are shown. The maximum *average* occupation is thus only 1 now, since all relevant energy levels are still far above the resonances with the right lead. When $\epsilon_\downarrow$ crosses the resonance with the left lead, it again almost reaches its maximum occupation (in this interval around μ_{L}). This time however, when $\epsilon_\uparrow$ reaches its resonance with the left lead, it also gets some probability to be occupied. In spite of this, the spin-up occupation is not translated in an equal increase of the total dot occupation N_z. Indeed: when a spin-up electron occupies the dot in this region, the spin-down electrons loose their potential for occupation, since they can not provide the additional charging energy for double occupation. The increase of $N_{\uparrow z}$ is thus partially compensated by a decrease of $N_{\downarrow z}$. Similar mechanisms are at play around the other resonances.

Using the duality relation (2.12), it is now easy to find the second eigenmode of the kernel W from the first eigenmode (4.4). This second eigenmode, which we call again the (fermion-)parity mode, its corresponding rate and amplitude covector are given by

$$\begin{aligned}
\gamma_p =& 2\Gamma = \Gamma_\uparrow + \Gamma_\downarrow \\
(p'| =& [\mathcal{P}\mathcal{I}|z)]^\dagger = ((-\mathbb{1})^N z_i| \\
=& \left(\frac{1}{4} - \frac{1}{2}\Delta N_i + \frac{1}{4}p_i\right)|0) + \left(\frac{1}{4} + \frac{1}{2}\sigma_i - \frac{1}{4}p_i\right)|\uparrow) \\
&+ \left(\frac{1}{4} - \frac{1}{2}\sigma_i - \frac{1}{4}p_i\right)|\downarrow) + \left(\frac{1}{4} + \frac{1}{2}\Delta N_i + \frac{1}{4}p_i\right)|2) \\
|p) =& |\mathcal{P}) = |(-\mathbb{1})^N).
\end{aligned} \tag{4.5}$$

In these expressions, we again used the notation for the inverted stationary state, $z_i = \mathcal{I}z = z\,(-\epsilon_\uparrow, -\epsilon_\downarrow, -U, -\mu)$. We also defined the following additional expectation values with respect to the inverted stationary state: the spin-resolved particle numbers $N_{\uparrow i} = (N_\uparrow|z_i)$ and $N_{\downarrow i} = (N_\downarrow|z_i)$, and the total spin $\sigma_i = (\sigma|z_i)$.

As can be seen from all these expressions, there are no large changes in the stationary and fermion-parity modes with respect to the system without an applied magnetic field. All differences originate from the splitting of the spin-degeneracy, which allows for different energies for spin-up and -down levels. This introduces non-vanishing total spins σ_z and σ_i. It also further complicates the expressions in terms of Fermi-functions, which is why we omitted them from the main text. This demonstrates the powerful approach of working with observables, amplitude covectors and operators as we do here. Without the present approach the calculations (that follow) would be much more cumbersome than they are now.

4.2.2 Mixed charge and spin modes

When an external magnetic field is applied, the charge and spin modes that were present in the non-magnetic case are altered more drastically than the stationary and fermion-parity modes. Most importantly, these modes couple such that we cannot speak any longer about a charge and spin mode, but rather of combinations of both.

In order to find expressions for the third and fourth eigenvalues and eigenvectors, one needs to consider that the matrix representation of W is always given with respect to a certain basis as we have seen in Eq. (2.8):

$$W = \sum_{i,j} W_{ij}|i)(j|, \text{ with } W_{ij} = (i|W|j).$$

Until now, we have used two different basis sets. Either we used the basis of the physical possible states of the dot $\{0, \uparrow, \downarrow, 2\}$, for which the kernel elements for the dot with an applied magnetic field are given by Eq. (4.3). In the non-magnetic case, we also used the eigenbasis $\{z, p, c, s\}$ of the kernel W. In that basis the kernel was diagonal with the eigenvalues on the diagonal. Although we will use another basis set for the quantum dot in a magnetic field, the charge and spin operators and amplitude covectors will still be very useful. We thus restate and redefine them here in the presence of a magnetic field,

such that they retain their physical interpretation. Keep in mind however that they are *not* any more the eigenvectors of the magnetic kernel W! The charge amplitude covector and operator remain unchanged with respect to the original definition Eq. (2.19):

$$\begin{aligned}(c'| &= (N| - N_z(\mathbb{1}| \\ |c) &= \frac{1}{2}(-\mathbb{1})^N [|N) - N_i|\mathbb{1})] .\end{aligned} \tag{4.6}$$

The spin amplitude covector and operator on the other hand now have to take into account the possibility of non-zero spin in the stationary state σ_z. In analogy to Eq. (4.6), and to its original definition Eq. (2.20), we now define the spin amplitude covector and operator as

$$\begin{aligned}(s'| &= (\sigma| - \sigma_z(\mathbb{1}| \\ |s) &= \frac{1}{2}\left[|\sigma) + \sigma_i|(-\mathbb{1})^N)\right] = \frac{1}{2}(-\mathbb{1})^N [-|\sigma) + \sigma_i|\mathbb{1})] .\end{aligned} \tag{4.7}$$

This reduces to the old equation (2.20) when the system is spin-independent. Whenever we use $(c'|$, $(s'|$, $|c)$ or $|s)$ in this chapter, we refer to these new definitions.

We will now use temporarily another basis set in order to find the two last eigenmodes of the kernel with an applied magnetic field. Since the first two eigenmodes of W (stationary and parity mode) are already known, we use these in our basis set. The other two, yet to be introduced basis states will be denoted by x and y. The basis set is then $\{z, p, x, y\}$. Notice that this is still not the eigenbasis of W, but rather a basis set that will help us find that eigenbasis. The basis states x and y should be chosen such that they are orthogonal to both the eigenstates z and p, as well as to each other. This is important for two reasons. First, it makes sure that the kernel W is block-diagonal, which makes it particularly easy to find its remaining eigenmodes. Second, it ensures that these unknown eigenmodes can be expressed as a linear combination of only the basis operators x and y. With these considerations in mind, we choose the amplitude covectors and operators to be

$$(x'| = (N_\uparrow| - N_\uparrow(\mathbb{1}| \tag{4.8a}$$
$$(y'| = (N_\downarrow| - N_\downarrow(\mathbb{1}| \tag{4.8b}$$
$$|x) = |\mathcal{P}N_\downarrow) - N_{\downarrow i}|(-\mathbb{1})^N) \tag{4.8c}$$
$$|y) = |\mathcal{P}N_\uparrow) - N_{\uparrow i}|(-\mathbb{1})^N). \tag{4.8d}$$

It can be checked that these vectors indeed satisfy biorthogonality. In the basis spanned by $\{z, p, x, y\}$, the kernel W now contains the elements

$$W = \begin{bmatrix} -\gamma_z & 0 & 0 & 0 \\ 0 & -\gamma_p & 0 & 0 \\ 0 & 0 & (x'|W|x) & (x'|W|y) \\ 0 & 0 & (y'|W|x) & (y'|W|y) \end{bmatrix} = \begin{bmatrix} 0 & 0 & 0 & 0 \\ 0 & -2\Gamma & 0 & 0 \\ 0 & 0 & -\Gamma_\uparrow & -f^+_{\epsilon\uparrow} + f^+_{U\uparrow} \\ 0 & 0 & -f^+_{\epsilon\downarrow} + f^+_{U\downarrow} & -\Gamma_\downarrow \end{bmatrix} . \tag{4.9}$$

From this expression for the magnetic kernel W, we deduce the two remaining eigenvectors. We will denote these by a and b, such that the orthogonal eigenbasis for the magnetic kernel W becomes $\{z, p, a, b\}$. The rates γ_a and γ_b of the eigenmodes a and b, which are the negated eigenvalues, are

$$\begin{aligned}\gamma_a &= -\lambda_a = \Gamma + \sqrt{\left(f^+_{\epsilon\uparrow} - f^+_{U\uparrow}\right)\left(f^+_{\epsilon\downarrow} - f^+_{U\downarrow}\right) + \frac{1}{4}\left(\Gamma_\uparrow - \Gamma_\downarrow\right)^2} \\ \gamma_b &= -\lambda_b = \Gamma - \sqrt{\left(f^+_{\epsilon\uparrow} - f^+_{U\uparrow}\right)\left(f^+_{\epsilon\downarrow} - f^+_{U\downarrow}\right) + \frac{1}{4}\left(\Gamma_\uparrow - \Gamma_\downarrow\right)^2}.\end{aligned} \tag{4.10}$$

The eigenmodes $|a)$ and $|b)$, and amplitude covectors $(a|$ and $(b|$ are given in App. B.2. They can be expressed in several (lengthy) ways, both in terms of x and y and in terms of the charge c and s modes. Both of these forms will prove to be useful in specific cases.

These eigenvectors a and b are normalised in the sense that $(a'|a) = (b'|b) = 1$. These normalisation conditions left us however for both the a and b mode with a relative multiplication factor of the vectors that can be chosen freely. When we consider the modes a and b in the limit without a magnetic field, i.e. $B \to 0$, it is desirable that they reduce to the modes in the absence of a magnetic field. This fixes the prefactors. One can indeed check that in the limit $B \to 0$, the modes a and b become

$$|a) \to \frac{1}{2}\left[|x) + |y)\right] = |c) \qquad |b) \to \frac{1}{2}\left[|x) - |y)\right] = |s) \tag{4.11a}$$

$$(a'| \to (x'| + (y'| = (c'| \qquad (b| \to (x'| - (y'| = (s'|. \tag{4.11b}$$

While in the case without a magnetic field the charge and spin eigenmodes are self-dual in the sense of the duality relation (2.12), this same duality relation now cross-links the a and b eigenmodes. Indeed, their rates, amplitude covectors and operators are related as

$$\begin{aligned}\gamma_b &= 2\Gamma - \mathcal{I}\gamma_a \\ |b) &= -\frac{1}{4}\frac{(\gamma_a - \gamma_b)}{f^+_{\epsilon\uparrow} - f^+_{U\uparrow}}\left[(a'|\mathcal{I}\mathcal{P}\right]^\dagger \\ |a) &= \frac{1}{4}\frac{(\gamma_a - \gamma_b)}{f^+_{\epsilon\uparrow} - f^+_{U\uparrow}}\left[(b'|\mathcal{I}\mathcal{P}\right]^\dagger.\end{aligned}$$

The extra factors in the last two of these equations arise from the specific normalisation of a and b that we chose. The duality relation (2.12) can here thus again be used to find one of the eigenmodes, once the other is known (apart from normalisation, which one has to choose anyway). This extension of the results of [30] to include spin-dependence, clearly shows that strategy presented there (and used in this thesis) is certainly not restricted to a single specific system.

4.3 Sudden switch: decay rates, charge and spin

In this section, we will briefly discuss the time-dependence of the expectation value of the total charge and spin of the quantum dot after a sudden switch in any of the parameters of the system. In contrast to the discussion in Sec. 2.4, we here fully take the spin-dependence that is due to the external magnetic field into account. As we discussed in the previous section, the charge c and spin s modes are now mixed into the new a and b eigenmodes. This will significantly change the dynamics of the charge and spin in the quantum dot system. Additional, explicit expressions that were omitted in the text can once again be found in App. B.3.

The expectation values for the total charge and spin in the dot are initially $\langle N\rangle(0) = (N|z_0) = N_{z0}$ and $\langle\sigma\rangle(0) = (\sigma|z_0) = ((\uparrow| - (\downarrow|)|z_0) = \sigma_{z0}$. Expanding the time-dependent density operator in eigenmodes of W (the decay modes from after the switch), we find for $t > 0$:

$$\begin{aligned}|\rho(t)) &= e^{Wt}|\rho_0) = e^{Wt}|z_0)\\ &= |z)(z'|z_0) + e^{-\gamma_p t}|p)(p'|z_0) + e^{-\gamma_a t}|a)(a'|z_0) + e^{-\gamma_b t}|b)(b'|z_0).\end{aligned} \tag{4.12}$$

By having the time-dependence of the density operator, we have everything we need to calculate the expectation values of the charge $\langle N\rangle(t)$ and spin $\langle\sigma\rangle(t)$. For the charge we find

$$\langle N\rangle(t) = (N|\rho(t)) = \Big[(\uparrow| + (\downarrow| + 2(2|\Big]\,|\rho(t)),$$

while the spin expectation value can be calculated as

$$\langle\sigma\rangle(t) = (\sigma|\rho(t)) = ((\uparrow| - (\downarrow|)\,|\rho(t)).$$

The final results of these calculations can be written in a compact form as

$$\langle N\rangle(t) = \sum_{k=a,b}\sum_{\sigma=\uparrow,\downarrow}\frac{(-1)^{\delta_{k,b}}}{\gamma_a-\gamma_b}\left[N_{\sigma z}\left(1-e^{-\gamma_k t}\right)+N_{\sigma z0}e^{-\gamma_k t}\right]\left[\gamma_k-\left(f^-_{\epsilon\bar\sigma}+f^+_{U\bar\sigma}\right)\right] \tag{4.13}$$

$$\langle\sigma\rangle(t) = \sum_{k=a,b}\sum_{\sigma=\uparrow,\downarrow}\frac{(-1)^{\delta_{k,b}}(-1)^{\delta_{\sigma,\downarrow}}}{\gamma_a-\gamma_b}\left[N_{\sigma z}\left(1-e^{-\gamma_k t}\right)+N_{\sigma z0}e^{-\gamma_k t}\right]\left[\gamma_k-\left(f^+_{\epsilon\bar\sigma}+f^-_{U\bar\sigma}\right)\right],$$

where

$$\delta_{k,b} = \begin{cases}0 & \text{if } k=a\\ 1 & \text{if } k=b\end{cases},\ \delta_{\sigma,\downarrow} = \begin{cases}0 & \text{if } \sigma=\uparrow\\ 1 & \text{if } \sigma=\uparrow\end{cases} \text{ and } \bar\sigma = \begin{cases}\uparrow & \text{if } \sigma=\downarrow\\ \downarrow & \text{if } \sigma=\uparrow\end{cases}.$$

These expressions for the evolution of the charge and spin expectation values show us clearly that there is not one specific relaxation rate related to either charge or spin. They are mixed together in the a and b modes, which is why $\langle N\rangle(t)$ and $\langle\sigma\rangle(t)$ have two characteristic rates: γ_a and γ_b. It is interesting to consider some limits to get a better understanding of the behaviour of the expectation values.

When we turn off the magnetic field (i.e. the limit $\epsilon_\uparrow = \epsilon_\downarrow = \epsilon$ and $\Gamma_\uparrow = \Gamma_\downarrow = \Gamma$), $\langle N\rangle(t)$ and $\langle\sigma\rangle(t)$ indeed reduce to the results without an applied magnetic field. As noted before, γ_a and γ_b are in this limit equal to γ_c and γ_s and the charge and spin expectation values only contain their respective relaxation rates.

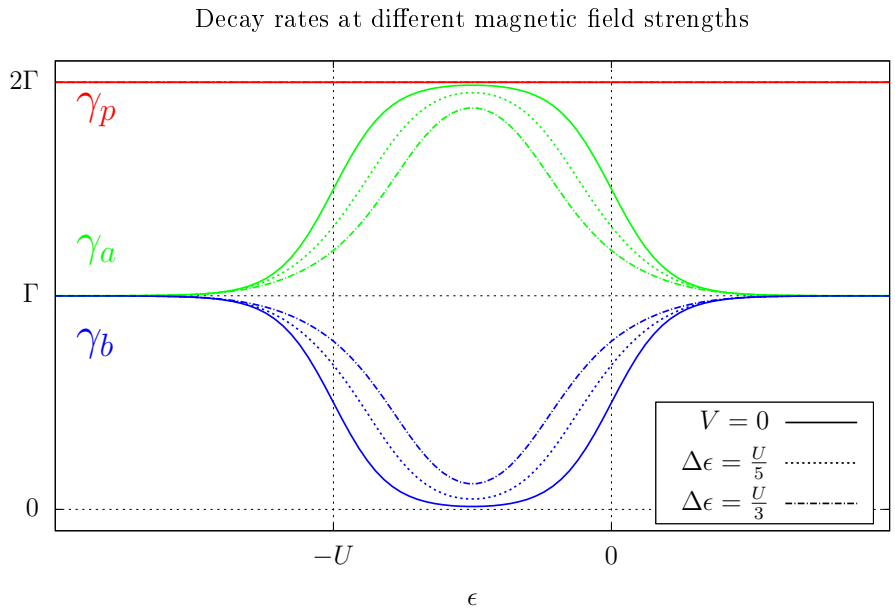

Figure 4.3: *The decay rates of the fermion-parity mode γ_p, the a mode γ_a and the b mode γ_b as a function of the dot energy level. The dot is connected to one lead (or multiple leads at the same electrochemical potential) with a spin-independent tunnel-coupling strength $\Gamma = \Gamma_\uparrow = \Gamma_\downarrow$. The on-site interaction is $U = 10T$. The different rates are shown without a magnetic field (solid), with a weak magnetic field (dotted) and a stronger magnetic field (dash-dotted). For these two last cases, we plot $\Delta\epsilon = \frac{U}{5}$ and $\Delta\epsilon = \frac{U}{3}$ respectively.*

We now again consider a non-zero magnetic field, but we assume that there is no on-site repulsion, i.e. $U = 0$. In this limit, $\gamma_a = \Gamma_\uparrow$ and $\gamma_b = \Gamma_\downarrow$. The charge and spin expectation values become rather simple:

$$\langle N \rangle (t) = N_{\uparrow z}\left(1 - e^{-\Gamma_\uparrow t}\right) + N_{\uparrow z0}e^{-\Gamma_\uparrow t} + N_{\downarrow z}\left(1 - e^{-\Gamma_\downarrow t}\right) + N_{\downarrow z0}e^{-\Gamma_\downarrow t}$$
$$\langle \sigma \rangle (t) = N_{\uparrow z}\left(1 - e^{-\Gamma_\uparrow t}\right) + N_{\uparrow z0}e^{-\Gamma_\uparrow t} - N_{\downarrow z}\left(1 - e^{-\Gamma_\downarrow t}\right) - N_{\downarrow z0}e^{-\Gamma_\downarrow t}.$$

This is indeed what one would expect. In the absence of local interaction, there is no interaction at all between spin-up and spin-down particles. They thus behave as independent, different entities with each their own decay rate $\Gamma_\uparrow$ and $\Gamma_\downarrow$.

To conclude this section, it is interesting to see the influence of the magnetic field on the decay rates γ_p, γ_a and γ_b. This is shown in Fig. 4.3. The strength of the magnetic field is here measured in terms of the Zeeman splitting $2\Delta\epsilon = \epsilon_\uparrow - \epsilon_\downarrow$. The parity rate stays constant as before. Without an applied magnetic field, the a and b rates are simply the charge and spin rates that we saw in Fig. 2.4. The stronger the magnetic field, the more the charge and spin rates mix. The difference between γ_a and γ_b becomes smaller. For a Zeeman splitting much larger than the on-site interaction U, these rates are indistinguishable and equal to Γ (not shown in figure). Similar to the limit $U \to 0$, the two spins behave as independent particles. Now this happens because always only one of the energy levels $\epsilon_\uparrow$ or $\epsilon_\downarrow$ is close to the electrochemical potential of the lead. As a result, only one spin-particle is of importance for the tunnelling at every ϵ. Moreover, mathematically the on-site interaction $U \ll \Delta\epsilon$, such that it can be neglected.

4.4 Dynamics for arbitrary driving

In this section, we calculate the particle, energy and heat currents through the system when there is an external magnetic field applied. We apply a similar strategy as in chapter 3. First, we find an expression for the density operator $|\rho(t))$. Since the complexity of the expressions grows very quickly with increasing orders in the adiabatic expansion, we will only proceed up to the first order in the driving frequency $\frac{\Omega}{\Gamma}$ (i.e. the first adiabatic correction). Later, we find expressions for the different currents through the system for general $|\rho)$. Finally, we fill in the explicitly calculated density operator up to first order in the driving frequency $\frac{\Omega}{\Gamma}$, which gives us explicit expressions for the currents up to the first adiabatic correction. Because of their lengthy nature, most of the derivations in this section can be found in App. B.

We do not show any results for a specific type of driving here. However, the generality of our results makes them applicable to simulations of a large variety of nanosystems placed in a magnetic field, including spintronics devices or adiabatic spin pumps.

4.4.1 Density operator

We find the instantaneous and first adiabatic correction ($n = 0$ and $n = 1$) of the expansion of the density operator $|\rho(t)) = \sum_n |\rho^{(n)})$ in orders of $\frac{\Omega}{\Gamma}$. The steps we employ to do so are carefully explained in App. B.4, and are analogous to the ones in Sec. 3.1.2. The final result is

$$\begin{aligned}
|\rho) \approx& |\rho^{(0)}) + |\rho^{(1)}) = |z) + P_p^{(1)}|p) + P_a^{(1)}|a) + P_b^{(1)}|b) \\
\approx& |z) - \frac{1}{2\gamma_p}\left[(2N_{\downarrow i} - 1)\,\partial_t N_{\uparrow z} + (2N_{\uparrow i} - 1)\,\partial_t N_{\downarrow z} + \frac{1}{2}\partial_t p_z\right]|p) \\
&- \frac{1}{\gamma_a\gamma_b}\left[\left(f_{\epsilon\downarrow}^{-} + f_{U\downarrow}^{+}\right)\partial_t N_{\uparrow z} + \left(f_{\epsilon\uparrow}^{-} + f_{U\uparrow}^{+}\right)\partial_t N_{\downarrow z}\right]|c) \\
&- \frac{1}{\gamma_a\gamma_b}\left[\left(f_{\epsilon\downarrow}^{+} + f_{U\downarrow}^{-}\right)\partial_t N_{\uparrow z} - \left(f_{\epsilon\uparrow}^{+} + f_{U\uparrow}^{-}\right)\partial_t N_{\downarrow z}\right]|s).
\end{aligned} \tag{4.14}$$

This result has a similar shape as the result in the absence of a magnetic field[1], Eq. (3.6). There are two main alterations with respect to the zero magnetic field case. First of all, the total occupation number is always separated into an occupation number for spin-up and -down electrons respectively. This is the expected behaviour, since the magnetic field alters the behaviour of the spin-up and -down electrons in a different way. We saw this already in the switching case, Sec. 4.3. Secondly, we see that both the operators $|c)$ and $|s)$ appear, with a prefactor that combines the rates γ_a and γ_b. The spin mode appears because the magnetic field lifts the spin-independence in the system. The appearance of both rates γ_a and γ_b in the prefactors can be seen as yet another consequence of the mixing of the spin and charge mode. The result (4.14) is used in the next subsection to calculate the instantaneous currents and their first adiabatic corrections.

[1] It also reduces to that result in the limit $B \to 0$, as it should.

4.4.2 Particle current

We now calculate the particle current, in the same way as we did in chapter 3. The calculation becomes more complicated however, since the charge mode is not longer an eigenmode of the kernel. Nevertheless, starting from Eq. (3.7), we can still find a general equation by splitting the amplitude covector $(N|$ into a spin-up and -down component:

$$I_{N\alpha} = (N|W_\alpha|\rho(t)) = (N_\uparrow|W_\alpha|\rho(t)) + (N_\downarrow|W_\alpha|\rho(t)).$$

In this way, we find after some algebra the general result

$$I_{N\alpha} = \gamma_{c\uparrow\alpha}\left(N_{\uparrow z\alpha} - (N_\uparrow|\rho(t))\right) + \gamma_{c\downarrow\alpha}\left(N_{\downarrow z\alpha} - (N_\downarrow|\rho(t))\right), \tag{4.15}$$

where we defined the new rates

$$\begin{aligned}\gamma_{c\uparrow\alpha} &= -(c'_\alpha|W_\alpha|x_\alpha) = \Gamma_{\uparrow\alpha} + f^+_{\epsilon\downarrow\alpha} - f^+_{U\downarrow\alpha}\\ \gamma_{c\downarrow\alpha} &= -(c'_\alpha|W_\alpha|y_\alpha) = \Gamma_{\downarrow\alpha} + f^+_{\epsilon\uparrow\alpha} - f^+_{U\uparrow\alpha}.\end{aligned}$$

The details of this derivation can be found in App. B.5.

We now need to be careful with the interpretation of these rates. $\gamma_{c\uparrow\alpha}$ denotes the total charge decay rate restricted to lead α *due to* spin-up occupation of the dot. It is thus *not* the charge decay rate *of* spin-up particles. Similarly, $\gamma_{c\downarrow\alpha}$ is the total charge decay rate restricted to lead α *due to* spin-down occupation of the dot.

Notice that the current equation (4.15) is written in the same structure as the corresponding equation without a magnetic field, Eq. (3.8). The only important difference lies in the separation into a term related to the spin-up and -down electrons. Be aware however: because of the specific interpretation of $\gamma_{c\uparrow\alpha}$ and $\gamma_{c\downarrow\alpha}$, these two terms do not correspond to the spin-resolved currents. Rather, they are the currents as a result of the occupation of the dot by respectively spin-up or -down electrons. By rearranging the terms of the particle current expression, we can however also express it as the sum of the spin-resolved currents:

$$I_{N\alpha} = I_{N\uparrow\alpha} + I_{N\downarrow\alpha}.$$

Detailed expressions for the spin-resolved currents can again be found in the appendix B.5. Each of these spin-resolved currents contain a part of both charge decay rates $\gamma_{c\uparrow\alpha}$ and $\gamma_{c\downarrow\alpha}$. This means that each spin-resolved current depends on the occupation of the dot with the same spin, as well as the dot occupation with the opposite spin. This effect arises due to the on-site interaction U between the two particles of opposite spin.

Now that we have a general form for the particle current through lead α, we can use the explicit expression for the density operator up to first order in $\frac{\Omega}{\Gamma}$, Eq. (4.14), to get explicit results. The instantaneous particle current and its first adiabatic correction are

$$\begin{aligned}I^{(0)}_{N\alpha} &= \gamma_{c\uparrow\alpha}\left(N_{\uparrow z\alpha} - N_{\uparrow z}\right) + \gamma_{c\downarrow\alpha}\left(N_{\downarrow z\alpha} - N_{\downarrow z}\right)\\ I^{(1)}_{N\alpha} &= \frac{1}{\gamma_a\gamma_b}\left[\gamma_{c\uparrow\alpha}\Gamma_\downarrow - \gamma_{c\downarrow\alpha}\left(f^+_{\epsilon\downarrow} - f^+_{U\downarrow}\right)\right]\partial_t N_\uparrow + \frac{1}{\gamma_a\gamma_b}\left[\gamma_{c\downarrow\alpha}\Gamma_\uparrow - \gamma_{c\uparrow\alpha}\left(f^+_{\epsilon\uparrow} - f^+_{U\uparrow}\right)\right]\partial_t N_\downarrow.\end{aligned}$$

Spin-resolved equations are again given in the appendix. As expected, the first order correction depends on the time derivatives of both the spin-up and -down occupation

numbers, as well as the two rate γ_a and γ_b (since the previous charge related rate γ_c gets mixed into these rates). Just as in the non-magnetic limit Eq. (3.11), the parity mode does not appear yet, since it is related to many-particle effects that do not enter the particle current as a single-particle quantity.

4.4.3 Energy and heat current

To conclude this chapter on the dynamics of a quantum dot when placed in an external magnetic field, we present the energy and heat currents through such a system. We focus on the energy current, since the heat current can simply be obtained from $I_{Q\alpha} = I_{E\alpha} - \mu_\alpha I_{N\alpha}$. The energy current is given by Eq. (3.12):

$$I_{E\alpha} = (H|W_\alpha|\rho).$$

Because of the lifted spin-degeneracy, the Hamiltonian is now different:

$$(H| = \epsilon_\uparrow (N_\uparrow| + \epsilon_\downarrow (N_\downarrow| + U(2|.$$

A calculation similar to the one that leads to Eq. (3.15) results in

$$I_{E\alpha} = (\epsilon_\uparrow + U\,(1 - N_{\downarrow i\alpha}))\, I_{N\uparrow\alpha} + (\epsilon_\downarrow + U\,(1 - N_{\uparrow i\alpha}))\, I_{N\downarrow\alpha} - U\gamma_{p\alpha}(p'_\alpha|\rho). \tag{4.16}$$

Details of this calculation are given in App. B.6. From the fact that $N_{\bar{\sigma} i\alpha}$ appears in the prefactor of the particle current of the opposite spin $I_{N\sigma\alpha}$, we see that the dynamics of spin-up and -down electrons are coupled through the interaction U. Also here we point out the similarity of Eq. (4.16) with its spin-degenerate counterpart Eq. (3.15). The tight-coupling contributions get split up in spin-resolved contributions. The prefactors of the tight-coupling terms have now a particularly clear interpretation. Every electron with spin σ carries an energy ϵ_σ. When the occupation of the level $\epsilon_{\bar{\sigma}}$ with opposite spin with respect to lead α is high enough (so $N_{\bar{\sigma} i\alpha} \approx 0$), the electron carries also the additional charging energy U. This can be explained based on the model: double occupation of the dot is necessary for the on-site repulsive interaction to be present. The energy current equation (4.16) provides us with the analytical expression of this fact.

Expressions for the energy current in zeroth and first order in $\frac{\Omega}{\Gamma}$ are not discussed here because of their lengthy nature. Nevertheless, they can be found (together with their derivation) in App. B.6.

5 Increasing thermoelectric efficiency by introducing time-dependence

The very general theoretical results that we obtained in the previous chapters can be used to study a wide variety of electronic nanosystems. This is the first of two chapters in which we use them to investigate a specific problem. The results in these chapters are preliminary, since the research is still on-going. As such, they should be considered as outlooks on a few of the many possibilities arising from the results obtained in this thesis.

5.1 Thermoelectric performance of time-dependent systems

The thermoelectric effect refers to the phenomenon in which an applied temperature gradient over a (nanoscale) structure generates a voltage gradient. This voltage gradient can then in turn be used to power an electrical device. The thermoelectric effect can thus be used to convert (waste) heat into useful electrical power. This is especially interesting for waste heat recovery in modern IC chips that must be cooled externally to avoid overheating. A review of this effect, specifically for quantum dots, can be found in [38]. The thermoelectric efficiency is defined as the ratio between the useful energy that is delivered to the electrical device and the heat absorbed from the source of the thermoelectric device. Optimising the thermoelectric efficiency is most often achieved by changing the used materials while operating the device in the steady state. In this stationary regime, the achieved efficiencies stay however insufficient for most practical applications [44].

More recent theoretical studies focussed on thermoelectrics in time-dependently driven nanosystems [31, 45–49]. They all study slightly different systems with varying assumptions on the exact time-dependence and other system parameters. Most of them use a Green's function formalism to calculate the thermoelectric quantities of interest. Here, we will mainly connect to the paper by Zhou et al. [31], in which the authors study the dynamic thermoelectric efficiency in a quantum dot system with time-dependent control[1] over the gate. Interestingly, they find that in certain regimes a boost of the thermoelectric efficiency is possible as a result of the induced time-dependence. The very general formulas for particle and heat current that were derived in this thesis (Sec. 3.2) provide an excellent and well-manageable alternative to the Green's function formalism used in [31]. While our approach is limited to weak tunnel coupling, $\Gamma \ll T$, it can account for

[1] This external input driving is not taken into account as an input energy when calculating the efficiency. One can imagine it to be some waste force induced by a nearby system.

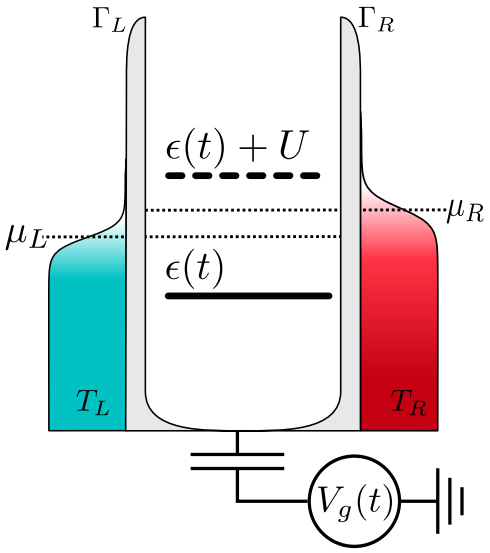

Figure 5.1: *The system under consideration in this chapter. The driving of the dot level $\epsilon(t)$ is explicitly given by $V_g(t)$. The applied voltage bias is small: $\mu_{\mathrm{R}} = \mu_{\mathrm{L}} + \Delta\mu$, with $\Delta\mu \ll \mu_{\mathrm{L}}$. In addition, a small temperature gradient is applied such that $T_{\mathrm{R}} = T_{\mathrm{L}} + \Delta T$, with $\Delta T \ll T_{\mathrm{L}}$.*

a large on-site Coulomb interaction $U \gg T$ which becomes a crucial ingredient of the heat current in the case of time-dependent driving with sudden voltage switches [29]. In this chapter, we give an outline on how the thermoelectric efficiency of a quantum dot with strong on-site interaction can be calculated using the formulas that were presented in this thesis. As in [31] and as detailed in the following, we assume small gradients in chemical potential and temperature, allowing us to a employ a linear response theory for which we need to determine the corresponding Onsager coefficients.

5.2 Linear response theory and Onsager reciprocal relation

We consider a quantum dot, such as shown in Fig. 5.1. The dot level ϵ is driven by a gate potential $V_g(t)$. The system is subject to a small bias in electrochemical potential $\Delta\mu \ll \mu$ as well as a small temperature bias[1] $\Delta T \ll T$, such that $\mu_{\mathrm{R}} = \mu_{\mathrm{L}} + \Delta\mu$ and $T_{\mathrm{R}} = T_{\mathrm{L}} + \Delta T$. We also denote $T_{\mathrm{L}} = T$ and $\mu_{\mathrm{L}} = \mu$. In this regime with small biases, linear response theory allows for a characterisation of the electrothermal properties of the electronic system [50]. Indeed, a linear expansion in $\Delta\mu$ and ΔT of the charge and heat currents $I_{N\alpha}$ and $I_{Q\alpha}$ through the lead α gives

$$\begin{bmatrix} I_{N\alpha} \\ I_{Q\alpha} \end{bmatrix} = \begin{bmatrix} I^D_{N\alpha} \\ I^D_{Q\alpha} \end{bmatrix} + \begin{bmatrix} G_\alpha & L_\alpha \\ M_\alpha & K_\alpha \end{bmatrix} \begin{bmatrix} \Delta\mu \\ \Delta T \end{bmatrix}. \tag{5.1}$$

[1] Notice that we never had a temperature bias before in this thesis, but all theory remains equally valid.

Here we used matrix notation to make the structure more clear. The first vector on the right-hand side represents the displacement currents

$$I^D_{N\alpha} = I_{N\alpha}|_{\Delta\mu=\Delta T=0} \qquad I^D_{Q\alpha} = I_{Q\alpha}|_{\Delta\mu=\Delta T=0}\,.$$

These currents account for the transport of charge and heat that is exclusively due to the time-dependent driving $V_g(t)$, even in the absence of electrochemical or thermal gradients, and hence do not appear in a usual, time-independent linear response theory.

The effect of the small biases on the system is given by the last term of Eq. (5.1). In a time-independent theory, the matrix that appears here is the so-called the Onsager matrix; here, we extend the definition of its elements – the Onsager or kinetic coefficients that characterise the thermal and electric response of the quantum dot in the linear regime – to the time-dependent regime. More precisely, the coefficients are defined as the low-bias limit of the derivatives of the *time-dependent* charge and heat currents with respect to both temperature and electrochemical potential biases:

$$\begin{aligned} G_\alpha &= \left.\frac{\partial I_{N\alpha}}{\partial\Delta\mu}\right|_{\Delta\mu=\Delta T=0} & L_\alpha &= \left.\frac{\partial I_{N\alpha}}{\partial\Delta T}\right|_{\Delta\mu=\Delta T=0} \\ M_\alpha &= \left.\frac{\partial I_{Q\alpha}}{\partial\Delta\mu}\right|_{\Delta\mu=\Delta T=0} & K_\alpha &= \left.\frac{\partial I_{Q\alpha}}{\partial\Delta T}\right|_{\Delta\mu=\Delta T=0}. \end{aligned} \tag{5.2}$$

The diagonal coefficients G_α and K_α are the electrical and thermal conductances, respectively. The off-diagonal ones, L_α and M_α, are the thermoelectric and electrothermal conductances. The latter quantify heat to charge current conversion (Seebeck effect) and charge current to heat conversion (Peltier effect). The larger L_α (M_α), the larger is the electrical (heat) current produced by a temperature gradient ΔT (voltage bias $\Delta\mu$) between the leads. Importantly, whenever micro-reversibility (time-reversal symmetry) is fulfilled by the system, L_α and M_α are not independent. They satisfy the so-called Onsager reciprocal relation [50, 51]

$$M_\alpha = T\ L_\alpha. \tag{5.3}$$

As soon as time-reversal symmetry is broken, this relation does not always hold any more, implying in particular that it does not any more *restrict* the achievable efficiencies in the same way. This breaking of time-reversal symmetry is exactly what we introduce by having a time-dependent driving scheme!

5.3 Onsager coefficients in stationary limit

We now show the results for the Onsager coefficients through the system of Fig. 5.1 in the stationary, time-independent limit. Already in this stationary regime, the notation in terms of modes and observables introduced in this thesis is very insightful. Results for a switch case, such as described in Sec. 2.4 have also been obtained already. These expressions still need some further investigation however, and are not shown here. In the limit $t \to \infty$ they reduce to the stationary Onsager coefficients that we discuss now.

The stationary currents $I_{N\alpha}^{(0)}$ and $I_{Q\alpha}^{(0)}$ are given by formulas (3.9), (3.17) and (A.4)[1]. By calculating the derivatives of these currents with respect to the voltage bias and temperature gradient according to Eq. (5.2), we find all elements of the Onsager matrix in Eq. (5.1). All derivatives can be expressed in terms of known variables.

For the electrical conductance we find

$$\begin{aligned} G_\alpha^{(0)} &= \frac{\Gamma_{\bar{\alpha}}}{\Gamma}\gamma_c \left.\frac{\partial N_z}{\partial \Delta\mu}\right|_{\Delta\mu=\Delta T=0} \\ &= \frac{\Gamma_\alpha \Gamma_{\bar{\alpha}}}{2T\Gamma^3}\gamma_c(2\Gamma-\gamma_c)N_z\,(2-N_z)\,, \end{aligned}$$

where $\bar{\alpha}$ is the opposite of α. The electrical conductance thus is proportional to the charge relaxation rate γ_c and to the variation of the average electron occupation number in the dot, N_z, due to a variation of the voltage bias $\Delta\mu$.

The thermoelectric and electrothermal conductances are

$$L_\alpha^{(0)} = \frac{1}{T}G_\alpha^{(0)}\left[\epsilon-\mu+\frac{U}{2}(2-N_i)\right]$$

and

$$M_\alpha^{(0)} = G_\alpha^{(0)}\left[\epsilon-\mu+\frac{U}{2}(2-N_i)\right],$$

which satisfy the reciprocal relation Eq. (5.3), i.e. $M_\alpha^{(0)} = T\ L_\alpha^{(0)}$. A direct consequence of this reciprocal relation is that only the charge mode enters $M_\alpha^{(0)}$ [28–30], since $L_\alpha^{(0)}$ determines the charge current which in general is not affected by the parity mode. This is interesting, as the heat current from which $M_\alpha^{(0)}$ derives in principle also depends on the parity mode. Besides $G_\alpha^{(0)}$, we see that the average effective energy $\langle E_\alpha\rangle$ of every tunnelling electron (the renormalised energy in the square bracket, as we discussed in Sec. 3.2.2) gives the magnitude of the heat to charge current conversion and vice versa in this stationary state regime. In particular, the Seebeck coefficient or thermopower, which sets the voltage drop per Kelvin generated by a temperature gradient across the two leads, is

$$S_\alpha^{(0)} = \frac{L_\alpha^{(0)}}{G_\alpha^{(0)}} = \frac{1}{T}\left[\epsilon-\mu+\frac{U}{2}(2-N_i)\right] = \frac{\langle E_\alpha\rangle}{T}.$$

This result is in agreement with Mott and Matveev relations valid for a generic diffusive conductor [52, 53]. The larger $\langle E_\alpha\rangle$, the higher the electric current produced by ΔT and the larger the efficiency of this process. Moreover, because this Seebeck coefficient contains the inverted dot occupation N_i, this linear response regime quantity can provide us with a nice way to access N_i experimentally.

Finally, the thermal conductance is

$$K_\alpha^{(0)} = \frac{1}{T}G_\alpha^{(0)}\left\{\left[\epsilon-\mu+\frac{U}{2}(2-N_i)\right]^2+\left(\frac{U}{2}\right)^2 N_i\,(2-N_i)\right\}.$$

From this equation, we see that the heat produced by the temperature gradient is again proportional to $G_\alpha^{(0)}$ and the renormalised average energy squared $\langle E_\alpha\rangle^2$. The additional

[1]Indeed, if there is no time-dependence, there are only instantaneous contributions to the currents.

renormalisation factor $\frac{U}{2}N_i(2-N_i)$ originates from the fermion-parity mode. As discussed in Sec. 2.3, N_i is typically 0 or 2. This means that this additional renormalisation factor has typically a very small contribution, with the exception of a small region around the particle-hole symmetric point.

5.4 Outlook

As mentioned before, the Onsager coefficients for a fast switch case have also been calculated. These results are still work in progress and we are cross-checking them with the corresponding data from [31] in the limit $U \to 0$. It is remarkable that our formalism allows to write down *analytical* expressions for the quantities involved, whereas the final results in [31] had to be obtained numerically. These analytical expressions can hopefully tell us something more about the origin of the increase in efficiency. The system studied in [31] does not take into account an on-site interaction U. We want to see which effect this additional interaction has on the thermoelectric efficiency, and more generally on the Onsager coefficients.

6 Signatures of fermion-parity mode and inverted dot model

In chapters 2 to 4, we have shown the theoretical approach of this thesis to be a very useful tool in the study of the dynamics of a quantum dot with a general time-dependent driving. However, several recent works [27–30, 32] have pointed out that the main concepts of this approach – the fermion-parity mode [28, 54, 55] and the inverted dot model [29, 30] – also have important practical consequences for experiments measuring the energy emitted via electron tunnelling from a quantum dot after a fast level switch. One possible example is already approached in chapter 5. With the core result of this thesis at hand, we have been able to extend this analysis of the experimental relevance to moderately fast, but otherwise completely *arbitrary* time-dependent driving schemes. Our main finding, as discussed and explained in detail in the following sections, is that the average heat current flowing from the dot per driving cycle typically *does not* exhibit features that can unambiguously be related to the fermion-parity mode or the inverted model. On the one hand, this shows that the study of time-resolved currents after sudden level shifts seem more suitable to find experimental evidence for the underlying fundamental fermion-parity duality relation [29]. On the other hand, it also yields a more concrete picture for the specific elements in experiments and applications for which the physical implications of the parity mode have to be taken into account. As already noted in the previously mentioned works, a minimum requirement for the fermion-parity mode to play a role is that two-particle effects are at play. The following treatment thus mainly focusses on the energy (heat) current which directly contains the Coulomb interaction energy as a two-particle contribution.

6.1 Stationary features

Since even the instantaneous (stationary) energy current $I^{(0)}_{E\alpha}$ as written in Eq. (A.4) contains variables that are directly related to the inverted dot model, it is already worth studying whether this stationary limit exhibits any clearly visible features. This is of particular interest for experiments, as the measurement of a *stationary* current is more feasible than the measurement of time-resolved currents. In this section, we therefore focus on a system that is not time-dependently driven. To be able to study the contributions of different quantities of the inverted dot model ($N_{i\alpha}$ and $p_{i\alpha}$) in $I^{(0)}_{E\alpha}$, we separate the latter into different terms:

$$\begin{aligned} I^{(0)}_{E\alpha} = &(\epsilon + U)\, I^{(0)}_{N\alpha} - \frac{U}{2}\gamma_{p\alpha}\left(\frac{p_z}{2} - N_z + 1\right) \\ &- \frac{U}{2}\left[\gamma_{c\alpha}\left(N_{z\alpha} - N_z\right) + \gamma_{p\alpha}\left(N_z - 1\right)\right] N_{i\alpha} - \frac{U}{4}\gamma_{p\alpha} p_{i\alpha}. \end{aligned} \tag{6.1}$$

Here, the terms on the first line do not contain any inverted dot model quantities, while on the second line two terms containing $N_{i\alpha}$ and $p_{i\alpha}$ are separated. Figure 6.1 shows all relevant variables appearing in this equation as a function of ϵ for one of the two leads (left) to which the dot is coupled. It was already discussed in connection to Fig. 2.3 that $N_{i\mathrm{L}}$ only shows a (strong) ϵ-dependence around $\epsilon = \mu_{\mathrm{L}} - \frac{U}{2} \equiv \epsilon_s$ (the particle-hole symmetric point). Also $p_{i\mathrm{L}}$ has its only feature around this same ϵ_s. From Fig. 6.1 it is immediately clear that in none of the considered cases a sudden increase/decrease (signature of N_{iL}, second row) nor a local minimum/maximum (signature of p_{iL}, third row) can be seen in $I^{(0)}_{EL}$ around $\epsilon = \epsilon_s$ (top row). As argued in the following, this holds more generally for all the situations in which our dot model is valid.

To this, let us estimate the terms in the second line of Eq. (6.1), which could in principle contain signatures of the inverted model. We start with the contribution proportional to $N_{i\alpha}$. Expressing all terms explicitly in terms of Fermi-functions, one can show that for a level position set to the signature point ϵ_s, the prefactor is bounded as

$$\left|\frac{U}{2}\left[\gamma_{c\alpha}\left(N_{z\alpha} - N_z\right) + \gamma_{p\alpha}\left(N_z - 1\right)\right]\right| \leq \Gamma_\alpha \left|U\right| \exp\!\left(-\frac{U}{2T}\right).$$

The factor in front of $N_{i\alpha}$ is algebraically suppressed for $U \ll T$, and even exponentially suppressed when $U \gg T$. Since $N_{i\alpha}$ itself is bounded by the maximal dot occupation 2, the term can only become relevant in the regime $U \approx T$ in which any possible signature of the inverted model at ϵ_s is already too smeared to be clearly distinguishable (see also Fig. 6.1).

The observable $p_{i\alpha}$ is almost always 1, as the attractive interaction in the inverted dot model prohibits a stable single occupation. At the point $\epsilon = \epsilon_s$, $p_{i\alpha}$ reaches a global minimum. Its deviation from 1 at this point can be shown to be limited by

$$\left|1 - p_{i\alpha}\right| \leq 2 \exp\!\left(-\frac{U}{2T}\right). \tag{6.2}$$

This confirms again Fig. 6.1, showing that the deviation from unity is exponentially suppressed when $U \gg T$. For higher temperatures, the signature becomes larger, but again also more smeared out due to thermal broadening. It can again not be distinguished.

Our first main conclusion is thus that the contributions related to the parity mode and the inverted dot model are either very small or indistinguishable from other features, and hence do not play any role for experiments or applications which rely on the *stationary* energy current in the absence of time-dependent driving. On the one hand, this result is consistent with the fact that the time scales of the charge mode, γ_c, and the parity mode, γ_p, do not play a role in the stationary long-time limit, since this limit is time-independent. On the other hand, recalling that the effect of the parity mode on the transient heat current in the highly *non-stationary* situation after a sudden level switch is substantially different from that of the charge mode, our finding immediately gives rise to the question how the transition from the completely stationary case to the transient behaviour in the switch case takes place. With the main result of this thesis at hand, we can now analytically explore this transitional regime of moderately fast time-dependent driving. This enables us, in the following, to narrow down the conditions under which the parity mode becomes essential for the physical description.

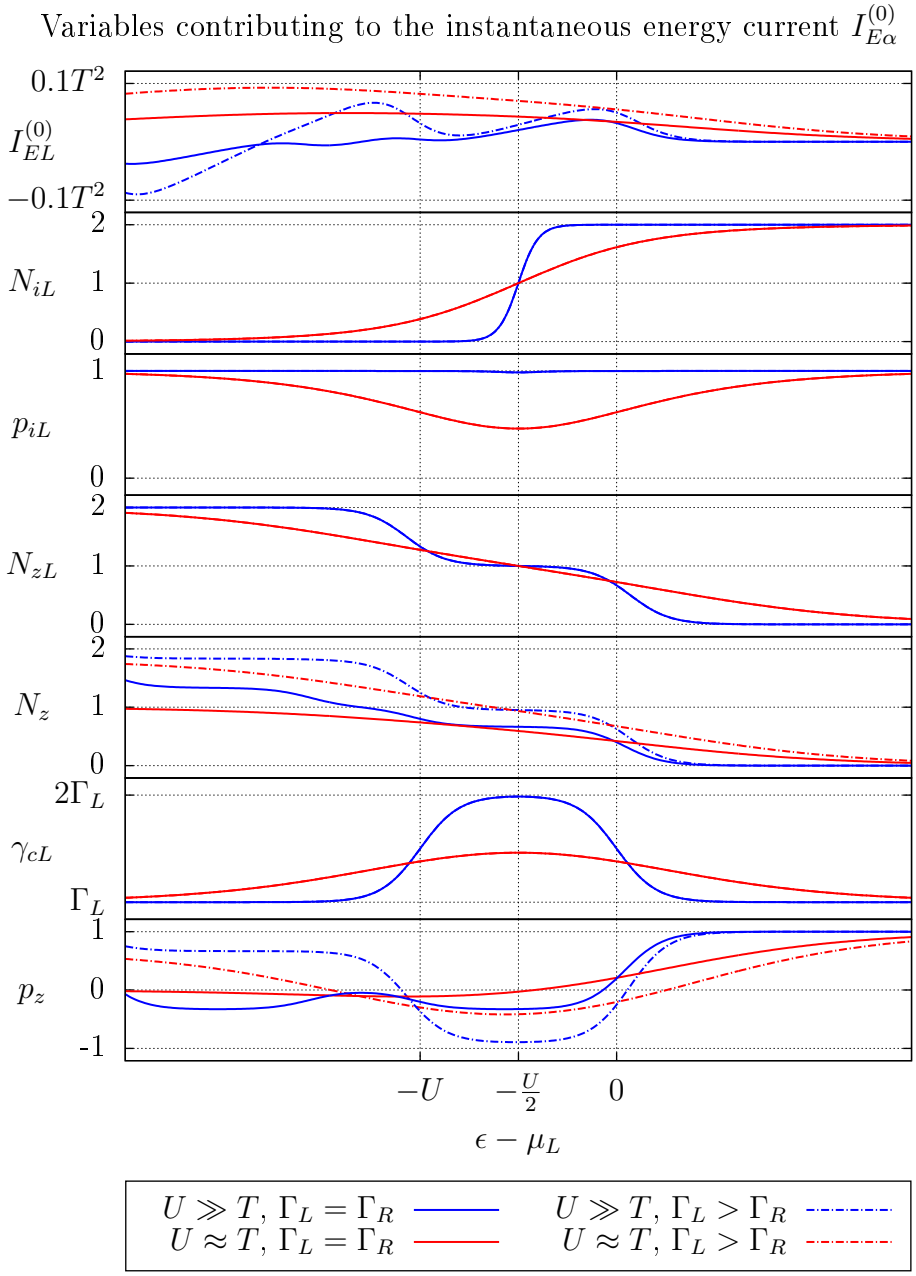

Figure 6.1: *All non-constant variables that appear in equation (6.1) as a function of ϵ. The plots are for the case of a dot coupled to only two leads ($\alpha = \mathrm{L}, \mathrm{R}$), with $\mu_\mathrm{L} > \mu_\mathrm{R}$. The on-site interaction U is such that $\mu_\mathrm{L} - \mu_\mathrm{R} \gg U$. All plots are made in two temperature regimes: one in which $T \ll U$ (blue curves) and one in which $T \approx U$ (red curves) was chosen such that the factor in front of $N_{i\alpha}$ in Eq. (6.1) would be maximal. Next to different temperature regimes, the dependence is also plotted for varying coupling strength to the different leads. For the solid lines, the coupling strength to both leads is the same ($\Gamma_\mathrm{L} = \Gamma_\mathrm{R}$). The dashed lines show the situation for a much (ten times) stronger coupling to the left lead than to the right lead ($\Gamma_\mathrm{L} > \Gamma_\mathrm{R}$). In case there is no dashed line drawn, the values for asymmetric coupling coincide with those of the symmetric coupling. The variables are plotted for the left lead ($\alpha = \mathrm{L}$). We are interested in signatures of N_{iL} or p_{iL}. These signatures are expected to be seen around $\epsilon_s = \mu_L - \frac{U}{2}$, so only a limited interval centred on this ϵ is shown.*

6.2 Tight coupling in small bias regime

To introduce non-stationary conditions into the system, we consider a driven quantum dot for which it is sufficient to study the time evolution only up to a finite non-vanishing order n in the adiabatic expansion parameter $\frac{\Omega}{\Gamma}$. The non-instantaneous energy current contributions are then given by Eq. (3.16):

$$I_{Q\alpha}^{(n)} \overset{n\neq 0}{=} \underbrace{\left[\epsilon - \mu_\alpha + \left((2|c_\alpha) + \frac{\gamma_{p\alpha}}{\gamma_{c\alpha}}(p'_\alpha|c)\right) U\right] I_{N\alpha}^{(n)}}_{\text{TC}} \underbrace{-\gamma_{p\alpha} U (p'|\rho^{(n)})}_{\text{NTC}}, \tag{6.3}$$

where (N)TC is the (non-)tight coupling contribution to this current, as we discussed in Sec. 3.2.2. In this equation, the fermion-parity mode is clearly present in the last, non-tight coupling term. We know that the fermion-parity mode is only expected to play a role when two-particle effects are present. Such two-particle effects can be expected when the driving frequency is sufficiently high. The parity-related NTC term is shown time-resolved in Fig. 6.2(a), where no bias is applied across the leads and only the dot level is driven as $\epsilon(t) = \bar{\epsilon} + \delta\epsilon \sin(\Omega t)$ with driving amplitude $\delta\epsilon = 0.1U$. As can be seen in the figure, this term shows a clear time-dependent pattern. Performing these kind of time-resolved measurements on the energy or heat current is infeasible in an experimental setting. Experimentally, there are typically two relevant types of measurements possible.

Either one filters out specific components, which corresponds to measuring the Fourier spectrum of the signal. The frequency spectrum of the non-tight coupling term is different from the other terms in Eq. (6.3). The main distinction of the NTC term with respect to other contributions is namely that it is made up of less frequency components. Nevertheless, we could show (not specifically discussed here), that it is not possible to detect these differences in an experiment.

Alternatively, one can average the results over one driving cycle. The average current per period is defined as

$$\bar{I}_{X\alpha} = \frac{1}{\mathcal{T}} \int_t^{t+\mathcal{T}} \mathrm{d}t' I_{X\alpha}(t'),$$

where $\mathcal{T} = \frac{2\pi}{\Omega}$ is the driving period, t any time during the periodic driving and X can represent either the particle, energy or heat current. Fig. 6.2(b) shows the exact numerically calculated average heat current $\bar{I}_{Q\alpha}$ (see Sec. 3.1.1) for all orders in $\frac{\Omega}{\Gamma}$ as a function of the average energy level $\bar{\epsilon}$. The plots are in the absence of an applied bias over the leads. As such, no stationary current is present. Moreover, since this is a single-parameter periodic driving, the lowest order non-vanishing contribution in $\frac{\Omega}{\Gamma}$ will be $n = 2$ [56]. This second order contribution to the average heat current $\bar{I}_{Q\alpha}^{(2)}$ is shown in Fig. 6.2(b). This same figure also shows the NTC contribution to this current.

Importantly, the lowest order contribution $\bar{I}_{Q\alpha}^{(2)}$ is already very close to $\bar{I}_{Q\alpha}$. It is more generally true that a few low order corrections give already a very good approximation of the full currents. This is in favour of the formalism presented in this thesis, since it means that even with a very limited number of contributions in $\left(\frac{\Omega}{\Gamma}\right)^n$ a good convergence can be achieved.

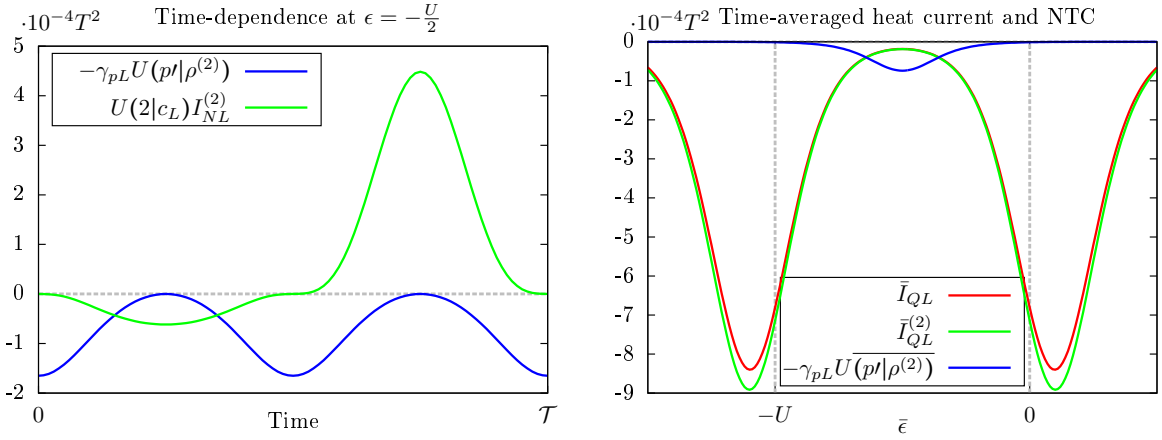

(a) **(b)**

Figure 6.2: *Plots for quantum dot coupled to two leads, without an applied bias. The on-site interaction is* $U = 10T$ *and the coupling strengths are* $\Gamma_{\mathrm{L}} = \Gamma_{\mathrm{R}} = 0.1T$*. The dot level is driven as* $\epsilon(t) = \bar{\epsilon} + \delta\epsilon \sin(\Omega t)$*, with driving amplitude* $\delta\epsilon = 0.1U$ *and frequency* $f = \frac{\Omega}{2\pi} = 0.01$*. Different quantities of Eq. (6.3) and* $\bar{I}_{Q\alpha}$ *are shown* **(a)** *time-resolved at the particle-hole symmetric point* $\bar{\epsilon} = -\frac{U}{2}$ *and* **(b)** *averaged over a driving period as function of average dot level* $\bar{\epsilon}$*.*

Notice that the signature related to the parity mode (i.e. the signature of the NTC term at the particle-hole symmetric point $\bar{\epsilon} = -\frac{U}{2}$) can not be distinguished in the heat current $\bar{I}^{(2)}_{Q\alpha}$. It turns out that the two terms of the heat current Eq. (6.3) plotted in a time-resolved way in Fig. 6.2(a) exactly cancel in the time-average at the particle-hole symmetric point, such that the signature can not be seen in Fig. 6.2(b). This means that, while there is a non-tight coupling contribution for the time-resolved heat current, it is not present any more in the averaged heat current. This is remarkable, since electrons can have either an energy ϵ or $\epsilon + U$ and therefore no tight coupling between the particle and heat current is in general expected.

In the case without applied voltage bias between the leads, the cancellation of the NTC term can be understood from the fact that the same charging energy U (which is itself time-independent) is both emitted and absorbed again during each driving period. This adds up to a zero operation in the average over a driving period. To show this in a mathematically more rigorous way, we start from Eq. (3.12):

$$I_{E\alpha}(t) = \epsilon(N|W_\alpha|\rho(t)) + U(2|W_\alpha|\rho(t)). \tag{6.4}$$

The second term of Eq. (6.3) that we are interested in originates from the last term in this equation. However, without a bias and without an asymmetry in the couplings Γ_α, all leads are equivalent for the system. Considering that there are two leads, we can thus write $W_\alpha = \frac{1}{2}W$. The last term in Eq. (6.4) can thus be calculated as

$$U(2|W_\alpha|\rho(t)) = \frac{U}{2}(2|W|\rho(t)) = \frac{U}{2}(2|\frac{\mathrm{d}}{\mathrm{d}t}|\rho(t)) = \frac{\mathrm{d}}{\mathrm{d}t}\left(\frac{U}{2}(2|\rho(t))\right),$$

where we used the Born-Markov master equation (2.7) in the second equality and the crucial fact that we assume the local interaction U to be time-independent in the third

equality. The long-time limit of the Born-Markov solution $|\rho(t))$ is periodic in time (since the driving parameter is periodic). This implies in particular that any order in the expansion in $\frac{\Omega}{\Gamma}$ is periodic in time. Moreover, as a consequence $\frac{U}{2}(2|\rho(t))$ has the same periodicity. Hence, taking the time-integral over a period $\mathcal{T}$ gives

$$\int_t^{t+\mathcal{T}} \mathrm{d}t \frac{\mathrm{d}}{\mathrm{d}t}\left(\frac{U}{2}(2|\rho(t))\right) = \left[\frac{U}{2}(2|\rho(t))\right]_t^{t+\mathcal{T}} = 0 = \int_t^{t+\mathcal{T}} \mathrm{d}t U(2|W_\alpha|\rho(t)).$$

From this we thus conclude that the second term of Eq. (6.3) cancels with other contributions to the energy or heat current in any order of $\frac{\Omega}{\Gamma}$ when no bias is applied. When there is a small applied bias $V \ll U$, this cancellation is not exact any more in the average over a period, but the remainder is still orders of magnitude smaller than $\bar{I}^{(2)}_{Q\alpha}$. This can again be understood from the fact that the difference in electrochemical potential between the leads is small, such that effectively the heat dissipation due to the charging energy U that is being emitted and absorbed again during each driving period is still the same.

The important conclusion with respect to experiments that we should draw is that the *time-averaged* currents, under single-parameter driving when only a small bias is applied, appear as if they are tightly coupled. For experiments of this type, the parity mode is thus still not essential for a physical description of the currents. In the mathematical analysis in this section, some conditions were posed on the system's parameters. These give an essential guideline on how to proceed to find characteristic features of the parity mode and the NTC term. First, in Sec. 6.3 we explore the characteristics of this term when a larger bias V is applied over the dot. This breaks the symmetry between the different leads. Secondly, in Sec. 6.4 we investigate the influence of a time-dependent on-site interaction U, which breaks the argument that the same constant U is both emitted and absorbed during each cycle. In this last section we also explore the possibility to break the directional symmetry by specific multi-parameter driving schemes.

6.3 Signatures under large bias

The mathematical cancellation argument made in the previous section can be broken upon the introduction of an asymmetry between the left and the right lead such that $W_\alpha \neq \frac{1}{2}W$. In this section, we break this directional symmetry by applying a large voltage bias over the attached leads. Because of the large bias, the charging energy is most often provided by the lead with the highest electrochemical potential, while it is emitted in the other lead, which might give a more interesting way of seeing the NTC term. In Fig. 6.3, the NTC term of Eq. (6.3) in lowest order contribution (apart from the instantaneous one) is shown under the same conditions as those in the previous section, but now with applied voltage biases ranging from $V = 0.4U$ up to $V = 1.6U$ (where the bias V is positive when $\mu_\mathrm{L} > \mu_\mathrm{R}$).

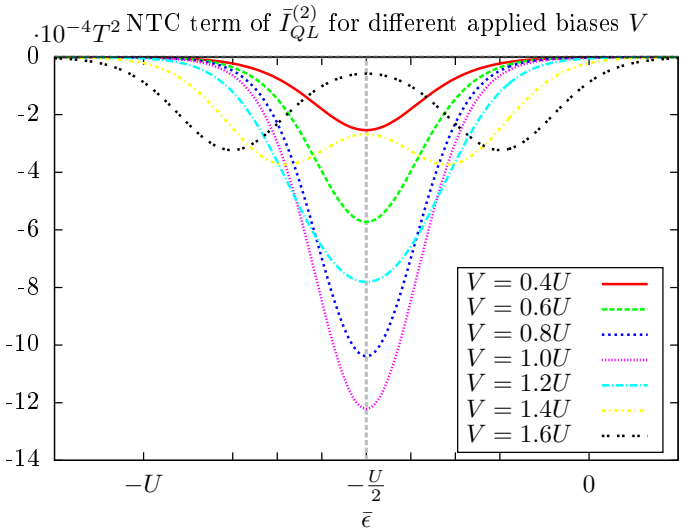

Figure 6.3: *Averages over a cycle period of the NTC term in Eq. (6.3), for different applied biases V between the left and right lead. Other parameters are the same as described in Fig. 6.2. The ticks on the horizontal axis show the resonances with the leads $\bar{\epsilon} = \mu_\mathrm{R}$ and $\bar{\epsilon} = \mu_\mathrm{L} - U$ for $V \geq U$. The two outermost unlabelled ticks are for the case $V = 1.6U$.*

For a bias $V < U$, which means that not both ϵ and $\epsilon + U$ can be within the bias window at the same time, the signature of the NTC term stays the same as before. This means that it is located at the particle-hole symmetric point. Moreover, the magnitude of the NTC term grows with increasing bias. As demonstrated in Sec. 6.2 however, it cancels with other terms in $\bar{I}^{(2)}_{Q\alpha}$.

The nature of the NTC term changes for a large bias $V > U$, which is the situation shown in Fig. 2.1. In this case, the NTC term has two features, one at both the resonances $\bar{\epsilon} = \mu_\mathrm{R}$ and $\bar{\epsilon} = \mu_\mathrm{L} - U$. These are exactly the boundaries for the range in which both dot levels ϵ and $\epsilon + U$ are located within the bias window. These locations can be explained by looking more closely at the overlap $(p'|\rho^{(2)})$ that is present in the NTC term. In between the aforementioned resonances, all physical dot states (empty, spin-up/down or doubly occupied) are equally well possible because the dot levels are within the bias window. This also holds for the inverted stationary state $(z_i|$ that determines $(p'|$. Outside the bias window, the inverted dot model is again always empty or doubly occupied, as discussed in Sec. 2.3. This occupation outside the bias window is such that the overlap with $|z)$, and more importantly $|\rho^{(2)})$, is always vanishing. On the other hand, the correction $|\rho^{(2)})$ is only non-zero at the resonances with the leads themselves[1]. This leads us to conclude that the overlap $(p'|\rho^{(2)})$, and thus also the NTC term in Eq. (6.3), can only have contributions at the resonances $\bar{\epsilon} = \mu_\mathrm{R}$ and $\bar{\epsilon} = \mu_\mathrm{L} - U$, as can be seen in Fig. 6.3. Moreover, apart from the decay rate $\gamma_{p\alpha}$, this term is completely lead-independent, such that this observation is equally well valid in all leads.

[1]Since this is where the dot occupation changes, and thus where corrections are needed

We have thus seen that the place of the time-averaged contribution of the NTC term is inherently different in the regimes $V < U$ (as studied in the previous section) and $V > U$. In the former they occur at the particle-hole symmetric point, while in the latter they occur exactly at the resonances with the leads and do not cancel any more with other terms in Eq. (6.3). Despite the fact that no cancellation takes place in this large bias regime, the NTC contributions can not be distinguished from other contributions to the energy and heat current that also occur at these resonances. From this, we obtain the important insight that the time-averaged *relevance* of the fermion-parity mode does not substantially depend on the presence of a bias. This insight is important for two reasons. Theoretically, it suggests that the parity mode is more likely related to a collective effect that involves all leads equally (remember also that the NTC term is apart from the tunnel-coupling strength lead-independent). Heating can be an example of such a collective, non-directional effect. For experimentalists, it means that one should not expect any behaviour that is *substantially* different from the tight coupling picture. With this, we mean that one should not expect signatures at places different from those expected in a tight coupled model for the moderately fast driving considered here.

6.4 Driving multiple system parameters

We now investigate the other method proposed at the end of Sec. 6.2. This proposal was to look at more elaborate driving schemes, in which multiple system parameters are driven.

An important example of such a scheme is the situation in which both the energy level ϵ and the on-site interaction U are driven in (counter)phase. This is physically very reasonable, since a change in ϵ can lead to a different confinement of the electrons in the system, and thus to a different Coulombic repulsion. Moreover, it can break the argument from Sec. 6.2 that the *same* charging energy U is both emitted and absorbed again during one cycle. In this case, the peak of the NTC term in Fig. 6.2(b) gets skewed, and the peak of $\bar{I}^{(2)}_{Q\alpha}$ at the resonance $\bar{\epsilon} = \mu_\alpha - U$ increases (or decreases when the driving is in counterphase). This can be understood because the effective amplitude of the dot energy level $\epsilon + U$ changes when driving both ϵ and U with respect to the case where only ϵ is driven.

Other examples of multi-parameter driving schemes include (adiabatic) particle and energy pumping by time-dependently breaking the directional symmetry of the system. This can be done by driving both the left coupling strength Γ_L and ϵ out of phase. Another possibility is to drive Γ_L, ϵ as well as Γ_R, each with a $\frac{\pi}{2}$ phase difference. These schemes mimic the experiment shown in Fig. 1.3.

Even though all the simulations described in this section (of which the results are not shown here) do break the mathematical and intuitive argument given in Sec. 6.2, they still do not exhibit a clear distinguishable feature that can be attributed solely to the fermion-parity mode or the inverted dot model. The final conclusion that we should draw from all the simulations discussed in this chapter is twofold. On the one hand can the fermion-parity mode not straightforwardly be detected in an experiment using simple, moderately fast periodic driving, either because it cancels with other terms or because its features are not clearly distinguishable from the resonant behaviour typical

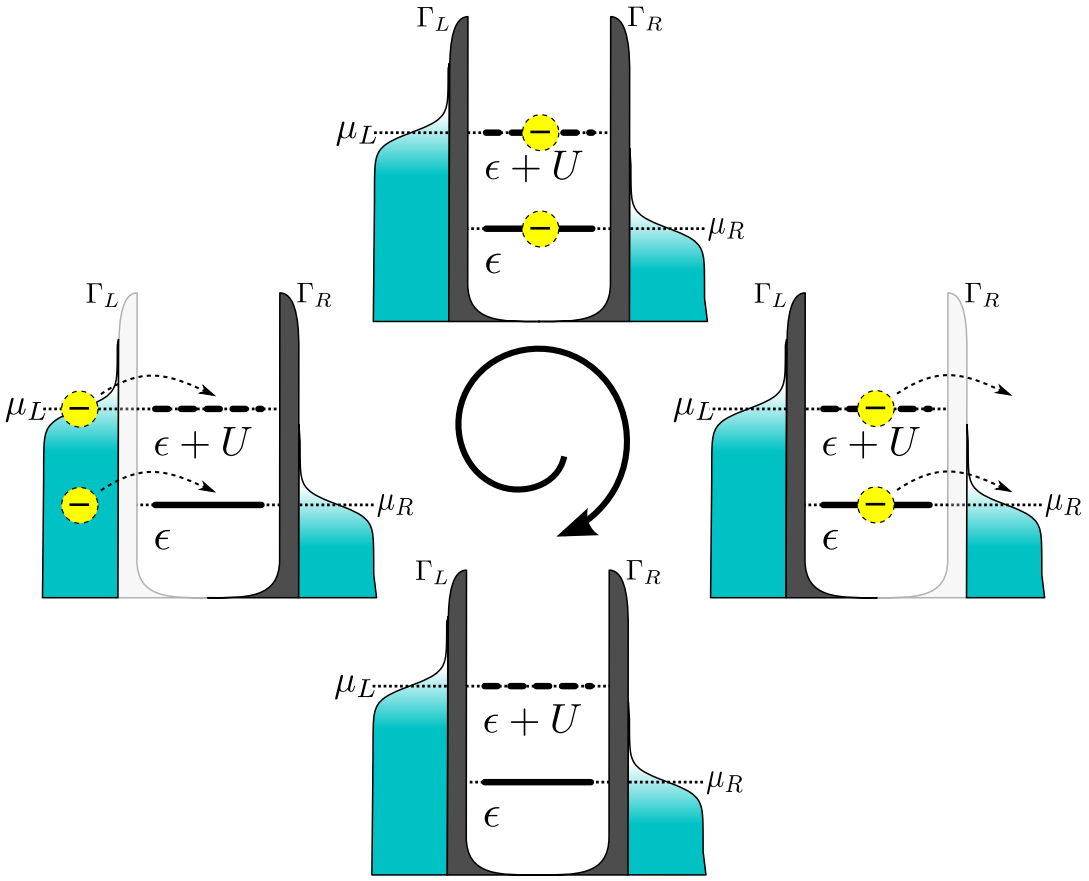

Figure 6.4: *Cyclic electron pumping scheme, in which the dot energy levels are kept constant, while the strength of the tunnel-coupling with the barriers is changed (dark (high) barrier represents weak tunnel-coupling, light (low) barrier represents strong tunnel-coupling). The scheme starts with a doubly occupied dot and two high barriers, such that the state of the dot stays fixed (top). Then the right barrier is lowered and the two electrons are given time to leave the dot (right). Next the right barrier is raised again (bottom), after which the left barrier is lowered (left). Electrons from the left are given time to enter the dot, after which the left barrier is raised again.*

for the charge mode. On the other hand however, plays the fermion-parity mode an essential role in the general description of the system dynamics presented in this thesis. This both in the derivation of the formulas, as well as in the final expressions. An important remark on this conclusion is that all driving schemes shown and studied here have one common characteristic. In all of them, the interaction of the dot with the lead involves only a single electron (even though two-particle effects are expected when the driving frequency is high enough). With this, we mean that the expected occupation of the dot differs at most by one from the instantaneous stationary occupation at every time[1]. This is important, since we know that the fermion-parity mode is associated with two-particle phenomena [28]. When real two-particle processes are involved in a periodic driving scheme, one might thus expect to find better distinguishable features related to this parity mode.

As mentioned before, the research related to this chapter is still ongoing, such that this conclusion is certainly not an endpoint. One of the possible interesting driving schemes is shown and described in Fig. 6.4. It is a driving scheme in which only the tunnel barriers are changed in strength, while the dot levels are kept both at a resonance. This periodic scheme mimics at two stages the switch case, for which it was shown in [29] that a characteristic of the parity mode can be detected. As discussed in the previous paragraph, the important point is that there are two-particle processes at play, whereas in the other schemes it was always a single level that was exchanging electrons with the leads.

[1] With the exception of the large bias case $V > U$, in which all physical states are equally probable in the stationary state.

7 Conclusion

7.1 Summary

In this thesis we have studied the dynamics of a single-level quantum dot with strong on-site interaction, weakly tunnel-coupled to multiple electronic leads. More specifically we studied the time-dependent evolution of the density operator and currents through the system for arbitrary, moderately fast driving schemes and found practical analytical solutions.

In chapter 1 we sketched the general context in which this thesis is situated. This included a description of quantum dots and their practical realisation, as well as the usefulness of studying single electron dynamics for, among others, metrology and quantum electron optics. The most important and relevant findings from the on-going research on interacting open quantum systems, in which this thesis fits, were also highlighted. Especially the newly found duality relation for a large class of fermionic open quantum systems [29] plays a key role in obtaining the results of this thesis.

In chapter 2, the general model of the quantum dot studied in this thesis was introduced, as well as some assumptions concerning this model. Next we presented the Born-Markov master equation based on a superoperator approach in Liouville space that governs the system dynamics. The eigenmodes of the system were found, based on the duality relation presented in [29]. A sudden switch case was treated, which allowed for a discussion on the different existing decay rates.

The main result of this thesis, Eq. (3.4), was then derived and discussed in chapter 3. An expansion in driving rate allowed for an analytical solution of the Born-Markov master equation for arbitrary, not necessarily periodic, driving schemes in any of the system's parameters. Together with these very general time-dependences, this main result covers a very wide range of situations. These include quantum dots with a finite local interaction U, coupled to multiple leads and with different voltage biases applied between these leads. From this main result, important analytical expressions for the currents through the system were derived. These equations are very practical in their use and have a virtually unlimited potential for studying new interesting driving schemes and understanding specific features in currents.

The quantum dot model under consideration was further extended to include the influence of an external magnetic field in chapter 4. This magnetic field lifts the spin-degeneracy of the dot energy level and introduces a spin-dependence in the tunnel-coupling strengths. We studied how the eigenmodes and decay rates of the system change under these conditions. Furthermore, we generalised the results for the density operator and currents to incorporate the spin-dependence. Expressions up to the first adiabatic correction in $\frac{\Omega}{\Gamma}$ were obtained and discussed in relation to their spin-degenerate analogues.

In chapter 5 we presented a first of two ongoing research projects enabled by the general formulas obtained in chapter 3. It concerns thermoelectrics in driven nanosystems, since recently an increased efficiency was predicted when a specific time-dependence is introduced [31]. We showed how the main results of this thesis can be used in practice to calculate Onsager coefficients, which are inherently related to the thermoelectric efficiency.

The second ongoing research project is related to the detection and a better understanding of the fermion-parity mode. In chapter 6, we discussed this and showed some specific uses of the main results of this thesis. Although we could show that the fermion-parity mode is of absolute importance for the description and derivations in this work, so far, no concrete signatures related to this mode could be distinguished in periodic driving schemes.

7.2 Open questions

Since the last two chapters of this thesis are part of ongoing research efforts, there are still many open question related to them. Concerning chapter 5, our interest is in seeing which factors contribute to the increased thermoelectric efficiency. This will enable us to narrow down the conditions for such an increased efficiency and in that way guide the study for driving schemes that provide the largest enhancement. Furthermore, it will be interesting to see whether a strong on-site interaction has an important effect on the thermoelectric behaviour, and if so, whether this effect is positive or negative for the efficiency of these nanoscale devices. In chapter 6 we already narrowed down the conditions under which the parity mode becomes essential for the physical description and experimental observations. This enabled us to propose a new driving scheme at the end of that chapter, which mimics a switch case. In that way, two-particle processes and thus the fermion-parity mode, play an enhanced role and are possibly experimentally detectable.

Further applications and questions concerning the results can be found both in the experimental reality as well as on the theory side. When in an experiment the dot energy level ϵ is being driven, it is very reasonable to assume that also other system parameters change unintentionally. This can be the on-site interaction U, but also the tunnel-coupling strength can be altered by this. It is therefore important to see how much influence this has in general on the results of an experiment and whether this has to be taken into account by an experimentalist. If these unintentional time-dependences turn out to have a substantial influence, we need to predict where and in what form they should be expected to appear in the results. Theory-wise, it is of interest to see how the main result of this thesis, Eq. (3.4), could be extended. This could be either to find a formula that is as general as this one for the spin-dependent dot model presented in chapter 4. But one can also ask the question whether a similar, general result would still be possible taking into account higher orders in the tunnel-coupling strength Γ. This would allow to describe, among others, cotunnelling and the Kondo effect.

Appendices

Appendix A

Expressions and derivations for a time-dependent, spin-degenerate quantum dot

A.1 Derivation formula $|\rho^{(n)})$

Here, we derive the general formula for $|\rho^{(n)})$ as described in the main text in Sec. 3.1.2. We start where we left in that section, namely Eq. (3.3b). To be able to do the recursion, we first take the derivative of this expression:

$$\partial_t|\rho^{(n)}) = \partial_t\left(-\frac{1}{\gamma_c}\partial_t|\rho^{(n-1)})\right) + \partial_t\left[\left(\frac{1}{\gamma_c}-\frac{1}{\gamma_p}\right)(p'|\partial_t|\rho^{(n-1)})\right]|p). \tag{A.1}$$

Repeatedly plugging this equation back into Eq. (3.3b), allows us to express $|\rho^{(n)})$ in terms of $|\rho^{(j)})$, with $n > j \geq 0$. After one iteration, we find

$$\begin{aligned}
|\rho^{(n)}) =& -\frac{1}{\gamma_c}\partial_t\left(-\frac{1}{\gamma_c}|\rho^{(n-2)})\right) - \frac{1}{\gamma_c}\partial_t\left[\left(\frac{1}{\gamma_c}-\frac{1}{\gamma_p}\right)(p'|\partial_t|\rho^{(n-2)})\right]|p) \\
&+\left(\frac{1}{\gamma_c}-\frac{1}{\gamma_p}\right)(p'|\partial_t\left(-\frac{1}{\gamma_c}\partial_t|\rho^{(n-2)})\right)|p) \\
&+\left(\frac{1}{\gamma_c}-\frac{1}{\gamma_p}\right)\partial_t\left[\left(\frac{1}{\gamma_c}-\frac{1}{\gamma_p}\right)(p'|\partial_t|\rho^{(n-2)})\right]|p) \\
=& -\frac{1}{\gamma_c}\partial_t\left(-\frac{1}{\gamma_c}|\rho^{(n-2)})\right) - \frac{1}{\gamma_p}\partial_t\left[\left(\frac{1}{\gamma_c}-\frac{1}{\gamma_p}\right)(p'|\partial_t|\rho^{(n-2)})\right]|p) \\
&+\left(\frac{1}{\gamma_c}-\frac{1}{\gamma_p}\right)(p'|\partial_t\left(-\frac{1}{\gamma_c}\partial_t|\rho^{(n-2)})\right)|p).
\end{aligned}$$

One can repeat the process by substituting Eq. (A.1) into this equation. The very general relation to express $|\rho^{(n)})$ in terms of $|\rho^{(n-k)})$ with $n \geq k \geq 1$ is then found to be:

$$|\rho^{(n)}) = \left(-\tfrac{1}{\gamma_c}\partial_t\right)^k|\rho^{(n-k)}) + \sum_{l=1}^{k}\left(-\tfrac{1}{\gamma_p}\partial_t\right)^{l-1}\left(\tfrac{1}{\gamma_c}-\tfrac{1}{\gamma_p}\right)(p'|\partial_t\left(-\tfrac{1}{\gamma_c}\partial_t\right)^{k-l}|\rho^{(n-k)})|p). \tag{A.2}$$

The special case $n = k$ gives Eq. (3.4) from the main text.

We now prove Eq. (A.2) by induction. As can be seen in Eq.(3.3b) and the subsequent calculation, the result holds for both $k = 1$ and $k = 2$. Now assume that the result holds for $k = k'$. We will show that it also holds for $k = k' + 1$, assuming $n \geq k' + 1$. Substituting the derivative equation (A.1) into equation (A.2) results in

$$\begin{aligned}|\rho^{(n)}) = &\left(-\frac{1}{\gamma_c}\partial_t\right)^{k'+1} |\rho^{(n-k'-1)}) + \left(-\frac{1}{\gamma_c}\partial_t\right)^{k'} \left(\frac{1}{\gamma_c} - \frac{1}{\gamma_p}\right) (p'|\partial_t|\rho^{(n-k'-1)})|p) \\ &+ \sum_{l=1}^{k'} \left(-\frac{1}{\gamma_p}\partial_t\right)^{l-1} \left(\frac{1}{\gamma_c} - \frac{1}{\gamma_p}\right) (p'|\partial_t \left(-\frac{1}{\gamma_c}\partial_t\right)^{k'+1-l} |\rho^{(n-k'-1)})|p) \\ &+ \sum_{l=1}^{k'} \left(-\frac{1}{\gamma_p}\partial_t\right)^{l-1} \left(\frac{1}{\gamma_c} - \frac{1}{\gamma_p}\right) \partial_t \left(-\frac{1}{\gamma_c}\partial_t\right)^{k'-l} \left(\frac{1}{\gamma_c} - \frac{1}{\gamma_p}\right) (p'|\partial_t|\rho^{(n-k'-1)})|p),\end{aligned}$$

where we made crucially use of $\partial_t|p) = 0$ to be able to shift $|p)$ through the derivatives in the second and the last terms. Now we can sum the second term with the first term in the summation of the last term. The second term in the equation is then gone, while the last term becomes

$$\begin{aligned}&\left(-\frac{1}{\gamma_p}\partial_t\right) \left(-\frac{1}{\gamma_c}\partial_t\right)^{k'-1} \left(\frac{1}{\gamma_c} - \frac{1}{\gamma_p}\right) (p'|\partial_t|\rho^{(n-k'-1)})|p) \\ &+ \sum_{l=2}^{k'} \left(-\frac{1}{\gamma_p}\partial_t\right)^{l-1} \left(\frac{1}{\gamma_c} - \frac{1}{\gamma_p}\right) \partial_t \left(-\frac{1}{\gamma_c}\partial_t\right)^{k'-l} \left(\frac{1}{\gamma_c} - \frac{1}{\gamma_p}\right) (p'|\partial_t|\rho^{(n-k'-1)})|p).\end{aligned}$$

In this expression, the term on the first line, can again be combined with the first term of the summation. This effect keeps appearing, until we are left with only one term. After having performed this telescoping summation, the result can be added as an extra term to the other summation (on the second line) that appears in the expression of $|\rho^{(n)})$. The result is then

$$\begin{aligned}|\rho^{(n)}) = &\left(-\frac{1}{\gamma_c}\partial_t\right)^{k'+1} |\rho^{(n-(k'+1))}) \\ &+ \sum_{l=1}^{k'+1} \left(-\frac{1}{\gamma_p}\partial_t\right)^{l-1} \left(\frac{1}{\gamma_c} - \frac{1}{\gamma_p}\right) (p'|\partial_t \left(-\frac{1}{\gamma_c}\partial_t\right)^{k'+1-l} |\rho^{(n-(k'+1))})|p).\end{aligned}$$

Equation (A.2) thus also holds for $k = k' + 1$ when it holds for $k = k'$. This concludes the proof.

A.2 Instantaneous energy current in first adiabatic correction

To demonstrate the use of Eq. (3.16), we calculate again the instantaneous ($n = 0$) energy current and the adiabatic correction ($n = 1$). We did this before for the density operator and particle current in respectively sections 3.1.3 and 3.2.1 Since we already have expressions for the particle currents, we only need to consider the last term of Eq. (3.16). For the instantaneous energy current, we need to evaluate $(p'_\alpha|z)$. This becomes easy by using the orthogonal operators $\mathbb{1}$, $N - \mathbb{1} = \Delta N$ and $(-\mathbb{1})^N$. The orthogonality of these operators can be checked explicitly. They are not normalised, but their scalar products are $(\mathbb{1}|\mathbb{1}) = ((-\mathbb{1})^N|(-\mathbb{1})^N) = 4$ and $(N - \mathbb{1}|N - \mathbb{1}) = 2$. Using these operators, the stationary state (2.14) and inverted stationary state (2.18) with respect to lead α can be written as

$$
\begin{aligned}
|z) &= \frac{1}{4}|\mathbb{1}) + \frac{1}{2}\left(N_z - 1\right)|N - \mathbb{1}) + \frac{1}{4}p_z|(-\mathbb{1})^N) \\
|z_{i\alpha}) &= \frac{1}{4}|\mathbb{1}) + \frac{1}{2}\left(N_{i\alpha} - 1\right)|N - \mathbb{1}) + \frac{1}{4}p_{i\alpha}|(-\mathbb{1})^N).
\end{aligned}
$$

Acting with $\mathcal{P} = (-\mathbb{1})^N$ on either $|z)$ or $|z_{i\alpha})$ interchanges in both cases the coefficients of $|\mathbb{1})$ and $|(-\mathbb{1})^N)$. With this observation, one immediately finds

$$
(z_{i\alpha}|\mathcal{P}|\rho) = \frac{1}{4}\left(p_z + p_{i\alpha}\right) + \frac{1}{2}\left(N_z - 1\right)\left(N_{i\alpha} - 1\right). \tag{A.3}
$$

The instantaneous energy current through lead α is thus

$$
I^{(0)}_{E\alpha} = \left(\epsilon + \frac{U}{2}\left(2 - N_{i\alpha}\right)\right) I^{(0)}_{N\alpha} - \gamma_{p\alpha} U \left[\frac{1}{4}\left(p_z + p_{i\alpha}\right) + \frac{1}{2}\left(N_z - 1\right)\left(N_{i\alpha} - 1\right)\right], \tag{A.4}
$$

with $I^{(0)}_{N\alpha}$ given by Eq. (3.9). The last term of Eq. (A.4) still looks rather complicated. We will further discuss it in chapter 6.

Finally, we also calculate the adiabatic correction to the energy current. For the first term, one just has to substitute the adiabatic correction to the particle current $I^{(1)}_{N\alpha}$ (3.11). For the second term of Eq. (3.16), we now use the expression for $|\rho^{(1)})$ (Eq. (3.6)) and further evaluate

$$
\begin{aligned}
(z_{i\alpha}|(-\mathbb{1})^N|p) &= (z_{i\alpha}|\mathbb{1}) = 1 \\
(z_{i\alpha}|(-\mathbb{1})^N|c) &= \frac{1}{2}(z_{i\alpha}|N - N_i\mathbb{1}) = \frac{1}{2}\left(N_{i\alpha} - N_i\right).
\end{aligned}
$$

The adiabatic correction to the energy current through lead α is then

$$
I^{(1)}_{E\alpha} = \left(\epsilon + \tfrac{U}{2}\left(2 - N_{i\alpha}\right)\right) I^{(1)}_{N\alpha} + \tfrac{U}{2}\tfrac{\gamma_{p\alpha}}{\gamma_c}\left(N_{i\alpha} - N_i\right)\partial_t N_z + \tfrac{U}{2}\tfrac{\gamma_{p\alpha}}{\gamma_p}\left(\left(N_i - 1\right)\partial_t N_z + \tfrac{1}{2}\partial_t p_z\right). \tag{A.5}
$$

Appendix B

Expressions quantum dot in magnetic field

This appendix has two goals. On the one hand we use it to give long explicit expression that were omitted in chapter 4. On the other hand it gives some additional steps for derivations of certain results from the main text.

B.1 Stationary state and fermion-parity mode

The stationary mode $|z)$ can be written in two additional useful ways:

$$\begin{aligned}
|z) =& \frac{2}{(\Gamma_\uparrow+\Gamma_\downarrow)\left[\left(f^+_{\epsilon\uparrow}+f^-_{U\uparrow}\right)\left(f^-_{\epsilon\downarrow}+f^+_{U\downarrow}\right)+\left(f^-_{\epsilon\uparrow}+f^+_{U\uparrow}\right)\left(f^+_{\epsilon\downarrow}+f^-_{U\downarrow}\right)\right]}\times \\
& \Big\{\left[f^-_{\epsilon\uparrow}f^-_{U\downarrow}\left(f^-_{\epsilon\downarrow}+f^+_{U\uparrow}\right)+f^-_{\epsilon\downarrow}f^-_{U\uparrow}\left(f^-_{\epsilon\uparrow}+f^+_{U\downarrow}\right)\right]|0) \\
& +\left[f^+_{\epsilon\uparrow}f^-_{\epsilon\downarrow}\left(f^-_{U\downarrow}+f^-_{U\uparrow}\right)+f^+_{U\uparrow}f^-_{U\downarrow}\left(f^+_{\epsilon\downarrow}+f^+_{\epsilon\uparrow}\right)\right]|\uparrow) \\
& +\left[f^+_{\epsilon\downarrow}f^-_{\epsilon\uparrow}\left(f^-_{U\uparrow}+f^-_{U\downarrow}\right)+f^+_{U\downarrow}f^-_{U\uparrow}\left(f^+_{\epsilon\uparrow}+f^+_{\epsilon\downarrow}\right)\right]|\downarrow) \\
& +\left[f^+_{\epsilon\uparrow}f^+_{U\downarrow}\left(f^+_{U\uparrow}+f^-_{\epsilon\downarrow}\right)+f^+_{\epsilon\downarrow}f^+_{U\uparrow}\left(f^+_{U\downarrow}+f^-_{\epsilon\uparrow}\right)\right]|2)\Big\} \\
=& \left(\frac{3}{4}-\frac{1}{2}N_z+\frac{1}{4}p_z\right)|0)+\left(\frac{1}{4}+\frac{1}{2}\sigma_z-\frac{1}{4}p_z\right)|\uparrow) \\
& +\left(\frac{1}{4}-\frac{1}{2}\sigma_z-\frac{1}{4}p_z\right)|\downarrow)+\left(-\frac{1}{4}+\frac{1}{2}N_z+\frac{1}{4}p_z\right)|2).
\end{aligned} \tag{B.1}$$

The particle number in the stationary state is now

$$N_z=(N|z)=\frac{2\left[f^+_{\epsilon\uparrow}\left(f^+_{U\downarrow}+f^-_{\epsilon\downarrow}\right)+f^+_{\epsilon\downarrow}\left(f^+_{U\uparrow}+f^-_{\epsilon\uparrow}\right)\right]}{\left(f^+_{\epsilon\uparrow}+f^-_{U\uparrow}\right)\left(f^-_{\epsilon\downarrow}+f^+_{U\downarrow}\right)+\left(f^-_{\epsilon\uparrow}+f^+_{U\uparrow}\right)\left(f^+_{\epsilon\downarrow}+f^-_{U\downarrow}\right)}.$$

The spin-resolved particle numbers on the other hand are given by

$$\begin{aligned}
N_{\uparrow z}=(N_\uparrow|z)&=\frac{2\left(f^+_{\epsilon\downarrow}f^+_{U\uparrow}+f^+_{\epsilon\uparrow}f^-_{\epsilon\downarrow}\right)}{\left(f^+_{\epsilon\uparrow}+f^-_{U\uparrow}\right)\left(f^-_{\epsilon\downarrow}+f^+_{U\downarrow}\right)+\left(f^-_{\epsilon\uparrow}+f^+_{U\uparrow}\right)\left(f^+_{\epsilon\downarrow}+f^-_{U\downarrow}\right)} \\
N_{\downarrow z}=(N_\downarrow|z)&=\frac{2\left(f^+_{\epsilon\uparrow}f^+_{U\downarrow}+f^-_{\epsilon\uparrow}f^+_{\epsilon\downarrow}\right)}{\left(f^+_{\epsilon\uparrow}+f^-_{U\uparrow}\right)\left(f^-_{\epsilon\downarrow}+f^+_{U\downarrow}\right)+\left(f^-_{\epsilon\uparrow}+f^+_{U\uparrow}\right)\left(f^+_{\epsilon\downarrow}+f^-_{U\downarrow}\right)}.
\end{aligned}$$

The spin expectation value in terms of Fermi functions is

$$\sigma_z = (\sigma|z) = \frac{2\left(f^+_{\epsilon\uparrow}f^-_{U\downarrow} - f^+_{\epsilon\downarrow}f^-_{U\uparrow}\right)}{\left(f^+_{\epsilon\uparrow}+f^-_{U\uparrow}\right)\left(f^-_{\epsilon\downarrow}+f^+_{U\downarrow}\right)+\left(f^-_{\epsilon\uparrow}+f^+_{U\uparrow}\right)\left(f^+_{\epsilon\downarrow}+f^-_{U\downarrow}\right)}.$$

An important identity that was used in rewriting the stationary state in the forms of Eq. (4.4) and Eq. (B.1) is

$$|2) = \frac{1}{2}|N) + \frac{1}{4}|p) - \frac{1}{4}|\mathbb{1}), \text{ such that } (2|z) = \frac{1}{2}N_z + \frac{1}{4}p_z - \frac{1}{4}.$$

This relation can easily be checked explicitly.

Alternative expression for the inverted stationary state $|z_i)$ are

$$\begin{aligned}
|z_i) =& \frac{2}{(\Gamma_\uparrow+\Gamma_\downarrow)\left[\left(f^+_{\epsilon\uparrow}+f^-_{U\uparrow}\right)\left(f^-_{\epsilon\downarrow}+f^+_{U\downarrow}\right)+\left(f^-_{\epsilon\uparrow}+f^+_{U\uparrow}\right)\left(f^+_{\epsilon\downarrow}+f^-_{U\downarrow}\right)\right]}\times \\
&\Big\{\left[f^+_{\epsilon\uparrow}f^+_{U\downarrow}\left(f^+_{\epsilon\downarrow}+f^-_{U\uparrow}\right)+f^+_{\epsilon\downarrow}f^+_{U\uparrow}\left(f^+_{\epsilon\uparrow}+f^-_{U\downarrow}\right)\right]|0) \\
&+\left[f^-_{\epsilon\uparrow}f^+_{\epsilon\downarrow}\left(f^+_{U\downarrow}+f^+_{U\uparrow}\right)+f^-_{U\uparrow}f^+_{U\downarrow}\left(f^-_{\epsilon\downarrow}+f^-_{\epsilon\uparrow}\right)\right]|\uparrow) \\
&+\left[f^-_{\epsilon\downarrow}f^+_{\epsilon\uparrow}\left(f^+_{U\uparrow}+f^+_{U\downarrow}\right)+f^-_{U\downarrow}f^+_{U\uparrow}\left(f^-_{\epsilon\uparrow}+f^-_{\epsilon\downarrow}\right)\right]|\downarrow) \\
&+\left[f^-_{\epsilon\uparrow}f^-_{U\downarrow}\left(f^-_{U\uparrow}+f^+_{\epsilon\downarrow}\right)+f^-_{\epsilon\downarrow}f^-_{U\uparrow}\left(f^-_{U\downarrow}+f^+_{\epsilon\uparrow}\right)\right]|2)\Big\} \\
=& \left(\frac{3}{4}-\frac{1}{2}N_i+\frac{1}{4}p_i\right)|0) + \left(\frac{1}{4}+\frac{1}{2}\sigma_i-\frac{1}{4}p_i\right)|\uparrow) \\
&+\left(\frac{1}{4}-\frac{1}{2}\sigma_i-\frac{1}{4}p_i\right)|\downarrow) + \left(-\frac{1}{4}+\frac{1}{2}N_i+\frac{1}{4}p_i\right)|2).
\end{aligned} \tag{B.2}$$

As a reminder, in the notation of Fermi-functions, the energy inversion is done by swapping $f^+ \leftrightarrow f^-$. This makes it easy to find the particle number in the inverted stationary state N_i, by starting from the particle number in the normal stationary state N_z. We find

$$N_i = (N|z_i) = \frac{2\left[f^-_{\epsilon\uparrow}\left(f^-_{U\downarrow}+f^+_{\epsilon\downarrow}\right)+f^-_{\epsilon\downarrow}\left(f^-_{U\uparrow}+f^+_{\epsilon\uparrow}\right)\right]}{\left(f^+_{\epsilon\uparrow}+f^-_{U\uparrow}\right)\left(f^-_{\epsilon\downarrow}+f^+_{U\downarrow}\right)+\left(f^-_{\epsilon\uparrow}+f^+_{U\uparrow}\right)\left(f^+_{\epsilon\downarrow}+f^-_{U\downarrow}\right)}.$$

Notice that the denominator stays unchanged under the swapping operation. The other inverted quantities can be obtained in exactly the same way.

B.2 Mixed charge and spin modes

The amplitude covectors and modes x and y that are introduced in the main text, can be written more explicitly as

$$\begin{aligned}
(x'| &= -N_\uparrow(0| + (1-N_\uparrow)(\uparrow| - N_\uparrow(\downarrow| + (1-N_\uparrow)(2| \\
(y'| &= -N_\downarrow(0| - N_\downarrow(\uparrow| + (1-N_\downarrow)(\downarrow| + (1-N_\downarrow)(2| \\
|x) &= -N_{\downarrow i}|0) + N_{\downarrow i}|\uparrow) + (N_{\downarrow i}-1)(\downarrow) + (1-N_{\downarrow i})|2) \\
|y) &= -N_{\uparrow i}|0) + (N_{\uparrow i}-1)|\uparrow) + N_{\uparrow i}|\downarrow) + (1-N_{\uparrow i})|2).
\end{aligned}$$

The eigenvectors a and b (modes and amplitude covectors) of the magnetic kernel W (4.9) are, when expressed in terms of x and y, given by

$$\begin{aligned}
|a) &= \frac{1}{2}|x) + \frac{f^+_{\epsilon\downarrow} - f^+_{U\downarrow}}{(\gamma_a - \gamma_b) + (\Gamma_\uparrow - \Gamma_\downarrow)}|y) \\
|b) &= \frac{1}{2}|x) - \frac{f^+_{\epsilon\downarrow} - f^+_{U\downarrow}}{(\gamma_a - \gamma_b) - (\Gamma_\uparrow - \Gamma_\downarrow)}|y) \\
(a'| &= \frac{(\gamma_a - \gamma_b) + (\Gamma_\uparrow - \Gamma_\downarrow)}{(\gamma_a - \gamma_b)}(x'| + 2\frac{f^+_{\epsilon\uparrow} - f^+_{U\uparrow}}{(\gamma_a - \gamma_b)}(y'| \\
(b'| &= \frac{(\gamma_a - \gamma_b) - (\Gamma_\uparrow - \Gamma_\downarrow)}{(\gamma_a - \gamma_b)}(x'| - 2\frac{f^+_{\epsilon\uparrow} - f^+_{U\uparrow}}{(\gamma_a - \gamma_b)}(y'|.
\end{aligned} \tag{B.3}$$

To understand the eigenmodes a and b better, they can be rewritten in several different ways. First of all, we rewrite $|a)$ and $|b)$ in terms of the charge mode $|c)$ and spin mode $|s)$ of the system without applied magnetic field. For this, we make use of the relations in Eq. (4.11).

$$\begin{aligned}
|a) =& \frac{1}{(\gamma_a - \gamma_b) + (\Gamma_\uparrow - \Gamma_\downarrow)} \left\{ \left[\frac{(\gamma_a - \gamma_b)}{2} + \frac{(\Gamma_\uparrow - \Gamma_\downarrow)}{2} + \left(f^+_{\epsilon\downarrow} - f^+_{U\downarrow} \right) \right] |c) \right. \\
&\left. + \left[\frac{(\gamma_a - \gamma_b)}{2} + \frac{(\Gamma_\uparrow - \Gamma_\downarrow)}{2} - \left(f^+_{\epsilon\downarrow} - f^+_{U\downarrow} \right) \right] |s) \right\}
\end{aligned} \tag{B.4a}$$

$$= \left[\frac{1}{2} + \frac{f^+_{\epsilon\downarrow} - f^+_{U\downarrow}}{(\gamma_a - \gamma_b) + (\Gamma_\uparrow - \Gamma_\downarrow)} \right] |c) + \left[\frac{1}{2} - \frac{f^+_{\epsilon\downarrow} - f^+_{U\downarrow}}{(\gamma_a - \gamma_b) + (\Gamma_\uparrow - \Gamma_\downarrow)} \right] |s) \tag{B.4b}$$

$$\begin{aligned}
|b) =& \frac{1}{(\gamma_a - \gamma_b) - (\Gamma_\uparrow - \Gamma_\downarrow)} \left\{ \left[\frac{(\gamma_a - \gamma_b)}{2} - \frac{(\Gamma_\uparrow - \Gamma_\downarrow)}{2} - \left(f^+_{\epsilon\downarrow} - f^+_{U\downarrow} \right) \right] |c) \right. \\
&\left. + \left[\frac{(\gamma_a - \gamma_b)}{2} - \frac{(\Gamma_\uparrow - \Gamma_\downarrow)}{2} + \left(f^+_{\epsilon\downarrow} - f^+_{U\downarrow} \right) \right] |s) \right\}
\end{aligned} \tag{B.4c}$$

$$= \left[\frac{1}{2} - \frac{f^+_{\epsilon\downarrow} - f^+_{U\downarrow}}{(\gamma_a - \gamma_b) + (\Gamma_\uparrow - \Gamma_\downarrow)} \right] |c) + \left[\frac{1}{2} + \frac{f^+_{\epsilon\downarrow} - f^+_{U\downarrow}}{(\gamma_a - \gamma_b) + (\Gamma_\uparrow - \Gamma_\downarrow)} \right] |s) \tag{B.4d}$$

Similarly, $(a'|$ and $(b'|$ can be rewritten in terms of $(c'|$ and $(s'|$:

$$\begin{aligned}
(a'| =& \frac{1}{\gamma_a - \gamma_b} \left\{ \left[\frac{(\gamma_a - \gamma_b)}{2} + \frac{(\Gamma_\uparrow - \Gamma_\downarrow)}{2} + \left(f^+_{\epsilon\uparrow} - f^+_{U\uparrow} \right) \right] (c'| \right. \\
&\left. + \left[\frac{(\gamma_a - \gamma_b)}{2} + \frac{(\Gamma_\uparrow - \Gamma_\downarrow)}{2} - \left(f^+_{\epsilon\uparrow} - f^+_{U\uparrow} \right) \right] (s'| \right\}
\end{aligned} \tag{B.4e}$$

$$\begin{aligned}
(b'| =& \frac{1}{\gamma_a - \gamma_b} \left\{ \left[\frac{(\gamma_a - \gamma_b)}{2} - \frac{(\Gamma_\uparrow - \Gamma_\downarrow)}{2} - \left(f^+_{\epsilon\uparrow} - f^+_{U\uparrow} \right) \right] (c'| \right. \\
&\left. + \left[\frac{(\gamma_a - \gamma_b)}{2} - \frac{(\Gamma_\uparrow - \Gamma_\downarrow)}{2} + \left(f^+_{\epsilon\uparrow} - f^+_{U\uparrow} \right) \right] (s'| \right\}.
\end{aligned} \tag{B.4f}$$

Using some relations between the different variables, these expressions can be further rewritten. Two of the most used relations are

$$\Gamma + \frac{(\gamma_a - \gamma_b)}{2} = \gamma_a \qquad \text{and} \qquad \Gamma - \frac{(\gamma_a - \gamma_b)}{2} = \gamma_b. \tag{B.5}$$

We then find the following final expressions for $|a)$ and $|b)$ in terms of c and s:

$$\begin{aligned}
|a) =& \frac{1}{(\gamma_a-\gamma_b)+(\Gamma_\uparrow-\Gamma_\downarrow)}\left\{\left[\gamma_a-\left(f^-_{\epsilon\downarrow}+f^+_{U\downarrow}\right)\right]|c)+\left[\gamma_a-\left(f^+_{\epsilon\downarrow}+f^-_{U\downarrow}\right)\right]|s)\right\}\\
|b) =& \frac{-1}{(\gamma_a-\gamma_b)-(\Gamma_\uparrow-\Gamma_\downarrow)}\left\{\left[\gamma_b-\left(f^-_{\epsilon\downarrow}+f^+_{U\downarrow}\right)\right]|c)+\left[\gamma_b-\left(f^+_{\epsilon\downarrow}+f^-_{U\downarrow}\right)\right]|s)\right\}\\
(a'| =& \frac{-1}{\gamma_a-\gamma_b}\left\{\left[\gamma_b-\left(f^+_{\epsilon\uparrow}+f^-_{U\uparrow}\right)\right](c'|+\left[\gamma_b-\left(f^-_{\epsilon\uparrow}+f^+_{U\uparrow}\right)\right](s'|\right\}\\
(b'| =& \frac{1}{\gamma_a-\gamma_b}\left\{\left[\gamma_a-\left(f^+_{\epsilon\uparrow}+f^-_{U\uparrow}\right)\right](c'|+\left[\gamma_a-\left(f^-_{\epsilon\uparrow}+f^+_{U\uparrow}\right)\right](s'|\right\}.
\end{aligned} \tag{B.6}$$

We will stop here in rewriting the eigenmodes a and b, since these are about the most elegant ways to write them. Notice however that they can be written in many more forms by using the relations

$$\begin{aligned}
\gamma_a-\Gamma_\downarrow &= \frac{1}{2}\left[(\Gamma_\uparrow-\Gamma_\downarrow)+(\gamma_a-\gamma_b)\right]=\Gamma_\uparrow-\gamma_b\\
\gamma_b-\Gamma_\downarrow &= \frac{1}{2}\left[(\Gamma_\uparrow-\Gamma_\downarrow)-(\gamma_a-\gamma_b)\right]=\Gamma_\uparrow-\gamma_a\\
\gamma_a-\gamma_b &= 2\gamma_a-2\Gamma=2\Gamma-2\gamma_b.
\end{aligned}$$

B.3 Sudden switch: decay rates, charge and spin

The time-dependence of the density operator after the switch as given in the main text is

$$|\rho(t)) = |z)(z'|z_0) + e^{-\gamma_p t}|p)(p'|z_0) + e^{-\gamma_a t}|a)(a'|z_0) + e^{-\gamma_b t}|b)(b'|z_0).$$

The overlaps in this expression are

$$\begin{aligned}
(z'|z_0) &= 1 \text{ (conservation of probability)}\\
(p'|z_0) &= \frac{1}{4}(p_{z0}-p_i)+\frac{1}{2}\Delta N_{z0}\Delta N_i-\frac{1}{2}\sigma_{z0}\sigma_i\\
(a'|z_0) &= \left(\frac{\Gamma_\uparrow-\Gamma_\downarrow}{\gamma_a-\gamma_b}+1\right)(N_{\uparrow z0}-N_{\uparrow z})+2\frac{f^+_{\epsilon\uparrow}-f^+_{U\uparrow}}{\gamma_a-\gamma_b}(N_{\downarrow z0}-N_{\downarrow z})\\
(b'|z_0) &= \left(1-\frac{\Gamma_\uparrow-\Gamma_\downarrow}{\gamma_a-\gamma_b}\right)(N_{\uparrow z0}-N_{\uparrow z})-2\frac{f^+_{\epsilon\uparrow}-f^+_{U\uparrow}}{\gamma_a-\gamma_b}(N_{\downarrow z0}-N_{\downarrow z}).
\end{aligned}$$

An important identity that was used several times to simplify things in the calculations of the charge and spin expectation values is

$$\frac{1}{4}\frac{(\gamma_a-\gamma_b)+(\Gamma_\uparrow-\Gamma_\downarrow)}{f^+_{\epsilon\uparrow}-f^+_{U\uparrow}}=\frac{f^+_{\epsilon\downarrow}-f^+_{U\downarrow}}{(\gamma_a-\gamma_b)-(\Gamma_\uparrow-\Gamma_\downarrow)}.$$

The charge and spin expectation values were calculated using the expressions for $|\rho(t))$ and the expressions in Eq. (B.4) for modes $|a)$ and $|b)$ in terms of $|c)$ and $|s)$ (which

give much nicer results then the expressions in terms of $|x)$ and $|y)$, (B.3)) The solutions that are less compact than Eq. (4.13), but easier to read and understand are

$$\begin{aligned}\langle N\rangle(t) =& \frac{1}{\gamma_a-\gamma_b}\left\{N_{\uparrow z}\left[\gamma_a-\left(f^-_{\epsilon\downarrow}+f^+_{U\downarrow}\right)\right]+N_{\downarrow z}\left[\gamma_a-\left(f^-_{\epsilon\uparrow}+f^+_{U\uparrow}\right)\right]\right\}\left(1-e^{-\gamma_a t}\right)\\ &+\frac{1}{\gamma_a-\gamma_b}\left\{N_{\uparrow z0}\left[\gamma_a-\left(f^-_{\epsilon\downarrow}+f^+_{U\downarrow}\right)\right]+N_{\downarrow z0}\left[\gamma_a-\left(f^-_{\epsilon\uparrow}+f^+_{U\uparrow}\right)\right]\right\}e^{-\gamma_a t}\\ &+\frac{-1}{\gamma_a-\gamma_b}\left\{N_{\uparrow z}\left[\gamma_b-\left(f^-_{\epsilon\downarrow}+f^+_{U\downarrow}\right)\right]+N_{\downarrow z}\left[\gamma_b-\left(f^-_{\epsilon\uparrow}+f^+_{U\uparrow}\right)\right]\right\}\left(1-e^{-\gamma_b t}\right)\\ &+\frac{-1}{\gamma_a-\gamma_b}\left\{N_{\uparrow z0}\left[\gamma_b-\left(f^-_{\epsilon\downarrow}+f^+_{U\downarrow}\right)\right]+N_{\downarrow z0}\left[\gamma_b-\left(f^-_{\epsilon\uparrow}+f^+_{U\uparrow}\right)\right]\right\}e^{-\gamma_b t}\end{aligned}$$

and

$$\begin{aligned}\langle\sigma\rangle(t) =& \frac{1}{\gamma_a-\gamma_b}\left\{N_{\uparrow z}\left[\gamma_a-\left(f^+_{\epsilon\downarrow}+f^-_{U\downarrow}\right)\right]-N_{\downarrow z}\left[\gamma_a-\left(f^+_{\epsilon\uparrow}+f^-_{U\uparrow}\right)\right]\right\}\left(1-e^{-\gamma_a t}\right)\\ &+\frac{1}{\gamma_a-\gamma_b}\left\{N_{\uparrow z0}\left[\gamma_a-\left(f^+_{\epsilon\downarrow}+f^-_{U\downarrow}\right)\right]-N_{\downarrow z0}\left[\gamma_a-\left(f^+_{\epsilon\uparrow}+f^-_{U\uparrow}\right)\right]\right\}e^{-\gamma_a t}\\ &+\frac{-1}{\gamma_a-\gamma_b}\left\{N_{\uparrow z}\left[\gamma_b-\left(f^+_{\epsilon\downarrow}+f^-_{U\downarrow}\right)\right]-N_{\downarrow z}\left[\gamma_b-\left(f^+_{\epsilon\uparrow}+f^-_{U\uparrow}\right)\right]\right\}\left(1-e^{-\gamma_b t}\right)\\ &+\frac{-1}{\gamma_a-\gamma_b}\left\{N_{\uparrow z0}\left[\gamma_b-\left(f^+_{\epsilon\downarrow}+f^-_{U\downarrow}\right)\right]-N_{\downarrow z0}\left[\gamma_b-\left(f^+_{\epsilon\uparrow}+f^-_{U\uparrow}\right)\right]\right\}e^{-\gamma_b t}.\end{aligned}$$

B.4 Density operator

Here we derive the expressions for the instantaneous density operator and its first adiabatic correction (zeroth and first order in $\frac{\Omega}{\Gamma}$). We start from the second line of Eq. (2.9), where the chosen basis states are still allowed to be time-dependent. Choosing the eigenmodes of the magnetic kernel W_{ij} as the orthonormal basis, W_{ij} is diagonal such that

$$\sum_i \left(\partial_t P_i\right)|i) + P_i\partial_t|i) = \sum_i W_{ii}P_i|i).$$

We now need to calculate the coefficients $P_i^{(0)}$ and $P_i^{(1)}$ for the zeroth and first order contributions in $\frac{\Omega}{\Gamma}$ of the eigenmode $|i)$. These expansion factors can be found as the solution for the set of equations

$$\begin{aligned}0 &= W_{ii}P_i^{(0)}|i)\\ \sum_i\left(\partial_t P_i^{(0)}\right)|i) + P_i^{(0)}\partial_t|i) &= \sum_i W_{ii}P_i^{(1)}|i).\end{aligned}$$

The first equation is the stationary Born-Markov equation with solution $P_z^{(0)}=1$, while $P_p^{(0)}=P_a^{(0)}=P_b^{(0)}=0$. Plugging this into the next equation, we find $\partial_t P_i^{(0)}=0$ for all i. Because of probability conservation, we also know that $P_z^{(1)}=0$. The second equation is then reduced to

$$\partial_t|z) = -\gamma_p P_p^{(1)}|p) - \gamma_a P_a^{(1)}|a) - \gamma_b P_b^{(1)}|b).$$

From this, we can obtain $P_p^{(1)}$, $P_a^{(1)}$ and $P_b^{(1)}$ as

$$P_p^{(1)} = -\frac{1}{\gamma_p}(p'|\partial_t|z)$$
$$P_a^{(1)} = -\frac{1}{\gamma_a}(a'|\partial_t|z)$$
$$P_b^{(1)} = -\frac{1}{\gamma_b}(b'|\partial_t|z).$$

The expression for $\partial_t|z)$ in these equation can immediately be found by taking the time derivative of Eq. (4.4):

$$\begin{aligned}\partial_t|z) = &\left(-\frac{1}{2}\partial_t N_z + \frac{1}{4}\partial_t p_z\right)|0) + \left(\frac{1}{2}\partial_t\sigma_z - \frac{1}{4}\partial_t p_z\right)|\uparrow) \\ &+ \left(-\frac{1}{2}\partial_t\sigma_z - \frac{1}{4}\partial_t p_z\right)|\downarrow) + \left(\frac{1}{2}\partial_t N_z + \frac{1}{4}\partial_t p_z\right)|2).\end{aligned}$$

Using this, and the expressions for $(p'|$, $(a'|$ and $(b'|$, all the adiabatic expansion coefficients can be found. For the parity mode, we obtain

$$\begin{aligned}P_p^{(1)} &= -\frac{1}{-\gamma_p}(p'|\partial_t|z) = -\frac{1}{\gamma_p}(z_i|\,(-\mathbb{1})^N\,\partial_t|z) \\ &= \frac{1}{2\gamma_p}\left[(1-N_i)\,\partial_t N_z + \sigma_i\partial_t\sigma_z - \frac{1}{2}\partial_t p_z\right].\end{aligned}$$

And using $N = N_\uparrow + N_\downarrow$ and $\sigma = N_\uparrow - N_\downarrow$,

$$= \frac{1}{2\gamma_p}\left[(1-2N_{\downarrow i})\,\partial_t N_{\uparrow z} + (1-2N_{\uparrow i})\,\partial_t N_{\downarrow z} - \frac{1}{2}\partial_t p_z\right].$$

To calculate the adiabatic correction coefficients $P_a^{(1)}$ and $P_b^{(1)}$, we make use of the expressions of $(a'|$ and $(b'|$ in terms of $(c'|$ and $(s'|$, as given in Eq. (B.6). For the a mode, we find

$$P_a^{(1)} = \frac{1}{\gamma_a(\gamma_a-\gamma_b)}\left\{\left[\gamma_b - \left(f_{\epsilon\uparrow}^+ + f_{U\uparrow}^-\right)\right](c'|\partial_t|z) + \left[\gamma_b - \left(f_{\epsilon\uparrow}^- + f_{U\uparrow}^+\right)\right](s'|\partial_t|z)\right\}.$$

Filling in the relations for $(c'|$ and $(s'|$, Eq. (4.6) and (4.7), and using several relations between the different quantities, this finally becomes

$$P_a^{(1)} = -\frac{1}{\gamma_a(\gamma_a-\gamma_b)}\left\{\left[(\gamma_a-\gamma_b) + (\Gamma_\uparrow - \Gamma_\downarrow)\right]\partial_t N_{\uparrow z} + 2\left[f_{\epsilon\uparrow}^+ - f_{U\uparrow}^+\right]\partial_t N_{\downarrow z}\right\}.$$

For the b mode, we have similarly

$$P_b^{(1)} = -\frac{1}{\gamma_b(\gamma_a-\gamma_b)}\left\{\left[\gamma_a - \left(f_{\epsilon\uparrow}^+ + f_{U\uparrow}^-\right)\right](c'|\partial_t|z) + \left[\gamma_a - \left(f_{\epsilon\uparrow}^- + f_{U\uparrow}^+\right)\right](s'|\partial_t|z)\right\}.$$

After analogous operations as for the a mode, this results in

$$P_b^{(1)} = -\frac{1}{\gamma_b(\gamma_a-\gamma_b)}\left\{\left[(\gamma_a-\gamma_b) - (\Gamma_\uparrow - \Gamma_\downarrow)\right]\partial_t N_{\uparrow z} + 2\left[-f_{\epsilon\uparrow}^+ + f_{U\uparrow}^+\right]\partial_t N_{\downarrow z}\right\}.$$

With these expressions, we are in principle able to write down $|\rho(t))$ up to first order in $\frac{\Omega}{\Gamma}$.

It is however useful to consider the combination $P_a^{(1)}|a) + P_b^{(1)}|b)$ that is present in that expression. We will write this combination in a more insightful way. By inserting the expressions for $|a)$ and $|b)$ in terms of $|c)$ and $|s)$, as given in Eq. (B.6), in the combination, we find after a lot of algebra

$$\begin{aligned} P_a^{(1)}|a) + P_b^{(1)}|b) =& \partial_t N_{\uparrow z} \frac{-1}{\gamma_a \gamma_b} \left[\left(f_{\epsilon\downarrow}^- + f_{U\downarrow}^+ \right) |c) + \left(f_{\epsilon\downarrow}^+ + f_{U\downarrow}^- \right) |s) \right] \\ &+ \partial_t N_{\downarrow z} \frac{-1}{\gamma_a \gamma_b} \left[\frac{\gamma_a \gamma_b - \Gamma_\uparrow \left(f_{\epsilon\downarrow}^- + f_{U\downarrow}^+ \right)}{f_{\epsilon\downarrow}^+ - f_{U\downarrow}^+} |c) + \frac{\gamma_a \gamma_b - \Gamma_\uparrow \left(f_{\epsilon\downarrow}^+ + f_{U\downarrow}^- \right)}{f_{\epsilon\downarrow}^+ - f_{U\downarrow}^+} |s) \right]. \end{aligned}$$

We would expect some more symmetry between the terms that contain the derivatives of $N_{\uparrow z}$ and $N_{\downarrow z}$. Since there is nothing fundamentally different between spin-up and -down electrons, the quantities related to them should be interchangeable with the exception of some sign changes. The factor in the term containing $\partial_t N_{\downarrow z}$ can be rewritten by using the relation

$$\gamma_a \gamma_b = \Gamma_\uparrow \Gamma_\downarrow - \left(f_{\epsilon\uparrow}^+ - f_{U\uparrow}^+ \right) \left(f_{\epsilon\downarrow}^+ - f_{U\downarrow}^+ \right).$$

We then have

$$\begin{aligned} P_a^{(1)}|a) + P_b^{(1)}|b) =& \frac{-1}{\gamma_a \gamma_b} \left\{ \left[\left(f_{\epsilon\downarrow}^- + f_{U\downarrow}^+ \right) \partial_t N_{\uparrow z} + \left(f_{\epsilon\uparrow}^- + f_{U\uparrow}^+ \right) \partial_t N_{\downarrow z} \right] |c) \right. \\ &\left. + \left[\left(f_{\epsilon\downarrow}^+ + f_{U\downarrow}^- \right) \partial_t N_{\uparrow z} - \left(f_{\epsilon\uparrow}^+ + f_{U\uparrow}^- \right) \partial_t N_{\downarrow z} \right] |s) \right\}. \end{aligned}$$

And using Eq. (4.11), this can also be written as

$$\begin{aligned} P_a^{(1)}|a) + P_b^{(1)}|b) =& \frac{-1}{\gamma_a \gamma_b} \left\{ \left[\Gamma_\downarrow \partial_t N_{\uparrow z} - \left(f_{\epsilon\uparrow}^+ - f_{U\uparrow}^+ \right) \partial_t N_{\downarrow z} \right] |x) \right. \\ &\left. + \left[- \left(f_{\epsilon\downarrow}^+ - f_{U\downarrow}^+ \right) \partial_t N_{\uparrow z} + \Gamma_\uparrow \partial_t N_{\downarrow z} \right] |y) \right\}. \end{aligned} \tag{B.7}$$

We are now finally in a position to write an expression for the density operator $|\rho(t))$ up to first order in $\frac{\Omega}{\Gamma}$, as we did in Eq. (4.14).

B.5 Particle current

Here we calculate the general particle current through the quantum dot in an external magnetic field. Later we also show the calculation for the instantaneous particle current and its adiabatic correction. Some additional useful expressions are also given.

We start our calculations from Eq. (3.7):

$$I_{N\alpha} = (N|W_\alpha|\rho(t)),$$

where W_α is the magnetic kernel for lead α. However, since the charge mode is not an eigenmode of the kernel any more, we need to proceed differently. First we write the particle number as the sum of spin-up and -down particle numbers:

$$I_{N\alpha} = (N_\uparrow|W_\alpha|\rho(t)) + (N_\downarrow|W_\alpha|\rho(t)).$$

Next, we use the fact that $(\mathbb{1}|$ is still an eigenvector of the kernel W_α, which corresponds to the eigenvalue 0:

$$I_{N\alpha} = ((N_\uparrow| - N_{\uparrow z\alpha}(\mathbb{1}|)\, W_\alpha|\rho(t)) + ((N_\downarrow| - N_{\downarrow z\alpha}(\mathbb{1}|)\, W_\alpha|\rho(t)).$$

The quantities between the brackets, can be recognised as the modes $(x'_\alpha|$ and $(y'_\alpha|$:

$$I_{N\alpha} = (x'_\alpha|W_\alpha|\rho(t)) + (y'_\alpha|W_\alpha|\rho(t)).$$

Even though $(x'_\alpha|$ and $(y'_\alpha|$ are not eigenvectors of W_α, they do allow us to employ the block-diagonalised form of the kernel Eq. (4.9). Using that expression, we can get rid of the kernel in our equation and arrive at

$$I_{N\alpha} = \left(-\Gamma_{\uparrow\alpha} - f^+_{\epsilon\downarrow\alpha} + f^+_{U\downarrow\alpha}\right)(x'_\alpha|\rho(t)) + \left(-\Gamma_{\downarrow\alpha} - f^+_{\epsilon\uparrow\alpha} + f^+_{U\uparrow\alpha}\right)(y'_\alpha|\rho(t)).$$

Now we use probability conservation, i.e. $(\mathbb{1}|\rho(t)) = 1$, and the definitions of $(x'_\alpha|$ and $(y'_\alpha|$ to find

$$I_{N\alpha} = \left(\Gamma_{\uparrow\alpha} + f^+_{\epsilon\downarrow\alpha} - f^+_{U\downarrow\alpha}\right)(N_{\uparrow z\alpha} - (N_\uparrow|\rho(t))) + \left(\Gamma_{\downarrow\alpha} + f^+_{\epsilon\uparrow\alpha} - f^+_{U\uparrow\alpha}\right)(N_{\downarrow z\alpha} - (N_\downarrow|\rho(t)))\,.$$

We can define two new quantities to better understand the prefactors in this equation:

$$\begin{aligned}\gamma_{c\uparrow\alpha} &= -(c'_\alpha|W_\alpha|x_\alpha) = \Gamma_{\uparrow\alpha} + f^+_{\epsilon\downarrow\alpha} - f^+_{U\downarrow\alpha}\\ \gamma_{c\downarrow\alpha} &= -(c'_\alpha|W_\alpha|y_\alpha) = \Gamma_{\downarrow\alpha} + f^+_{\epsilon\uparrow\alpha} - f^+_{U\uparrow\alpha}.\end{aligned}$$

The interpretation of these rates is given in the main text. With these definitions, we end up at Eq. (4.15):

$$I_{N\alpha} = \gamma_{c\uparrow\alpha}\,(N_{\uparrow z\alpha} - (N_\uparrow|\rho(t))) + \gamma_{c\downarrow\alpha}\,(N_{\downarrow z\alpha} - (N_\downarrow|\rho(t)))\,.$$

This particle current, separated in spin-resolved currents is

$$I_{N\alpha} = I_{N\uparrow\alpha} + I_{N\downarrow\alpha},$$

where

$$\begin{aligned}I_{N\uparrow\alpha} &= \Gamma_{\uparrow\alpha}\,(N_{\uparrow z\alpha} - (N_\uparrow|\rho(t))) + \left(f^+_{\epsilon\uparrow\alpha} - f^+_{U\uparrow\alpha}\right)(N_{\downarrow z\alpha} - (N_\downarrow|\rho(t)))\\ &= (x'_\alpha|W_\alpha|\rho(t))\\ I_{N\downarrow\alpha} &= \Gamma_{\downarrow\alpha}\,(N_{\downarrow z\alpha} - (N_\downarrow|\rho(t))) + \left(f^+_{\epsilon\downarrow\alpha} - f^+_{U\downarrow\alpha}\right)(N_{\uparrow z\alpha} - (N_\uparrow|\rho(t)))\\ &= (y'_\alpha|W_\alpha|\rho(t)).\end{aligned}$$

Now we substitute the density operator (4.14) to find the particle current up to first order in $\frac{\Omega}{\Gamma}$. For the instantaneous particle current (so zeroth order in $\frac{\Omega}{\Gamma}$), we use $(N_\sigma|\rho(0)(t)) = (N_\sigma|z) = N_{\sigma z}$. This immediately gives us

$$I^{(0)}_{N\alpha} = \gamma_{c\uparrow\alpha}\,(N_{\uparrow z\alpha} - N_{\uparrow z}) + \gamma_{c\downarrow\alpha}\,(N_{\downarrow z\alpha} - N_{\downarrow z})\,,$$

which is also the sum of the two spin-resolved currents

$$I^{(0)}_{N\uparrow\alpha} = \Gamma_{\uparrow\alpha}\left(N_{\uparrow z\alpha} - N_{\uparrow z}\right) + \left(f^+_{\epsilon\uparrow\alpha} - f^+_{U\uparrow\alpha}\right)\left(N_{\downarrow z\alpha} - N_{\downarrow z}\right)$$
$$I^{(0)}_{N\downarrow\alpha} = \Gamma_{\downarrow\alpha}\left(N_{\downarrow z\alpha} - N_{\downarrow z}\right) + \left(f^+_{\epsilon\downarrow\alpha} - f^+_{U\downarrow\alpha}\right)\left(N_{\uparrow z\alpha} - N_{\uparrow z}\right).$$

Next we calculate the first order correction in $\frac{\Omega}{\Gamma}$ by substituting $|\rho^{(1)})$ (the terms that do not contain $|\rho(t))$ in Eq. (4.15) were already taken into account by the instantaneous current, so we drop them for the corrections). We then have

$$I^{(1)}_{N\alpha} = -\gamma_{c\uparrow\alpha}\underbrace{(N_\uparrow|\rho^{(1)}(t))}_{=(x'|\rho^{(1)}(t))} - \gamma_{c\downarrow\alpha}\underbrace{(N_\downarrow|\rho^{(1)}(t))}_{=(y'|\rho^{(1)}(t))},$$

where the two additional equalities are true because $(\mathbb{1}|\rho^{(1)}(t)) = 0$. Finally we fill in $|\rho^{(1)})$ from Eq. (4.14), but now with alternative form Eq. (B.7). After the rearrangement of some terms, we get

$$I^{(1)}_{N\alpha} = \frac{1}{\gamma_a\gamma_b}\left[\gamma_{c\uparrow\alpha}\Gamma_\downarrow - \gamma_{c\downarrow\alpha}\left(f^+_{\epsilon\downarrow} - f^+_{U\downarrow}\right)\right]\partial_t N_\uparrow + \frac{1}{\gamma_a\gamma_b}\left[\gamma_{c\downarrow\alpha}\Gamma_\uparrow - \gamma_{c\uparrow\alpha}\left(f^+_{\epsilon\uparrow} - f^+_{U\uparrow}\right)\right]\partial_t N_\downarrow.$$

For completeness (ans because we need them for the energy and heat current), we also give the expressions for the first order correction in $\frac{\Omega}{\Gamma}$ of the spin-resolved currents:

$$\begin{aligned} I^{(1)}_{N\uparrow\alpha} =& \frac{1}{\gamma_a\gamma_b}\left\{\left[\Gamma_{\uparrow\alpha}\Gamma_\downarrow - \left(f^+_{\epsilon\uparrow\alpha} - f^+_{U\uparrow\alpha}\right)\left(f^+_{\epsilon\downarrow} - f^+_{U\downarrow}\right)\right]\partial_t N_{\uparrow z}\right. \\ &\left. + \left[-\Gamma_{\uparrow\alpha}\left(f^+_{\epsilon\uparrow} - f^+_{U\uparrow}\right) + \left(f^+_{\epsilon\uparrow\alpha} - f^+_{U\uparrow\alpha}\right)\Gamma_\uparrow\right]\partial_t N_{\downarrow z}\right\} \\ I^{(1)}_{N\downarrow\alpha} =& \left\{\left[-\Gamma_{\downarrow\alpha}\left(f^+_{\epsilon\downarrow} - f^+_{U\downarrow}\right) + \left(f^+_{\epsilon\downarrow\alpha} - f^+_{U\downarrow\alpha}\right)\Gamma_\downarrow\right]\partial_t N_{\uparrow z}\right. \\ &\left. + \frac{1}{\gamma_a\gamma_b}\left[\Gamma_{\downarrow\alpha}\Gamma_\uparrow - \left(f^+_{\epsilon\downarrow\alpha} - f^+_{U\downarrow\alpha}\right)\left(f^+_{\epsilon\uparrow} - f^+_{U\uparrow}\right)\right]\partial_t N_{\downarrow z}\right\}. \end{aligned}$$

B.6 Energy current

The energy current is calculated from Eq. (3.12)

$$I_{E\alpha} = (H|W_\alpha|\rho),$$

with

$$(H| = \epsilon_\uparrow(N_\uparrow| + \epsilon_\downarrow(N_\downarrow| + U(2|.$$

To proceed, we can first rewrite $(2|W_\alpha$ as

$$(2|W_\alpha = (2|z_\alpha)(z'_\alpha|W_\alpha + (2|p_\alpha)(p'_\alpha|W_\alpha + (2|x_\alpha)(x'_\alpha|W_\alpha + (2|y_\alpha)(y'_\alpha|W_\alpha,$$

which we are allowed to do since the set $\{z, p, x, y\}$ forms a biorthonormal basis. We can calculate several quantities in this equation, such that it becomes

$$(2|W_\alpha = -\gamma_{p\alpha}(p'_\alpha| + (1 - N_{\downarrow i\alpha})(x'_\alpha|W_\alpha + (1 - N_{\uparrow i\alpha})(y'_\alpha|W_\alpha.$$

Furthermore, we also realise that $(N_\uparrow|W_\alpha = (x'_\alpha|W_\alpha$ and $(N_\downarrow|W_\alpha = (y'_\alpha|W_\alpha$, since $(\mathbb{1}|W_\alpha = 0$. Combining all these results, we can write the expression (4.16) for the energy current through lead α, given the time-dependence of the density operator $|\rho)$:

$$I_{E\alpha} = (\epsilon_\uparrow + U\,(1 - N_{\downarrow i\alpha}))\, I_{N\uparrow\alpha} + (\epsilon_\downarrow + U\,(1 - N_{\uparrow i\alpha}))\, I_{N\downarrow\alpha} - U\gamma_{p\alpha}(p'_\alpha|\rho).$$

With the expression for the energy current with general $|\rho)$ in place, we can now calculate the zeroth and first order terms in $\frac{\Omega}{\Gamma}$ by plugging in the corresponding density operator Eq. (4.14). Since we already have the expression for the particle currents in these two orders, we only need to calculate the last term. First we consider the instantaneous case (zeroth order in $\frac{\Omega}{\Gamma}$). To start, notice that $\left\{|\mathbb{1}),\, |N - \mathbb{1}),\, |\,(-\mathbb{1})^N),\, |\sigma)\right\}$ forms an orthogonal basis, which is however not normalised since $(\mathbb{1}|\mathbb{1}) = ((-\mathbb{1})^N\,|\,(-\mathbb{1})^N) = 4$ and $(N - \mathbb{1}|N - \mathbb{1}) = (\sigma|\sigma) = 2$. Both $|z)$ and $|z_i)$, respectively Eq. (4.4) and (4.5), can be expressed in this basis as

$$\begin{aligned}
|z) &= \frac{1}{4}|\mathbb{1}) + \frac{1}{2}\,(N_z - 1)\,|N - \mathbb{1}) + \frac{1}{4}p_z|\,(-\mathbb{1})^N) + \frac{1}{2}\sigma_z|\sigma)\\
|z_{i\alpha}) &= \frac{1}{4}|\mathbb{1}) + \frac{1}{2}\,(N_{i\alpha} - 1)\,|N - \mathbb{1}) + \frac{1}{4}p_{i\alpha}|\,(-\mathbb{1})^N) + \frac{1}{2}\sigma_{i\alpha}|\sigma).
\end{aligned}$$

The advantage of writing these state in this basis, is that acting with $\mathcal{P}$ on either $|z)$ or $|z_{i\alpha})$ will just switch the coefficients of $|\mathbb{1})$ and $|\,(-\mathbb{1})^N)$. We can then easily calculate

$$(p'_\alpha|\rho^{(0)}) = (z_{i\alpha}|\,(-\mathbb{1})^N\,|z) = \frac{1}{4}\,(p_{i\alpha} + p_z) + \frac{1}{2}\,(N_z - 1)\,(N_{i\alpha} - 1) + \frac{1}{2}\sigma_z\sigma_{i\alpha}.$$

Notice that this equation is the same as Eq. (A.3) for the non-magnetic case, except for an additional term that only depends on the spins in the dot. The final instantaneous energy current is then

$$\begin{aligned}
I^{(0)}_{E\alpha} = (\epsilon_\uparrow + U\,(1 - N_{\downarrow i\alpha}))\, I^{(0)}_{N\uparrow\alpha} + (\epsilon_\downarrow + U\,(1 - N_{\uparrow i\alpha}))\, I^{(0)}_{N\downarrow\alpha}\\
- \frac{U}{2}\gamma_{p\alpha}\left[\frac{1}{2}\,(p_{i\alpha} + p_z) + (N_z - 1)\,(N_{i\alpha} - 1) + \sigma_z\sigma_{i\alpha}\right].
\end{aligned}$$

Next, for calculating the first order correction in $\frac{\Omega}{\Gamma}$, we again only need to calculate the last term of Eq. (4.16), since we already have expressions for the first order corrections of the spin-resolved particle currents. We can calculate the necessary overlaps separately:

$$\begin{aligned}
(p'_\alpha|p) &= (z_{i\alpha}|\mathbb{1}) = 1 \text{ (normalised)}\\
(p'_\alpha|c) &= (zi_\alpha|\mathcal{P}\frac{\mathcal{P}}{2}\,(-|N) - N_i|\mathbb{1})) = \frac{1}{2}\,(N_{i\alpha} - N_i)\\
(p'_\alpha|s) &= (z_{i\alpha}|\mathcal{P}\frac{\mathcal{P}}{2}\,(-|\sigma) + \sigma_i|\mathbb{1})) = \frac{1}{2}\,(\sigma_i - \sigma_{i\alpha})\,.
\end{aligned}$$

Combining these with the expression for $|\rho^{(1)})$, Eq. (4.14), we find the first order correc-

tion to the energy current:

$$
\begin{aligned}
I^{(1)}_{E\alpha} = &\left(\epsilon_\uparrow + U\left(1 - N_{\downarrow i\alpha}\right)\right) I^{(1)}_{N\uparrow\alpha} + \left(\epsilon_\downarrow + U\left(1 - N_{\uparrow i\alpha}\right)\right) I^{(1)}_{N\downarrow\alpha} \\
&- \frac{U\gamma_{p\alpha}}{2}\left\{ -\frac{1}{4\gamma_p}\partial_t p_z \right. \\
&+ \left\{ \frac{1 - 2N_{\downarrow i}}{2\gamma_p} + \frac{1}{\gamma_a\gamma_b}\left[\left(f^+_{\epsilon\downarrow} - f^+_{U\downarrow}\right)\left(N_{\uparrow i\alpha} - N_{\uparrow i}\right) + \Gamma_\downarrow\left(N_{\downarrow i} - N_{\downarrow i\alpha}\right)\right] \right\} \partial_t N_{\downarrow z} \\
&\left. + \left\{ \frac{1 - 2N_{\uparrow i}}{2\gamma_p} + \frac{1}{\gamma_a\gamma_b}\left[\left(f^+_{\epsilon\uparrow} - f^+_{U\uparrow}\right)\left(N_{\downarrow i\alpha} - N_{\downarrow i}\right) + \Gamma_\uparrow\left(N_{\uparrow i} - N_{\uparrow i\alpha}\right)\right] \right\} \partial_t N_{\downarrow z} \right\}.
\end{aligned}
$$

We took the freedom here to immediately group the terms based on their proportionality to the time derivatives of either p_z, $N_{\uparrow z}$ and $N_{\downarrow z}$. Having found this, the energy (and heat) current is now fully determined up to first order in the driving frequency.

References

[1] G. E. Moore, "Cramming more components onto integrated circuits", Electronics **38** (1965) (cit. on p. 1).

[2] T. Simonite, "Intel Puts the Brakes on Moore´ s Law", MIT Technology Review (2016) (cit. on p. 1).

[3] G. Q. Zhang and A. Roosmalen, *More than Moore* (Springer US, 2009) (cit. on p. 1).

[4] C. Kittel, *Introduction to Solid State Physics*, 8th (Wiley, 2004) (cit. on p. 2).

[5] T. Ihn, *Semiconductor nanostructures* (Oxford University Press Inc., 2010) (cit. on pp. 2, 13, 14).

[6] S. M. Reimann and M. Manninen, "Electronic structure of quantum dots", Rev. Mod. Phys. **74**, 1283–1342 (2002) (cit. on p. 2).

[7] L. Kouwenhoven, C. Marcus, P. McEuen, S. Tarucha, R. Westervelt, and N. Wingreen, "Electron transport in quantum dots", Proceedings of the NATO Advanced Study Institute on Mesoscopic Electron Transport, 105–214 (1997) (cit. on p. 2).

[8] E. U. Rafailov, *The Physics and Engineering of Compact Quantum Dot-based Lasers for Biophotonics*, edited by E. U. Rafailov (Wiley-VCH Verlag GmbH & Co. KGaA, 2014) (cit. on p. 2).

[9] M. Houssa, *Lecture notes in Mesoscopic Physics*, 2014 (cit. on p. 2).

[10] C. Gorter, "A possible explanation of the increase of the electrical resistance of thin metal films at low temperatures and small field strengths", Physica **17**, 777 –780 (1951) (cit. on p. 3).

[11] T. A. Fulton and G. J. Dolan, "Observation of single-electron charging effects in small tunnel junctions", Phys. Rev. Lett. **59**, 109–112 (1987) (cit. on pp. 3, 4).

[12] H. W. C. Postma, T. Teepen, Z. Yao, M. Grifoni, and C. Dekker, "Carbon Nanotube Single-Electron Transistors at Room Temperature", Science **293**, 76–79 (2001) (cit. on p. 4).

[13] L. Kouwenhoven and C. Marcus, "Quantum Dots", Physics World, 35–39 (1998) (cit. on p. 4).

[14] M. Heyns, *Lecture notes in Materials Physics and Technology for Nanoelectronics*, 2014 (cit. on p. 4).

[15] S. De Feyter, *Lecture notes in Chemistry at Nanometre Scale*, 2015 (cit. on p. 5).

[16] G. A. Ozin, A. Arsenault, and L. Cademartiri, *Nanochemistry : A Chemical Approach to Nanomaterials*, 2nd ed. (Royal Society of Chemistry, 2008) (cit. on p. 5).

[17] L. Cademartiri, G. A. Ozin, and J.-M. Lehn, *Concepts of Nanochemistry* (Wiley-VCH Verlag GmbH, 2009) (cit. on p. 5).

[18] T. Bauch and J. Bylander, *Lecture notes in Quantum Optics and Quantum Informatics*, 2015 (cit. on p. 5).

[19] N.-H. Kaneko, S. Nakamura, and Y. Okazaki, "A review of the quantum current standard", Measurement Science and Technology **27**, 032001 (2016) (cit. on p. 5).

[20] T. Kontos, "Quantum physics: Single electrons take the bus", Nature **477**, 414–414 (2011) (cit. on p. 6).

[21] S. Hermelin, S. Takada, M. Yamamoto, S. Tarucha, A. D. Wieck, L. Saminadayar, C. Bauerle, and T. Meunier, "Electrons surfing on a sound wave as a platform for quantum optics with flying electrons", Nature **477**, 435–438 (2011) (cit. on p. 6).

[22] R. McNeil, M. Kataoka, C. Ford, C. Barnes, D. Anderson, G. Jones, I. Farrer, and D. Ritchie, "On-demand single-electron transfer between distant quantum dots", Nature **477**, 439–442 (2011) (cit. on p. 6).

[23] G. Fève, A. Mahé, J.-M. Berroir, T. Kontos, B. Plaçais, D. C. Glattli, A. Cavanna, B. Etienne, and Y. Jin, "An On-Demand Coherent Single-Electron Source", Science **316**, 1169–1172 (2007) (cit. on p. 6).

[24] M. Blumenthal, B. Kaestner, L. Li, S. Giblin, T. Janssen, M. Pepper, D. Anderson, G. Jones, and D. Ritchie, "Gigahertz quantized charge pumping", Nat Phys **3**, 343–347 (2007) (cit. on pp. 6, 7).

[25] M. R. Connolly, K. L. Chiu, S. P. Giblin, M. Kataoka, J. D. Fletcher, C. Chua, J. P. Griffiths, G. A. C. Jones, V. Fal'ko, C. G. Smith, and T. J. B. M. Janssen, "Gigahertz quantized charge pumping in graphene quantum dots", Nature Nanotechnology **8**, 417–420 (2013) (cit. on p. 7).

[26] S. d´ Hollosy, M. Jung, A. Baumgartner, V. A. Guzenko, M. H. Madsen, J. Nygard, and C. Schönenberger, "Gigahertz Quantized Charge Pumping in Bottom-Gate-Defined InAs Nanowire Quantum Dots", Nano Letters **15**, 4585–4590 (2015) (cit. on p. 7).

[27] J. Splettstoesser, M. Governale, J. König, and M. Büttiker, "Charge and spin dynamics in interacting quantum dots", Phys. Rev. B **81**, 165318 (2010) (cit. on pp. 8, 25, 55).

[28] L. D. Contreras-Pulido, J. Splettstoesser, M. Governale, J. König, and M. Büttiker, "Time scales in the dynamics of an interacting quantum dot", Phys. Rev. B **85**, 075301 (2012) (cit. on pp. 8, 24, 25, 52, 55, 64).

[29] J. Schulenborg, R. B. Saptsov, F. Haupt, J. Splettstoesser, and M. R. Wegewijs, "Fermion-parity duality and energy relaxation in interacting open systems", Phys. Rev. B **93**, 081411 (2016) (cit. on pp. 8, 9, 11, 14, 17, 22–24, 50, 52, 55, 64, 65).

[30] J. Schulenborg, *Time-dependent relaxation of charge and energy in electronic nanosystems*, Technical report MC2 - Department of Microtechnology and Nanoscience, Chalmers University of Technology, no: 331 (Department of Microtechnology and Nanoscience, Applied Quantum Physics, Chalmers University of Technology, 2016), eprint: https://publications.lib.chalmers.se/publication/232302-time-dependent-relaxation-of-charge-and-energy-in-electronic-nanosystems (cit. on pp. 9, 11, 15, 18, 22, 24, 34, 43, 52, 55).

[31] H. Zhou, J. Thingna, P. Hänggi, J.-S. Wang, and B. Li, "Boosting thermoelectric efficiency using time-dependent control", Sci. Rep. **5**, 14870 (2015) (cit. on pp. 9, 49, 50, 53, 66).

[32] J. Schulenborg, J. Splettstoesser, M. Governale, and L. D. Contreras-Pulido, "Detection of the relaxation rates of an interacting quantum dot by a capacitively coupled sensor dot", Phys. Rev. B **89**, 195305 (2014) (cit. on pp. 9, 24, 55).

[33] P. W. Anderson, "Localized Magnetic States in Metals", Phys. Rev. **124**, 41–53 (1961) (cit. on pp. 11, 37).

[34] G. W. Bryant, "Electronic structure of ultrasmall quantum-well boxes", Phys. Rev. Lett. **59**, 1140–1143 (1987) (cit. on p. 13).

[35] T. Brandes, W. Häusler, K. Jauregui, B. Kramer, and D. Weinmann, "Coulomb interaction and transport in tunnel junctions and quantum dots", Physica B: Condensed Matter **189**, 16 –26 (1993) (cit. on p. 13).

[36] K. K. Likharev, "Single-Electron Devices and Their Applications", Proc. IEEE **87**, 606–632 (1999) (cit. on p. 13).

[37] B. Kubala, *Doctoral thesis: Quantum transport through Coulomb-Blockade Systems* (2006) (cit. on p. 13).

[38] B. Sothmann, R. Sánchez, and A. N. Jordan, "Thermoelectric energy harvesting with quantum dots", Nanotechnology **26**, 032001 (2015) (cit. on pp. 14, 49).

[39] H. Thierschmann, R. Sánchez, B. Sothmann, F. Arnold, C. Heyn, W. Hansen, H. Buhmann, and L. W. Molenkamp, "Three-terminal energy harvester with coupled quantum dots", Nat. Nanotechnol. **10**, 854–858 (2015) (cit. on p. 14).

[40] H.-P. Breuer and F. Petruccione, *The Theory of Open Quantum Systems* (Oxford University Press, 2002) (cit. on p. 14).

[41] J. Splettstoesser, M. Governale, J. König, and R. Fazio, "Adiabatic pumping through a quantum dot with coulomb interactions: A perturbation expansion in the tunnel coupling", Phys. Rev. B **74**, 085305 (2006) (cit. on pp. 15, 27, 29, 31).

[42] F. Cavaliere, M. Governale, and J. König, "Nonadiabatic Pumping through Interacting Quantum Dots", Phys. Rev. Lett. **103**, 136801 (2009) (cit. on pp. 15, 27, 29, 31).

[43] S. Juergens, F. Haupt, M. Moskalets, and J. Splettstoesser, "Thermoelectric performance of a driven double quantum dot", Phys. Rev. B **87**, 245423 (2013) (cit. on pp. 29, 34).

[44] C. B. Vining, "An inconvenient truth about thermoelectrics", Nature Materials **8**, 83–85 (2009) (cit. on p. 49).

[45] G. Benenti, K. Saito, and G. Casati, "Thermodynamic Bounds on Efficiency for Systems with Broken Time-Reversal Symmetry", Phys. Rev. Lett. **106**, 230602 (2011) (cit. on p. 49).

[46] M. F. Ludovico, F. Battista, F. von Oppen, and L. Arrachea, "Adiabatic response and quantum thermoelectrics for ac-driven quantum systems", Phys. Rev. B **93**, 075136 (2016) (cit. on p. 49).

[47] J. S. Lim, R. López, and D. Sánchez, "Dynamic thermoelectric and heat transport in mesoscopic capacitors", Phys. Rev. B **88**, 201304 (2013) (cit. on p. 49).

[48] G. Rosselló, R. López, and J. S. Lim, "Time-dependent heat flow in interacting quantum conductors", Phys. Rev. B **92**, 115402 (2015) (cit. on p. 49).

[49] A.-M. Daré and P. Lombardo, "Time-dependent thermoelectric transport for nanoscale thermal machines", Phys. Rev. B **93**, 035303 (2016) (cit. on p. 49).

[50] H. B. Callen, *Thermodynamics and an Introduction to Thermostatics* (John Wiley and Sons, 1985) (cit. on pp. 50, 51).

[51] L. Onsager, "Reciprocal Relations in Irreversible Processes. I.", Phys. Rev. **37**, 405–426 (1931) (cit. on p. 51).

[52] M. Cutler and N. F. Mott, "Observation of Anderson Localization in an Electron Gas", Phys. Rev. **181**, 1336–1340 (1969) (cit. on p. 52).

[53] K. A. Matveev, *Statistical and Dynamical Aspects of Mesoscopic Systems* (Springer-Verlag Berlin Heidelberg, 1999) (cit. on p. 52).

[54] R. B. Saptsov and M. R. Wegewijs, "Fermionic superoperators for zero-temperature nonlinear transport: Real-time perturbation theory and renormalization group for Anderson quantum dots", Phys. Rev. B **86**, 235432 (2012) (cit. on p. 55).

[55] R. B. Saptsov and M. R. Wegewijs, "Time-dependent quantum transport: Causal superfermions, exact fermion-parity protected decay modes, and Pauli exclusion principle for mixed quantum states", Phys. Rev. B **90**, 045407 (2014) (cit. on p. 55).

[56] F. Haupt, M. Leijnse, H. L. Calvo, L. Classen, J. Splettstoesser, and M. R. Wegewijs, "Heat, molecular vibrations, and adiabatic driving in non-equilibrium transport through interacting quantum dots", Physica status solidi (b) **250**, 2315–2329 (2013) (cit. on p. 58).